

Synthesis And Characterization of Leucine Zipper Hydrogel For Tissue Regeneration

BY

CHUN-CHIEH HUANG
B.S., National Chiao Tung University, 2003
M.S., National Taiwan University, 2005

THESIS

Submitted as partial fulfillment of the requirements
for the degree of Doctor of Philosophy in Bioengineering
in the Graduate College of the
University of Illinois at Chicago, 2014

Chicago, Illinois

Defense Committee:

Anne George, Chair and Advisor
Michael Cho
Vuk Uskokovic
Luisa DiPietro, Department of Periodontics
Cortino Sukotjo, Department of Restorative Dentistry

Dedicated to my parents and family.
For their deep love, support and encouragement.

ACKNOWLEDGEMENTS

First and foremost, I would like to express my deepest appreciation to my primary advisor as well as my committee chair, Dr. Anne George. She continually and persuasively conveyed a spirit of adventure in regard to research and scholarship, and an excitement in regard to teaching. I attribute most of my success to her guidance, talent and encouragement. Without her guidance and persistent help, this dissertation would not have been possible.

I would also like to thank my thesis committee members Michael Cho, Vuk Uskokovic, Luisa DiPietro and Cortino Sukotjo for their unwavering support and assistance. They provided valuable suggestions in all areas that helped me accomplish my research goals and enjoy myself in the process of dissertation.

In addition, a thank you to all of my lab colleagues, Sriram Ravindran, Amsaveni Ramachandran, Asha Eapen, Qi Gao, Yiqiang Song, and Youbin Zhang. I am so grateful to work with you all. Your great help, kindness and friendliness were supportive in both research and daily life. It was really fun to work with you.

CONTRIBUTION OF AUTHORS

Chapter I is a literature review that places my dissertation topic in the context of the larger field and highlights the significance of my research topic. Chapter II is the materials and methods that have been used in my research topic in this dissertation. Chapter III-A represents a published manuscript [1] for which I was the primary author and major driver of the research. Dr. Sriram Ravindran assisted me in the experiments shown in Figure 9, 10, 11, and 12. Dr. Ziying Yin assisted me in the experiment shown in Figure 5(B). My research mentor, Dr. Anne George contributed to the guiding of the research topic and manuscript polishing. Chapter III-B and III-C represents a series of my own unpublished experiments directed at developing the mineralization ability of leucine zipper hydrogel by incorporating calcium binding domains; and the growth factor binding and releasing ability of leucine zipper hydrogel by incorporating heparin-binding domain and MMP-2 cleavage domain. I anticipate that both lines of research will be continued in the laboratory after I leave and that this work will ultimately be published as part of a co-authored manuscript. Chapter IV represents my synthesis of the research presented in this dissertation and my overarching conclusions. The future directions of this field and this research topic are discussed.

TABLE OF CONTENTS

<u>CHAPTER</u>	<u>PAGE</u>
I. INTRODUCTION.....	1
A. Background.....	1
A.1. Hydrogel for tissue engineering applications	1
A.2. Peptide-based self-assembly hydrogels	7
A.3. Leucine Zipper Hydrogel.....	15
A.5. Mechanical property of the hydrogel.....	19
A.6. Incorporation of growth factors for tissue regeneration.....	22
B. Purpose of the study	25
C. Specific aims of the study	27
C.1. To synthesize and develop stable LZ hydrogels with and without RGD domain and test its functionality in supporting 3-D cell culture	27
C.2. To synthesize and develop stable LZ hydrogels with mineralizing properties for hard tissue regeneration applications	27
C.3. To synthesize and develop stable LZ hydrogels for sustained growth factor release	28
II. MATERIALS AND METHODS.....	29
1. Construction of the chimeric LZ-Control protein	29
2. Cloning of the chimeric LZ proteins with functional motifs.....	29
3. Cloning of the chimeric LZ protein with heparin-binding domain and the MMP2 cleavage site	30
4. Expression and Purification of the LZ chimeric proteins.....	31
5. Preparation of the LZ hydrogel.....	31
6. Circular Dichroism (CD) spectroscopy	32
7. Scanning electron microscopy (SEM)	33
8. Cryo-transmission electron microscopy (Cryo-TEM).....	33
9. <i>In vitro</i> degradation study	33
10. <i>In vitro</i> calcium phosphate mineralization on the LZ hydrogels.....	34
11. Microscopic magnetic resonance elastography (μ MRE)	35
12. Oscillatory rheology	36
13. Selected Area Electron Diffraction (SAED)	37
14. Growth factor binding assay	37
15. Dot-blot assay to measure the release of heparin-binding growth factors	38
16. <i>In vitro</i> cell culture.....	39
17. 2-D cell culture.....	39
18. 3-D cell culture.....	40
19. MTS cell proliferation assay	40
20. Time-lapse live cell imaging	41
21. Live-dead cell assay	41
22. Actin staining	42
23. <i>In vivo</i> subcutaneous implantation of the LZ hydrogel scaffold	42
24. Histology and immunohistochemistry	43
25. Alizarin red staining	44
26. RNA isolation and quantitative RT-PCR.....	45
27. Statistical analysis	46
III. RESULTS AND DISCUSSIONS	48

TABLE OF CONTENTS (continued)

<u>CHAPTER</u>	<u>PAGE</u>
A. 3-D self-assembled leucine zipper hydrogel with tunable properties for tissue engineering.....	48
A.1. Synthesis of chimeric leucine zipper proteins	48
A.2. Secondary structure of chimeric leucine zipper proteins.....	52
A.3. Analysis of the surface characteristics and morphology of the leucine zipper hydrogels.....	54
A.4. Leucine zipper hydrogel mechanical properties.....	58
A.5. <i>In vitro</i> degradation rate of the leucine zipper hydrogels	61
A.6. Mesenchymal stem attachments on the leucine zipper hydrogels with RGDS motifs	63
A.7. Mesenchymal stem cell proliferation test on leucine zipper hydrogels with RGDS motifs.....	65
A.8. Cell viability within the leucine zipper hydrogels with RGDS motifs.....	66
A.9. Cell migration in 3-D leucine zipper hydrogel culture system	68
A.10. Foreign body response to leucine zipper hydrogels.....	70
A.11. Host cell response to LZ hydrogels.....	72
A.12. <i>In vivo</i> response of leucine zipper hydrogels pre-seeded with HMSCs	75
B. Stable leucine zipper hydrogels with calcium-binding properties for hard tissue engineering.....	79
B.1. <i>In vitro</i> nucleation of calcium phosphate polymorphs under physiological concentrations of calcium and phosphate ions by leucine zipper hydrogels containing the DMP-1 calcium-binding motif	79
B.2. <i>In vitro</i> nucleation of calcium phosphate under high concentrations of calcium and phosphate ions by leucine zipper hydrogels containing the DMP-1 calcium-binding motifs	83
B.3. Mechanical properties of the leucine zipper hydrogel with DMP-1 calcium-binding motifs after mineralization in high concentrations of calcium and phosphate buffer.....	89
B.4. Mesenchymal stem cell adhesion to the leucine zipper hydrogels with DMP-1 calcium-binding motifs after mineralization	93
B.5. Leucine zipper hydrogels containing DMP-1 calcium-binding motifs facilitated vascularization	95
B.6. Evaluation of osteogenic differentiation of HMSCs seeded on premineralized leucine zipper hydrogels with DMP-1 calcium-binding motifs.....	102
B.7. Calcified matrix formation in <i>in vivo</i> implanted 1:1:1 leucine zipper scaffold with calcium-binding DMP-1 motifs.....	107
B.8. Evaluation of osteogenic gene expression in leucine zipper hydrogel with DMP-1 motifs	110
C. Synthesis of leucine zipper hydrogels with growth factor releasing properties for hard tissue engineering	115
C.1. The LZ-MMPHEP hydrogel can bind heparin and heparin-binding growth factors.....	115
C.2. Growth factor binding efficiency of the LZ-MMPHEP hydrogel.....	117
C.3. Growth factor release profile from the LZ-MMPHEP hydrogel.....	119
C.4. Angiogenesis in the growth factor loaded LZ-MMPHEP hydrogels	121

TABLE OF CONTENTS (continued)

<u>CHAPTER</u>	<u>PAGE</u>
C.5. Osteogenic differentiation of HMSCs in the growth factor loaded LZ-MMPHEP hydrogels in vivo.....	127
C.6. Regulation of osteogenic gene expression in LZ-MMPHEP hydrogels loaded with TGF- β 1 or BMP-1	132
IV. CONCLUSION.....	135
A. Synthesis and characteristic of a stable leucine zipper hydrogel; evaluation of the incorporated RGDS motif	135
B. Evaluation of the incorporated DMP-1 derived calcium binding motifs and the effect of high calcium and phosphate concentration on mineralization and cellular response of the leucine zipper hydrogel scaffold	136
C. Evaluation of the incorporated heparin-binding domain and MMP-2 cleavage site for leucine zipper hydrogel growth factor release	137
APPENDICES	139
Appendix A	139
Appendix B	141
CITED LITERATURES	143
VITA	159

LIST OF TABLES

<u>TABLE</u>	<u>PAGE</u>
TABLE I LIST OF REAL TIME PCR PRIMERS	47

LIST OF FIGURES

<u>FIGURE</u>	<u>PAGE</u>
Figure 1. Schematic representation showing the peptide sequences used in the synthesis of the second generation chimeric leucine zipper protein.	50
Figure 2. Schematic representation of the assembled hydrogel from chimeric leucine zipper protein construct.	51
Figure 3. Secondary structure analyses of chimeric leucine zipper proteins by Circular Dichroism (CD).	53
Figure 4. Microscopy-based characterization of the LZ hydrogel architecture.	57
Figure 5. Viscoelasticity measurements of LZ-Control hydrogel.	59
Figure 6. Stability of the LZ-Control hydrogel.	62
Figure 7. Attachment and Proliferation of HMSCs cultured on 2-D coated surfaces and 3-D LZ hydrogels with RGDS.	64
Figure 8. Live-dead cell assay of LZ hydrogel with RGDS.	67
Figure 9. Z-stack confocal microscopy of HMSC seeded LZ-Control hydrogel.	69
Figure 10. CD68 Immunohistochemistry of LZ hydrogel with RGDS.	71
Figure 11. Immunofluorescence staining of scaffold sections from LZ hydrogel implanted in wild type mice.	74
Figure 12. Histology and immunofluorescence staining of HMSC seeded LZ-scaffolds implanted in immunocompromised mice.	77
Figure 13. <i>In vitro</i> mineralization of the LZ hydrogel with different combinations of DMP-1 calcium-binding domains (LZ-ESQES and LZ- QESQSEQDS) under physiological concentrations of calcium and phosphate.	81
Figure 14. <i>In vitro</i> mineralization on LZ hydrogel with different combinations of DMP-1 calcium-binding domains (LZ-ESQES and LZ- QESQSEQDS) under high concentrations of calcium and phosphate.	85
Figure 15. <i>In vitro</i> mineralization on the LZ hydrogel with DMP-1 calcium-binding domains under high concentrations of calcium and phosphate.	87
Figure 16. Viscoelastic ity measurements of LZ hydrogel with different combinations of LZ-ESQES and LZ-QESQSEQDS under high concentrations of calcium and phosphate.	90
Figure 17. Proliferation rate of HMSCs cultured on 3-D LZ mineralized scaffold. LZ scaffold was subjected to mineralization under high concentrations of calcium and phosphate and used for culturing HMSCs.	94

LIST OF FIGURES (continued)

<u>FIGURE</u>	<u>PAGE</u>
Figure 18.	Histological staining and immunohistochemical analysis of angiogenic markers performed on HMSC-seeded LZ scaffolds with DMP-1 calcium-binding motifs before and after mineralization, implanted in immunocompromised mice. 97
Figure 19.	Immunofluorescence staining for angiogenic markers expressed by HMSC-seeded LZ scaffolds with DMP-1 calcium-binding motifs when implanted in immunocompromised mice. 100
Figure 20.	Immunofluorescence staining for osteogenic markers. HMSC-seeded LZ scaffolds with DMP-1 calcium-binding motifs were implanted in immunocompromised mice. 104
Figure 21.	Histology staining of HMSC-seeded LZ scaffolds with DMP-1 calcium-binding motifs implanted in immunocompromised mice. 108
Figure 22.	<i>In vitro</i> quantitative RT-PCR analysis was performed to determine osteogenic related gene expression levels on HMSCs seeded on LZ hydrogels. 112
Figure 23.	Functionality of the heparin-binding domain on the LZ-MMPHEP hydrogel. 116
Figure 24.	Growth factor binding efficiency of the LZ-MMPHEP hydrogel.... 118
Figure 25.	Release profile of VEGF loaded from the LZ-MMPHEP hydrogel in the presence of varying amounts of MMP-2. 120
Figure 26.	Images of the HMSC-seeded LZ scaffolds with heparin-binding domain and loaded with growth factors in immunocompromised mice. 122
Figure 27.	Histology staining and immunohistochemical analysis of HMSC-seeded LZ hydrogel scaffolds with heparin-binding domain loaded with growth factors and implanted in immunocompromised mice..... 123
Figure 28.	Immunofluorescence staining for angiogenesis markers of HMSC- seeded LZ scaffolds with heparin-binding domain loaded with growth factors and implanted in immunocompromised mice..... 125
Figure 29.	Immunofluorescence staining for osteogenic markers of HMSC-seeded LZ scaffolds with heparin-binding domain and loaded with growth factors and implanted in immunocompromised mice.129
Figure 30.	Histology staining and immunostaining for osteogenesis markers of HMSC-seeded LZ hydrogel scaffolds with heparin-binding domain and loaded with growth factors and implanted in immunocompromised mice..... 131
Figure 31.	<i>In vitro</i> quantitative RT-PCR analysis of mRNA expression from HMSCs seeded on LZ hydrogel and implanted in immunocompromised mice..... 134

LIST OF ABBREVIATIONS

AFM	Atomic force microscopy
ALP	Alkaline phosphatase
BMP	Bone Morphogenic Protein
CD	Circular Dichroism
CD31	Cluster of Differentiation 31
CD68	Cluster of Differentiation 68
COL	Collagen
DMP	Dentin Matrix Protein
DNA	Deoxyribonucleic Acid
DPP	Dentin phosphophoryn
ECM	Extracellular Matrix
EDX	Energy-Dispersive X-Ray
ELP	Elastin-like peptide
ER	Endoplasmic reticulum
FGF	Fibroblast Growth Factor
FN	Fibronectin
GAPDH	Glyceraldehyde 3-phosphate dehydrogenase
GDF	Growth/Differentiation Factor
GFP	Green Fluorescent Protein
GRP78	Glucose-Regulated Protein 78
HA	Hyaluronic Acid
HGF	Hepatocyte Growth Factor
H&E	Hematoxylin And Eosin
HMSC	Human Mesenchymal Stem Cell
LZ	Leucine Zipper
MMP	Matrix Metalloproteinases
MSC	Mesenchymal Stem Cell
MTS	(3-(4,5-dimethylthiazol-2-yl)-5-(3-carboxymethoxyphenyl)-2-(4-sulfophenyl)-2H-tetrazolium)
MRE	Magnetic Resonance Elastography
NGF	Nerve Growth Factor
OC	Osteocalcin
OPN	Osteopontin
PAAm	polyacrylamide
PBS	Phosphate Buffer Solution
PCR	Polymerase Chain Reaction
PEDF	Pigment Epithelium-Derived factor
PEG	Poly(ethylene glycol)
PEO	Poly(ethylene oxide)
PGA	Poly(glycolic acid)
PHEMA	Poly(hydroxyethyl methacrylate)
PHEX	Phosphate Regulating Endopeptidase Homolog, X-linked
PHSRN	Proline-Histidine-Serine-Arginine-Asparagine Acid
PLA	Poly(lactic acid)

LIST OF ABBREVIATIONS (continued)

PLGA	Poly(lactic-co-glycolic acid)
PVA	Poly(vinyl alcohol)
PVP	Polyvinylpyrrolidone
RGD	Arginine-Glycine-Aspartic Acid
RGDS	Arginine-Glycine-Aspartic-Serine Acid
RNA	Ribonucleic Acid
RT	Room Temperature
RT-PCR	Real-Time Polymerase Chain Reaction
RUNX2	Runt-Related Transcription Factor 2
SAED	Selected Area (Electron) Diffraction
SEM	Scanning Electron Microscopy
STEM	Scanning Transmission Electron Microscope
TCPS	Tissue Culture Plates
TEM	Transmission Electron Microscopy
TGF- β	Transforming Growth Factor Beta
TNF	Tumor Necrosis Factors
TRAF	TNF Receptor Associated Factors
TRIP	TRAF Interacting Protein
TRITC	Tetramethylrhodamine
VEGF	Vascular Endothelial Growth Factor
vWF	Von Willebrand Factor

SUMMARY

Tissue engineering is based on three major factors: cells, biological signals, and scaffold. The importance of biomaterial development for tissue engineering application is critical. Biomaterials are currently being developed for biological activity, and the essential property required for a functional biomaterial is cell attachment and cell viability. Scaffolds are also required to deliver specific biological signals at the specific time.

The Leucine Zipper (LZ) is a secondary α -helical coiled-coil structure found in several proteins. The LZ hydrogel is a novel biomaterial and is formed by the inherent self-assembly property of the LZ domain in the chimeric protein. Such native materials may be a better candidate for tissue engineering applications. However, the current LZ hydrogel is not stable enough to function as a scaffold for a desired period of time. Furthermore, the LZ hydrogel is not yet developed and explored as a scaffold. As LZ is synthesized as a recombinant protein, ideally it should be possible to incorporate the desired functional motifs with specific functions. Incorporating such functional domains in the scaffold may enable usage for a wide range of applications.

In this study, we developed a stable 3-D LZ hydrogel by using a dehydrothermal crosslinking method. The LZ hydrogel is porous. By altering the weight percentage of the hydrogel, the pore size and the mechanical properties can be changed. The LZ hydrogel is also tunable with respect to its functionality by incorporating different functional domains. We evaluated several different functional motifs after incorporated them into the LZ hydrogel. These motifs were

SUMMARY (continued)

RGDS, DMP-1 derived calcium-binding domain ESQES and QESQSEQDS and a heparin-binding domain with a MMP-2 cleavage site.

The LZ hydrogel by itself can provide good cell affinity for 3-D cell culture and did not trigger foreign body reaction when implanted subcutaneous in a wild type mouse. The RGDS incorporated LZ hydrogel can provide an even better cell culture environment by facilitating the cell attachment, proliferation and migration. The LZ hydrogel incorporated with DMP-1 derived calcium-binding domain (ESQES and QESQSEQS) showed the ability of accumulating calcium ions and further triggered biomineralization *in vivo*. This can also be used to enhance the hydrogel mechanical properties. The cell responses to the LZ hydrogel with an without pre-mineralization was also different when cultured subcutaneously in mice. The non-mineralized hydrogel could trigger osteogenic differentiation human mesenchymal stem cells (HMSCs). The HMSCs on the pre-mineralized hydrogel were able to undergo the osteogenic differentiation faster.

The incorporation of heparin-binding domain with MMP-2 cleavage site facilitated tethering of heparin-binding growth factors (VEGF, TGF- β 1 and BMP-2) and controlled release of active growth factor *in vitro* and *in vivo*. The growth factors could be released via proteolytic cleavage through the designated MMP-2 cleavage site. Two heparin-binding growth factors including TGF- β 1 and BMP-2 were evaluated *in vivo*. Both remained active and influenced HMSCs fate showing the feasibility of this approach.

Overall, we have shown that LZ, a self-assembling peptide can be utilized

SUMMARY (continued)

for the synthesis of a defined matrix for tissue regeneration. Synthesis of the engineered LZ domain can facilitate the formation of physical and covalent crosslinks in hydrogel structures leading to the formation of interconnected pores of varying sizes and mechanical properties based on peptide concentration or composition. The incorporated functional domains can also provide the hydrogel with tunable properties for varied applications. This is the first report on the development of a stable LZ hydrogel with tunable properties.

I. INTRODUCTION

A. Background

A.1. Hydrogel for tissue engineering applications

Tissue engineering is an interdisciplinary field combining cells, biological signaling molecules and scaffolds. Combination of these three could be used as therapeutic strategies for restoring or replacing damaged or malfunctioning tissues. Recently, several new biomaterials are being developed to function as a temporary scaffold to mimic the extracellular matrix (ECM) in the form of a hydrogel, to achieve a 3-D architecture and organization during tissue regeneration and also direct cells by providing biological and mechanical cues [2-7]. In living tissues, the cells are structurally supported and attached to the 3-D ECM that is synthesized and secreted by the cells themselves. The ECM regulate the cell fate by providing the biological and chemical cues through the intricately interwoven network made by hydrated proteoglycans and fibrous proteins such as collagen, fibronectin, laminin, and elastin [8]. Such a 3-D micro porous structure also facilitates cell-cell communications through signal transductions carried out by biological chemical molecules. The mechanical support provided by the 3-D ECM also initiates mechano-transduction events as the cells can exert forces with each other. In contrast, cells cultured in 2-D monolayer in the traditional way do not mimic the chemical and physical cues and possibly the functions observed *in vivo*. Several studies also have highlighted and stressed the importance and

necessity of a 3-D cell culture environment over the traditional 2-D culture [3, 9-14]. Hence it is important to design and synthesize a well defined 3-D artificial structure that is capable to accurately mimicing the microenvironment of the native ECM [15]. It has been shown that the refinement of the microstructure for 3-D cell culture significantly influences the behavior of how the cells respond to small biological molecules [16, 17]. Furthermore, scaffolds need to provide proper mechanical properties to allow cell attachment and migration, enable diffusion of oxygen and flow of biological substances for maintaining metabolic activity and also provide a localized and sustained release of growth factors depending on the demands of the specific application [18]. For different target tissue regeneration or specific biomedical applications such as wound healing or drug delivery, the hydrogels with different desired properties can be synthesized and the properties can be finely tuned according to the end use [6, 7, 19-22].

A hydrogel may be defined as a material made with water-insoluble and crosslinked polymer network that can absorb and hold a great amount of water [7, 23, 24]. Such a polymer network may be made from either synthetic or natural origin, as a homopolymer or a copolymer [25]. Although the hydrogel may contain a great amount of water as much as 99% of its volume, the material behavior of hydrogel still remains as a solid matter [19, 25]. To date, a large portion of the scaffolds for tissue engineering or biomedical materials are focused on synthetic polymers-based materials, as they are easy to synthesize with varying material properties. These properties are often easily tunable by

adjusting its monomer compounds or synthesis methodology [26-28]. Since 1995, one of the most important and still being widely used synthetic polymer hydrogel is poly(hydroxyethyl methacrylate) (polyHEMA, PHEMA) [29, 30]. Poly(ethylene glycol) (PEG), also known as poly(oxyethylene) or poly(ethylene oxide) (PEO), and its derivatives are another group that has been widely used as hydrogels made from synthetic polymer. The PEG family are characterized as having high biocompatibility, low toxicity and biodegradability makes them as favored candidates for biomedical applications like drug delivery and tissue engineering [31-33]. The other widely studied synthetic polymer-based hydrogel being used as a tissue engineering scaffold are poly(glycolic acid) (PGA), poly(lactic acid) (PLA) and their copolymer poly(lactic-co-glycolic acid) (PLGA). PGA, PLA, and PLGA are noted for their biodegradability and previous work have shown that such characteristic properties can benefit the repair of articular cartilage and facilitate tissue regeneration during implantation [34, 35]. The use of other synthetic polymer-based hydrogels such as poly(vinyl alcohol) (PVA) [36], polyvinylpyrrolidone (PVP) [37], polyimide [38], polyacrylate [39], and polyurethane [40] were also reported.

Although the synthetic polymer-based hydrogels are favored due to the convenience of manipulating its characteristic properties, however, these materials lack biological recognition domains, suppress cell affinity and are immunoreactive. In order to overcome these disadvantages, grafting cell recognition proteins or peptides on the scaffold surface were often being used [33, 41, 42]. This often requires chemical reactions and treatments, which

results in cytotoxicity [43, 44]. Besides, surface modifications still cannot fix the potential immunoreactivity caused by degraded polymer debris. On the other hand, natural biomaterials are often derived from components of the extracellular matrix that already exist in nature, hence it can be recognized by the cellular environment and can be degraded through cellular pathways. Often the hydrogels made from natural materials require crosslinking either covalently or non-covalently [45-47]. The native biomaterials can also have biological functions at the molecular level and are often enzymatically degraded without any need of additional cues [5].

Currently the use of natural material hydrogel can be categorized into two major groups, polymers derived from proteins and the polysaccharidic polymers. The advantage of using protein-origin polymers as hydrogel scaffold is the ease of mimicking the ECM characteristics and further potentially direct cell migration, proliferation and organization during tissue regeneration or wound healing. Collagen is the major content of the ECM which provides support to connective tissues, hence collagen-based hydrogel is widely used in tissue engineering or delivery systems [48-50]. Derived from denatured collagen, gelatin is commonly used in biomedical applications because of its biodegradability and biocompatibility when placed in physiological environments [51-53]. Fibrin and fibrinogen have been studied extensively as a tissue engineering scaffold because of the innate ability to facilitate cellular interaction and subsequently matrix remodeling [54-56]. Other polymers of protein-origin such as silk or silk fibroin [57-59] and elastin [60-62] hydrogels

were also reported. Peptide-based hydrogels is also a subgroup of the polymers of protein-origin..

The other major group of natural material is polysaccharides which are a class of polymers constituted by simple sugar monomers [63]. Polysaccharide based hydrogels are characterized as a material with good hemo-compatible properties that might arise because of its chemical properties being similar to heparin. Polysaccharides hydrogel are also non-cytotoxic, possess good cellular interaction ability and sometimes are cheaper than manufacturing other natural materials.[64, 65]. In nature, chitin is the second most abundant polysaccharide containing polymerized carbon and chitosan is fully or partially deacetylated derivative. Due to its proven biodegradable, biocompatible, biologically renewable, non-cytotoxic and biofunctional properties, chitosan has attracted a wide attention and employed in different applications including tissue engineering and drug delivery [66, 67]. In addition, chitosan is also easy to be chemically modified for surface grafting with biological signals and metabolically digested by enzymes, especially lysozyme, facilitating its biodegradability due to its amino and hydroxyl functional groups [68]. Among the polysaccharide hydrogel materials, alginate is one of the most studied and developed in tissue engineering and drug-delivery fields. Alginate-based hydrogels are useful and attractive because of their pH-sensitive characteristic properties and the mild process conditions for gelation [48, 68, 69]. Hyaluronan is often referred to as hyaluronic acid (HA) since it is exist in the form of a polyanion and not in the protonated acid form *in*

vivo. HA is also widely used in tissue engineering as a scaffold probably because of its high content in the ECM [48, 70, 71]. Starch is another promising polysaccharide hydrogel material, also because of its innate biodegradability, renewability, and excessive abundance. However, starch by itself is mechanically brittle making handling extremely difficult without adding any additives such as plasticizers or blending with other synthetic or natural polymers [72, 73]. Other polysaccharide hydrogels such as chondroitin sulphate [74, 75], dextran [64, 76], agar [77], carrageenans [78], cellulose [78], and gellan gum [64] were also reported from other studies as tissue engineering scaffolds or drug delivery carriers.

A.2. Peptide-based self-assembly hydrogels

Although there exists some benefit of using natural materials for hydrogel synthesis or tissue engineering or drug delivery applications, it possesses a major drawback: the difficulty of maintaining consistency from batch to batch during the synthesis of the hydrogel. However, this can be overcome by an alternate strategy using precisely designed recombinant or chimeric proteins as well as by the introduction of predictable crosslinking methodology. Bringing such a programmable methodology during the synthesis of natural polymer hydrogel can be extremely attractive as it will contain predictable properties such as degradation rate or concentration of bound biological signal motifs or growth factors which are useful for tissue engineering or drug delivery purposes [15, 61, 62].

The use of peptide-based hydrogels as a scaffold in regenerative medicine exhibits several advantages including mimicking the ECM contents, favorable for cell attachment, proliferation and organization during the regenerative process. In the molecular perspective, the peptide-based hydrogel can be considered as a series of combination of 20 distinct amino acids. By arranging the amino acids in different combinations, one can easily build the desired peptide sequence that exhibit unique functions. The current drawback of peptide-based hydrogel, however, is the fabrication difficulties of 3-D, stable, hierarchical scaffolds that can mimic the structural complexity of the natural ECM.

Self-assembly is defined as the spontaneous association of monomers or peptide building blocks following thermally equilibrium conditions and assemble into an ordered network structure through non-covalent interactions and therefore this assembly is reversible without any human interference. The phenomenon of molecular level self-assembly from the smaller building blocks to a super-structure network is not a simple and random aggregation. It is rather a specific interaction between these building blocks that result in a well-defined super-structure with a hierarchical order on larger scales [79]. These non-covalent interactions include electrostatic interactions, hydrogen bond binding, hydrophobic interactions, van der Waals interactions and aromatic π - π interaction. The hydrogel formation also involves a transition from a solution state into a gel state by the interaction of the building blocks (sol-gel transition). These transitions may be triggered by the change of solution conditions such as pH [80], changing of the solvent [81], addition salts [82], or thermal cycling [83]. The casting of the self-assembled hydrogel by different methods can also alter the properties [84]. These transitions are reversible in nature and can be easily interrupted by environmental stimuli. The self-assembled hydrogel are versatile and can be used in different forms as well as injected for medical applications [85, 86]. Since the hydrogel transition does not involve any covalent bond formation, it is often happens much faster then the crosslinked polymer based hydrogels [87-92]. The peptide-based hydrogel system offers a great opportunity for creating a chimeric protein based hydrogel with innate self-assembling property to build a hydrogel using a bottom-up strategy [93].

However, in order to increase the mechanical stability of the scaffold, some studies introduced covalent binding on top of the self-assembly hydrogel [94]. The easiest method used to detect the formation of the self-assembled hydrogel was performed by inverting the vial containing the hydrogel and further determined its mechanical properties by quantitative rheology measurements [95].

Chimeric proteins designed for hydrogel formation via self-assembly can efficiently form a stable 3-D hydrogel [88, 96-99]. In addition, these chimeric backbone proteins can be incorporated with functional motifs for fine tuning its properties to mimic the complexity of natural ECM. For example, the common drawback of covalent immobilization of biological molecules on the material surface with desired functions may be lost during the coupling process [100] but the use of chimeric proteins could alleviate this problem. The emergence of molecular self-assembly based hydrogels hold great promise in tissue engineering and regeneration applications.

The diversity of peptide building blocks that exist throughout the proteome in nature enables the greater possibility of peptide-based hydrogel that can be achieved. Researchers have found many examples of peptides that fold into 3-D structure and also identified different peptide motif domains for various end applications in tissue engineering. By careful designing and selecting the functional peptide motifs, we can manipulate the functional properties of the chimeric proteins.

In the field of peptide-based hydrogels, the coiled-coil α -helical structure is the one that has been explored extensively as a self-assembling motif in hydrogel formation. Proteins containing coiled-coil structure abundantly exist in nature and are critical for their physiological function. For example, the blood clots that are formed by the fibrin fibers are assembled by fibrin monomers containing coiled-coil structure. The fibrin monomers are a long chain and originate from the aggregation of the soluble plasma protein, fibrinogen, after activation by the protease thrombin. These fibrin monomers then further aggregate and assemble via its coiled-coil linkers to form the fibrin fiber and then form a polymerized network as blood clots [101]. The coiled-coil structure contains heptad repeats of amino acids. By simply having three heptad repeats (21 amino acids), a self-assembled hydrogel can form as nanofibers at a relatively high peptide concentrations and at low pH values [102]. Leucine zipper (LZ) domain is another example of coiled-coil structure and extensively studied as the self-assembling motif in the synthesis of hydrogel scaffolds for tissue engineering applications.

Just like the coiled-coil α -helical structure, the β -sheet structure is another structural group of self-assembling motif and is also abundantly present in nature and found in biomaterials such as silk fibroin. The β -sheet structure is known to form β -strands as observed in amyloid fibrils with the alignment of hydrogen bonds perpendicular to the fibril axis [103-105]. In early studies back to 1975, it was suggested that an alternative arrangement of the hydrophilic and the hydrophobic amino acids tends to form a β -sheet structure

with one side hydrophilic and the other side hydrophobic [106]. In recent years, there are many hydrogels made of β -sheet fibril-rich structures. For example, the domain K24 (KLEALYVLGFFGFFTLGIMLSYIR) is the residues 41-67 but without the residues 47-49 of the transmembrane domain of protein IsK. This is one of the first sequence taken from a native protein and shown to form a self-assembled β -sheet hydrogel with proper viscoelastic gel properties [107]. Originated from the yeast protein zuotin, the 16-residue peptide EKA16-II (AEAEAKAKAEAEAKAK) and its derivatives including RADA16-I, (RADA)₄, and RAD16-II (RARADADARARADADADA) can self-assemble into β -sheet structure by salt-induced method under physiological conditions [108-110]. Similar salt-induced β -sheet fibril formation for peptides like FEK-16 or (FEFEFKFK)₂ were also investigated and used for a variety of tissue engineering purposes [111]. Q11 (QQKFQFQFEQQ) is another well-studied peptide that was specifically designed to carry biological signal motifs such as RGDS or IKVAV at its N-termini to facilitate cell recognition and adhesiveness for tissue engineering applications [112, 113]. With proper design, a two-step self-assembled β -sheet hydrogel formation can be achieved by making the peptide fold into β -hairpin conformation by first stimulating environmental changes like pH, salt ion concentration, or temperature. MAX1, whose sequence is (VK)₄-V^DPPT-(KV)₄-CONH₂, and its derivative MAX8 are one of such peptides used for two-step self-assembly into β -sheet hydrogel [114, 115]. Some extremely short peptides can also be attached to aromatic components to create a π -stacking (stacking the aromatic rings) interaction

and further facilitate the peptide self-assembly. Examples including Boc (*tert*-butoxycarbonyl), Fmoc (9-fluorenylmethoxycarbonyl), and naphthyl group (Nap) conjugate with dipeptides [83, 116].

Sometimes the fused organic functional group can participate in the self-assembly together with the peptide just like the peptide amphiphiles. The peptide amphiphiles was first introduced in 1995 and usually includes three major domains: a hydrophobic alkyl tail, a peptide which is capable of forming a β -sheet with hydrogen bonds, and a functional peptide motif which is hydrophilic and can be incorporated with desired biological signals [117, 118]. At a certain concentration, these peptide amphiphiles can self-assemble into cylindrical micelle nanofibers with the hydrophobic amphiphile occupying the core space, and the nanofibers are further interwoven into a viscoelastic hydrogel. The relatively ease of synthesis and high flexibility for tuning the properties drew a lot of attentions to the peptide amphiphiles. For example, the amphiphile can be modified with different crosslinking cues like covalent bonds or UV crosslinking [98, 119, 120]. The peptide sequence can also be modified to delay the gelation time [121]. Different biological signal motifs such as RGDS or IKVAV[122, 123], or growth factor binding mechanism such as heparin-binding motifs can also be incorporated to the hydrophilic end [98, 124].

Another group of hydrogel is the elastin-like peptide-based hydrogel. The various peptide-based hydrogels mentioned above focuses on the sequence containing the structural assembly property. However, the elastin-

like peptide assembles into a specific natural protein as the name suggests into elastin. Elastin is a elastic protein that exist abundantly in mammalian tissues like blood vessels, lung parenchyma and skin, and is the major component of the ECM in these tissues. Elastin is synthesized as monomers called tropoelastin, and the self-assembly property of tropoelastin inspired the synthesis of recombinant elastin-like peptides (ELPs) and ELP hydrogel research [125, 126]. The ELPs are derived from a naturally occurring motive of repeating VPGXG sequence, where X can be any amino acid but proline [127], and the self-assembly property is driven by a process of temperature-induced phase separation or coacervation [128]. The modifications to the ELPs included changing its thermal transition temperature for gelation. By using a single repeat of VPGVG, the ELP thermal transition temperature can be tuned and capable for a local *in situ* gelation once the ELPs reach a tissue with higher temperature [129]. Or by replacing the fourth position amino acid to a hydrophobic one can bring the thermal transition temperature down below 37°C by the formation of the type II β -turns [130]. Another approach to ELP modification was carried on the tri-block by using the plastic domain VPAG on both ends and the elastomeric domain VPGVG in the middle block [131-133]. However, there was no mention of their capability to form 3-D hydrogels with the tri-block ELPs [134]. Recent researches conducted on ELP hydrogels were on its mechanical properties and ways to introduce covalent bonds to stabilize it [135]. The dependency of the ELP hydrogel mechanical properties to

chondrogenesis was also investigated for cartilage tissue engineering [127, 136, 137].

A.3. Leucine Zipper Hydrogel

Native biomaterials, including collagen, fibrin, chitosan and so on, are derived from naturally existing extracellular matrix [5]. Recently, peptide-based biomaterials are receiving increasing attention for tissue engineering applications. The ease of manipulating the peptide sequences makes it convenient to obtain the required biological response [138]. Hence, the idea of assembling each individual short domain peptides with specific functions to generate a “multi-domain peptide” was developed recently.

The LZ domains, as one of the coiled-coil superstructures, are structural motifs that exist abundantly in native proteins like transcription factors as part of DNA binding domain. The LZ domains form α -helices and are constituted by repeated heptad amino acids in the form of *abcdefg* where positions *a* and *d* are non-polar residues and positions *e* and *g* are charged residues. Such arrangement of the amino acids allow the formation of coiled-coil structures as the side chains of the non-polar residues provide a local hydrophobic environment. The non-polar residues in position *a* and *d* are often leucine residues and therefore reflect the name of this coiled-coil structure as leucine zippers [139, 140].

The LZ chimeric peptide is one example of the ABA multi-domain peptide, or tri-block peptide structure, with domain A consisting of the α -helix coiled-coil secondary structure named LZ domain and the domain B with a hydrophilic flexible peptide allowing the LZ motifs to move freely. When present in an ionic and neutral pH condition, the α -helix coiled-coil secondary

structure in domain A is formed and adhere together, thereby forming a large network by self-assembly. Pekta et al. was the first to demonstrate the idea of LZ hydrogel [138, 141, 142]. Such a network composed of LZ peptides is soft and paste-like in appearance, and it is also not stable enough for tissue engineering applications. The cysteine residues was later introduced in the LZ ABA tri-block structure in order to provide for the formation of the covalent disulfide bonds to prevent the naturally reversibility of the LZ binding and to enhance the integrity [143]. The later studies also reported the instability of the ABA tri-block due to the self-aggregation and self-loop-formation and introduced a dissimilar coiled-coil structure to improve the erosion rate [144, 145]. However, there has never been a stable LZ hydrogel synthesized as a 3-D scaffold. Hence, further modification to this material is necessary for its use in tissue engineering applications in clinical practice.

A.4. Incorporation of biological motifs for cell attachment in hydrogels

Stem cells are often favorable for tissue repair and regeneration and require attachment on the ECM or onto another cell. Hence when developing a new biomaterial, surface markers for cell recognition were often used for improving the cell attachment efficiency and motility during culture [146]. Hydrogels from native materials such as collagen, chitosan, alginate, HA or dextran are inherently biocompatible and bioactive, but the surface recognition markers still need to be incorporated for its use as a biomaterial [147].

In nature, cells bind to adhesive proteins such as laminin and fibronectin present on the ECM via integrins. Short peptide motifs RGD or RGDS are found in many adhesive proteins and has been well characterized as an integrin binding receptor $\alpha_v\beta_3$ [148]. PHSRN was another surface marker derived from fibronectin that also triggered integrin-based intracellular signaling pathways that altered cell proliferation or differentiation [149]. Both motifs were used either chemically or physically for biomaterial surface modifications in order to improve surface properties. Studies also showed that the biomaterial surface modified with laminin derived peptide motifs such as YIGSR and IKVAV can significantly improve neural cell attachment [122, 150, 151]. Longer laminin derived fragments (CDPGYIGSR and RNIAEIIKDI) modified agarose hydrogel surface and hyaluronic acid hydrogel surface were also reported for dorsal root ganglia cell growth guidance thereby improving neuron cell density [152-154].

The $\alpha_5\beta_1$ integrin-specific fragment from fibronectin was also used for coupling with HA for culturing mouse MSCs [155]. Other surface receptors such as CD44 and CD168 were used to provide attachment of stem cells in HA hydrogel [11]. The integrin-peptide motif affinity contributes to the efficiency of cell attachment and mobility. This affinity is effectively influenced by the concentration of the peptide motif. Cells respond to various concentrations of cell attachment ECM proteins coated on a surface and studies demonstrated a minimum concentration range of 100~1300 fmol/cm² of fibronectin and vitronectin is required for sufficient cell attachment and spreading [156]. For a RGD peptide motif immobilized surface, a minimum concentration of 1 fmol/cm² was determined for sufficient fibroblast spreading, and a minimum concentration of 10 fmol/cm² was required for $\alpha_v\beta_3$ binding, focal adhesion and cytoskeleton organization [157].

Many studies have shown the inclusion of the RGD domains in the hydrogel may favor cell attachment, migration, differentiation and organization in various tissue engineering applications [158, 159]. Published studies also show that the self-assembled hydrogel containing the fibronectin and laminin peptide domains [99]. Studies on the incorporation of RGD domains on the self-assembled LZ hydrogel were also reported, however, these results were carried out on a 2-D LZ tri-block peptide surface or on a unstable 3-D LZ hydrogel [160-162].

A.5. Mechanical property of the hydrogel

The primary purpose of developing a scaffold for tissue engineering is to make an artificial filling of the vacant space lost from the original tissue. Thus, it is favorable for tissue regeneration if the scaffold can match the mechanical properties of the original tissue. The cells are able to sense the mechanical microenvironment condition through the transmembrane proteins such as integrins and regulate its behavior by responding through mechanotransduction [163, 164]. In the tissue microenvironments, the cells may experience a wide range of stiffness changes depending on if they are present near soft tissues or hard tissues and that will directly affect the cell behavior responses or gene regulation [165, 166]. For example, the brain tissue stiffness is about 0.1 kPa and the precalcified bone can be around 80 kPa [167]. Many studies have shown how the mechanical properties of the hydrogel scaffold affect cell behaviors including attachment, migration, proliferation, and differentiation. The cells can alter its behavior through the response from the transmembrane proteins such as integrins or through mechanotransduction after sensing the mechanical property profile of the hydrogel.

From the perspective of tissue engineering, the mechanical properties are also important based on the stiffness of the regenerative tissue. Different cell type such as chondrocytes, fibroblasts, smooth muscle cells, endothelial cells, and mesenchymal stem cells may exhibit different response and behavior to the mechanical properties of ECM or hydrogels. For example,

HMSCs shows neurogenic, myogenic, or osteogenic when cultured on the PAAm surface with different stiffness ranging from 0.1 kPa to 34 kPa. It has also been reported the HMSCs differentiation can be controlled by the stiffness of the hydrogel [168].

The mechanical properties of the hydrogels may be tuned by three major methodologies. The most commonly used and the easiest method is to change the concentration of the hydrogel monomer. Higher concentrations than the critical gelling concentration can be used for strengthening the hydrogel mechanical properties [169-171]. Another approach is to increase the degree of crosslinking of the hydrogel. It has been reported that the changes of the cell growth behavior and morphology can be altered by the crosslinking density of the PEG-based hydrogel [172, 173]. The last method is to reinforce the hydrogel mechanical properties by coating or doping different materials. For instance, a coated layer of calcium phosphate or mixing some carbon nanotubes can increase the stiffness and stability of the hydrogel [174, 175].

Currently, either atomic force microscopy (AFM) or oscillatory rheometer is typically used for characterizing the mechanical properties of the hydrogel matrices. AFM had been used for collecting the material mechanical properties, including stiffness and viscoelasticity, by the micro- or nano-indenters for more than two decades [176]. Under the force mode, the AFM indents the tip into the hydrogel surface and detects the deflection of the cantilever based on the stiffness. In order to reduce the strain at the point of contact, a bead is usually attached to the AFM tip [177]. Conventional

nanoindenters can also be used for stiffer hydrogel matrices to characterize the mechanical properties with similar mechanism, only with a larger tip and contact point compared to AFM [178]. Since the hydrogel matrices are more often viscoelastic which is intermediate between an ideal solid and an ideal liquid, an oscillatory rheometer is used. Rheology is the study of the flow and deformation of matter, and the measurements are collected by shearing the samples. The oscillatory rheometer applies a controlled oscillatory sinusoidal shear strain through parallel plates on the samples and the responsive torque stress change is measured.

One of the major challenges in fine tuning the hydrogel mechanical properties is the change in its 3-D microenvironment properties. It is worth noting that an increase in the hydrogel stiffness is usually accompanied by a decrease in pore size. This further affects the mass diffusivity due to the inherent permeability and porosity of the hydrogel matrices [179, 180].

A.6. Incorporation of growth factors for tissue regeneration

Hydrogel scaffolds for tissue engineering applications are meant to temporarily replace the native tissue and mimic the native ECM. One of the important functions of the native ECM is to provide soluble signaling factors, including growth factors, in order to trigger the cellular response for promoting tissue regeneration [100, 181]. This is the reason why state-of-the-art hydrogel scaffolds are required to have a sustained growth factor release capability [18].

There are many studies that have demonstrated a spatial distribution of covalently immobilized growth factors in the scaffold [100, 182, 183]. However, the suitable binding sites of the growth factors for coupling are hard to obtain, and the reactions for coupling the growth factors to the material may damage its biofunctionality [100]. Thus, non-covalently binding of the growth factors through a specifically designed binding site provides an alternative method for sustained release. Such non-covalent binding interactive molecules is predominant in nature, for example, heparin-binding growth factors can bind specifically to heparan sulfate proteoglycans in the ECM via electrostatic binding mechanism [184].

Numerous peptide motifs in several growth factors show great binding affinity to heparin, and this binding affinity is important for the growth factors to bind to the native ECM in nature. This electrostatic heparin-binding mechanism provides growth factor activity locally thereby preventing growth factor degradation, and sometimes improving the cell surface receptor binding. Studies have shown the development of several strategies to bind growth

factors on material surfaces. For example, it has been shown that the incorporation of sulfated glycosaminoglycans inspired by heparan sulfate can provide the heparin-binding growth factors on the sulfated alginate hydrogels with superior binding affinity [185]. Another example is the use of 12-14, type three repeats of fibronectin functionalized fibrin matrices, which also showed good binding and growth factor release characteristics *in vitro* [186]. However, the issues of not able to determine optimum binding motif concentrations may be a drawback for several applications. Hydrogels such as fibrin matrices have relatively larger network frame that may limit the maximum binding of motifs, while hydrogels made from peptide amphiphiles may limit the porous network within for potential cell movement due to the smaller building blocks [98]. Considering these factors, the LZ self-assembled hydrogel may provide a way to fine tune the growth factor binding motif concentration by simply adjusting its concentration by dilution rate and also maintain a suitable framework with a reasonable pore size for cell activities.

The major heparin-binding growth factors include VEGF, TGF- β , BMP, HGF, FGF, NGF and so forth [187]. Studies in the past have demonstrated the practical use of heparin-binding growth factor sustained release in tissue engineering scaffolds [188-193]. So far, there are two approaches to develop a heparin-binding growth factor release hydrogel scaffold. One is to directly incorporate the heparin structure into the hydrogel backbone structure covalently via modified heparin functional groups [191] and the other is to non-covalently and electrostatically bind the heparin molecules by introducing

heparin-binding peptide domain in the hydrogel backbone structure [190]. Both methodologies are able to allow heparin-binding growth factors be attached on the hydrogels and act as a growth factor reservoir for sustained release.

B. Purpose of the study

In order to be considered as a suitable hydrogel scaffold to be used in tissue engineering applications, they must provide a good substratum cell attachment, cell motility, tunable mechanical properties and have the ability to provide controlled release of biomolecules such as growth factors. Ease of synthesis and non-cytotoxic are also critical for modifying the hydrogel scaffold.

The advantage of the LZ chimeric protein synthesis is that any amino acid residue can be added or changed easily by genetic engineering. Therefore, peptides with different biological functions can be incorporated in the LZ backbone to create a functional chimeric protein with self-assembling properties. Hence, developing a brand new stable hydrogel scaffold with tunable functions specifically designed and dedicated for various tissue engineering applications is the major goal of the study.

RGDS peptide sequence is commonly found in several native proteins and functions to promote cell attachment through integrin receptors. Therefore, the RGDS motif was engineered into the LZ chimeric protein in order to enhance cell attachment, spreading and motility.

Calcium-binding motifs (ESQES and QESQSEQDS) derived from DMP-1 protein were incorporated into the LZ chimeric protein. The calcium-binding motifs provide the surface for binding of calcium ions and facilitate calcium phosphate deposition. Deposition of calcium phosphate enhances the mechanical property of the hydrogel and function as an osteoinductive scaffold.

Heparin-binding domain (LRKKLGKA) was used in the LZ chimeric construct for binding of growth factors. The MMP-2 cleavage sequence (IPVSLRSG) was coupled with heparin-binding domain to provide a growth-factor release mechanism. This design was intended to make the LZ hydrogel capable of controlled-release for the heparin-binding growth factor.

Therefore, the overall goal of this project is to demonstrate the feasibility of constructing mechanically stable LZ hydrogel, ligands with cell surface binding properties, mineral deposition motifs and growth factor binding and controlled release of these growth factors. By fine-tuning the properties of the LZ hydrogel scaffold, this scaffold can have potential applications in the repair and regeneration of various tissues.

C. Specific aims of the study

C.1. To synthesize and develop stable LZ hydrogels with and without RGD domain and test its functionality in supporting 3-D cell culture

A new LZ design was used to synthesize stable hydrogels. To increase stability a novel method was developed. This consisted of lyophilizing the hydrogel pellets and subjecting it to dehydrothermal treatment at 120°C for 12 hours. This additional thermal processing made the LZ hydrogel a stable scaffold for tissue engineering applications after rehydration. It also facilitated sterilization of the solution. The mechanical properties of the hydrogel and its microstructure can also be fine tuned for specific applications by altering the LZ hydrogel concentrations. Biological functionality was achieved by incorporating the integrin binding domain RGDS into the LZ protein backbone. Such modifications might provide cell-binding properties to the LZ protein-based hydrogel scaffold.

C.2. To synthesize and develop stable LZ hydrogels with mineralizing properties for hard tissue regeneration applications

A scaffold that can facilitate mineralization is a requirement for hard tissue regeneration like dentin and bone. We selected two calcium-binding peptides derived from Dentin Matrix Protein-1 (DMP-1) and incorporated them in the LZ protein construct. This design will provide the scaffold with calcium-binding property when placed in mineralization media and initiate the process of mineral nucleation and growth. Such a functionalized scaffold will also

provide a stiffer matrix for bone and dentin tissue engineering for *in vivo* applications.

C.3. To synthesize and develop stable LZ hydrogels for sustained growth factor release

In order to provide biological signals to the cells, LZ hydrogel was designed to be bioactive. The consensus heparin-binding domain LRKKLGKA was introduced in the chimeric LZ protein. This domain ideally binds to heparin and further binds to the heparin-binding growth factors. Furthermore, we designed a growth-factor releasing cue by enabling the incorporation of the consensus matrix metalloproteinase-2 (MMP-2) cleavage site IPVSLRSG before the heparin-binding domain. This design would trigger the release of growth factors by extracellular proteases such as the MMP family members. This construct should provide a potential strategy for sustained release of growth factor from the LZ hydrogel scaffold.

II. MATERIALS AND METHODS

1. Construction of the chimeric LZ-Control protein

The previously published leucine zipper peptide containing the six heptad repeat amino acid sequence was used (A1: SGELENE VAQLERE VRSLEDE AAELEQK VSRLKNE IEDLKAE) [194]. This A1 sequence was modified by the introduction of a cysteine amino acid residue to generate A2 by site-directed mutagenesis kit (A2: **CS**GELENE VAQLERE VRSLEDE AAELEQK VSRLKNE IEDLKAE) in order to facilitate covalent binding by cysteine-cysteine cross-links. The site-directed mutation was done with the QuikChange kit (QIAGEN) according to the manufacturer's protocol. Two A2 sequences were then separated by a spacer of two sets of 5 repeat of flexible peptides [C1: 5(AGAGAGPEG)]. An extra flexible tail containing another cysteine [C2: (AGAGAGPEG)₂**C**] was also incorporated to the C-terminal end of the polypeptide. The combination of the peptide domains A2-C1-C1-A2-C2 formed the LZ-Control polypeptide.

2. Cloning of the chimeric LZ proteins with functional motifs

This initial construct of LZ-Control was then modified to incorporate the functional motifs including the integrin-binding motif (RGDS) and two calcium-binding motifs derived from DMP1 (ESQES, QESQSEQDS) in between the two C1 blocks in LZ-Control (A2-C1-motif-C1-A2-C2, motif = RGDS, ESQES, or QESQSEQDS). This polypeptide was designated as LZ-RGDS, LZ-ESQES, and LZ-QESQSEQDS respectively. These functional motifs were designed

with the same restriction sites of HindIII on the N terminus and XbaI on the C terminus. Such a design would allow the easy substitution of the desired functional motif into the chimeric LZ construct. The final LZ-Control, LZ-RGDS, LZ-ESQES, and LZ-QESQSEQDS chimeric protein constructs were cloned and verified by sequencing at the DNA Services Facility at the University of Illinois at Chicago Research Resources Center. The final constructs were then cloned into pQE9 vector (QIAGEN) and expressed recombinantly in *E. coli* strain SG13009 (QIAGEN).

3. Cloning of the chimeric LZ protein with heparin-binding domain and the MMP2 cleavage site

This initial construct of LZ-Control was modified with an insertion of C3 peptide sequence (C3: AGAGAGPEG IPVSLRSG AGPEG LRKKLGKA) in between the A2 and C1 peptide sequence (A2-C1-C1-A2-C3-C2) where the specific sequences of IPVSLRSG and LRKKLGKA were the consensus peptide sequences for the MMP-2 cleavage site and the heparin-binding site respectively. This polypeptide was designated as LZ-MMPHEP. The final LZ-MMPHEP chimeric protein construct was verified by sequencing at the DNA Services Facility at University of Illinois at Chicago Research Resources Center. The final constructs were then cloned into pQE9 vector (QIAGEN) and expressed recombinantly in *E. coli* strain SG13009 (QIAGEN).

4. Expression and Purification of the LZ chimeric proteins

For expression of the chimeric proteins, a single bacterial colony was inoculated in 500mL LB broth containing 100 µg/mL ampicillin and 30 µg/mL kanamycin and grown in a 37°C shaker overnight. The culture was then transferred into larger 5L LB broth culture with 100 µg/mL ampicillin and 30 µg/mL kanamycin and incubated in a 37°C shaker until OD 600 was reached. Protein production was induced using 1.0 ml of 1.5 mM isopropyl β-D-1-thiogalactopyranoside (IPTG) added to the culture and grown for an additional period of 5 hours. The cells were then pelleted and stored at -80°C. The LZ chimeric protein purification was carried out using Ni-NTA Superflow resin (QIAGEN) following manufacturer's protocol.

The elution buffer with LZ chimeric protein was extensively dialyzed for 5 days, lyophilized and stored at -20°C until use. The purified protein was then run on SDS-PAGE gel and stained with Coomassie blue. The size of the LZ chimeric protein was approximately 37 kDa and the yield was about 80 mg/L.

5. Preparation of the LZ hydrogel

LZ hydrogels were prepared by mixing specific ratios of the LZ-Control protein with LZ-RGDS, LZ-ESQES, LZ-QESQSEQDS, or LZ-MMPHEP at concentrations from 7% ~12% (w/v) by dissolving in 100 mM phosphate buffer. The pH was adjusted to 7.4. The self-assembled LZ hydrogel formed within 3 hours when incubated at 37°C. The hydrogel was then lyophilized and placed in a vacuum oven at 121°C and 1 Torr for 12 hours for dehydrothermal

treatment to facilitate further physical crosslinking and sterilization. Hydrogels were stored in sterile containers at room temperature.

In this study, 7% w/v LZ hydrogels were used if not stated otherwise. The ratios of different LZ chimeric proteins that were combined to form hydrogels are listed below,

LZ-Control:LZ-RGDS = 100:0, 75:25, or 50:50

LZ-Control:LZ-ESQES:LZ-QESQSEQDS = 3:0:0, 2:1:0, 2:0:1, or 1:1:1

LZ-Control:LZ-MMPHE = 90:10

6. Circular Dichroism (CD) spectroscopy

The CD spectrum was recorded using Jasco J-720 spectrometer at 25°C. 14 μ M LZ-Control, LZ-RGDS, LZ-ESQES, LZ-QESQSEQDS, or LZ-MMPHEP solution was prepared using 100 mM phosphate buffer and the pH adjusted with either HCl or NaOH to 4, 7.4, or 11. The samples were heated to 50°C for 30 minutes and slowly cooled down to room temperature before CD measurements to allow any possible refolding. A quartz cuvette with path length of 0.1 cm was used and the measurement was taken at a resolution of 1 nm, bandwidth of 1 nm, and the wavelength range was from 200- 250 nm. Final spectra were obtained by subtraction of the corresponding buffer readings. Each sample was scanned three times..

7. Scanning electron microscopy (SEM)

The LZ-Control hydrogels from 7%, 10% and 12% w/v were quenched in liquid nitrogen and then placed in a pre-cooled turbo freeze-drying chamber. The series of drying steps from -160°C to room temperature was performed in increments of 20°C/hour at 1x10⁻³mmHg ultra low pressure. After drying, the samples were fractured and the exposed inner structure was mounted onto SEM grids. The samples were coated with 10nm osmium tetroxide and the imaging was performed using a Field Emission Hitachi S-4800-II SEM operating at 5keV.

8. Cryo-transmission electron microscopy (Cryo-TEM)

Cryo-TEM was performed using a Hitachi HD-2300A STEM. A 7% w/v LZ-Control hydrogel was prepared and applied directly on the TEM carbon-coated grid and excess water was blotted with a filter paper. The samples were quickly frozen by plunging into liquid ethane and were kept in liquid nitrogen before and during the cryo-TEM imaging.

9. *In vitro* degradation study

The *in vitro* degradation rate was determined by immersing the hydrogel in PBS (Gibco) containing 0.5% sodium azide (Fisher Scientific). The 7% w/v LZ-Control hydrogel was weighed, and placed in a tube containing excess amount of PBS and stirred at 37°C for a period of up to 30 days. The hydrogel was then removed and rinsed with distilled water for several times to remove

the salts. After lyophilization, the hydrogel was weighed again. The weight loss (W_L) and remaining weight (RW) was calculated according to the equation

below $WL = \frac{W_0 - W_1}{W_0}$, where W_0 and W_1 represent the hydrogel weight before and after soaking in PBS respectively and Remaining weight $RW = 1 - W_L$.

10. *In vitro* calcium phosphate mineralization on the LZ hydrogels

Nucleation of calcium phosphate polymorphs was carried out using two different techniques on the 7% w/v LZ hydrogels. The three polypeptides namely LZ-Control, LZ-ESQES, and LZ-QESQSEQDS were mixed in different ratios ranging from 2:1:0, 2:0:1, and 1:1:1 respectively (LZ-Control:LZ-ESQES:LZ-QESQSEQDS). In the first *in vitro* mineralization method, nucleation was carried out in the presence of physiological concentrations of calcium and phosphate ions as previously described [195]. Briefly, the combined LZ hydrogel scaffolds were placed into a channel connecting two halves of an electrolyte cell, one compartment containing calcium buffer (165 mM NaCl, 10 mM HEPES, and 2.5 mM CaCl_2 [pH 7.4]) and the other phosphate buffer (165 mM NaCl and 10 mM HEPES KH_2PO_4 [pH 7.4]). A small electric current of 1 mA was passed through the system to facilitate movement of ions across the samples. The buffers were changed regularly (twice daily) to maintain a constant pH. The samples were subjected to nucleation for a period of 2 weeks. The method of facilitating mineralization

under physiological concentration of calcium and phosphate is developed and published in the previous publication from our lab [196].

In the second technique, nucleation was carried out under high concentrations of calcium and phosphate. Briefly, the scaffolds were immersed in a 1 M calcium chloride solution for a period of 30 min. They were then washed extensively in water to remove any nonspecifically bound calcium and then immersed in a 1 M sodium phosphate solution for a period of 30 min. The samples were then washed in water and lyophilized for further characterization and use. The method of facilitating mineralization under high concentration of calcium and phosphate is developed and published in the previous publication from our lab [196].

11. Microscopic magnetic resonance elastography (μ MRE)

μ MRE experiments were performed on a vertical bore (54 mm diameter) Bruker DRX 11.74 T (500 MHz for protons) Avance MR Spectrometer (Oxford Instruments, Oxford, UK) equipped with the MRE electro-mechanical setup [197]. Briefly, 7%, 10% and 12% w/v LZ-Control hydrogel samples (6 mm diameter discs) were embedded in 0.75% (w/v) agarose gel (SeaKem LE Agarose, Lonza, Rockland, ME USA, Catalog No: 50000) in MRE test tubes (I.D = 8.8 mm). Agarose gel was made with PBS to maintain osmotic and pH balance. The MRE tube was attached to a piezo-ceramic actuator. Axisymmetric mechanical harmonic shear wave excitation (frequencies from 1 kHz to 4 kHz) was applied to the entire test tube through

the actuator driven by a power amplifier. The agarose gel was used to promote the transfer of shear wave motions within the samples. Shear motions were generated within the sample and were synchronized with the motion-encoding gradient of a gradient-echo based MRE pulse sequence to create shear wave images. The gradient echo based MRE pulse sequence was used with the following imaging parameters: pulse repetition time/echo time = 400/6 ms; flip angle = 30°; field of view = 10 mm; slice thickness = 0.5 mm; 1 slices; in-plane resolution = 78 μm \times 78 μm ; MSG strength = 120 G/cm. From the wave image data, the shear stiffness was estimated using the local frequency estimation (LEF) inversion algorithm with directional filtering [198].

12. Oscillatory rheology

The dynamic viscoelastic properties of the hydrogel were obtained on a Bohlin Gemini rheometer (Malvern Instruments, Worcestershire, UK) with 8 mm/0° parallel plate geometry. Samples were prepared as described previously. 7%, 10% and 12% w/v LZ-Control hydrogel, and high concentrations of calcium and phosphate pre-mineralization treated 2:1:0, 2:0:1, and 1:1:1 LZ-Control:LZ-ESQES:LZ-QESQSEQDS hydrogel were fixed on a glass slide and placed on the rheometer sample stage. The upper plate was lowered until it was in uniform contact with the LZ hydrogel top surface. The corresponding gap distances were 1.3-1.6 mm. Dynamic time sweep experiments (DTS) were performed to monitor the storage (G') and loss (G'') modulus changes of the hydrogels with time. Frequency sweeps between 0.01

and 1 Hz at 0.1% strain at 25°C were performed. To prevent evaporation, a chamber cover was used to protect the samples during the analysis. All measurements were made in triplicates on 3 different preparations of LZ hydrogel.

13. Selected Area Electron Diffraction (SAED)

1:1:1 LZ-Control:LZ-ESQES:LZ-QESQSEQDS LZ hydrogel after mineralization under high calcium and phosphate concentrations were lyophilized, crushed and loaded onto the TEM grids. The electron diffraction spectra were obtained using Joel 3010EX TEM.

14. Growth factor binding assay

Heparin-binding growth factors namely VEGF, TGF- β 1 and BMP-2 were used to test for binding to LZ-MMPHEP hydrogels via heparin (prepared by 7% w/v of mixing 90:10 LZ-Control:LZ-MMPHEP). The LZ-MMPHEP hydrogels were placed in 50 μ l of heparin solution (5 mg/ml in PBS) overnight in 4°C and washed by PBS for three times, 10 minutes each wash. Then the heparin bound LZ-MMPHEP hydrogels were then placed in 10 ng or 20 ng of VEGF (Sigma), TGF- β 1 (R&D system) or BMP-2 (AKRON BIOTECH) in 50 μ l PBS solution, overnight at 4°C and washed in PBS for three times, 30 minutes each wash. The growth factor solution after binding, and the PBS washes were combined and stored at -80°C for quantitative dot-blot analysis.

15. Dot-blot assay to measure the release of heparin-binding growth factors

After the process of binding heparin and growth factors, the LZ-MMPHEP hydrogels were immediately immersed in PBS (Gibco) containing MMP-2 (10 ng/ 50 μ l, R&D system) and 0.5% sodium azide (Fisher Scientific) to characterize the growth factor release profile. The LZ hydrogels were placed on a (rotor shaker) at 37°C for a period of up to 11 days. Four samples were used for each time point. At each time point, the buffer containing the hydrogel was collected and the hydrogel was collected and washed 3 times with 150 μ l of PBS for 10 minutes and the PBS washings were also collected. The washings from each hydrogel were combined and dot-blotted on a nitrocellulose membrane (BIO-RAD) using Bio-Dot dot-blotting system (BIO-RAD). The membrane was allowed to dry and blocked with 5% BSA in PBS for 45 min at room temperature. After blocking, antigen detection was performed by incubating with anti-VEGF (1:100 Santa Cruz Biotechnology) antibody overnight at 4°C. After several washes with PBS, the blot was then incubated with HRP-conjugated goat anti-rabbit IgG secondary antibody (Chemicon International). The blot was again washed several times in PBS and the signal was developed by the SuperSignal West Femto Chemiluminescent Substrate (Thermo Scientific). The X-ray films were scanned and converted to a digital image and analyzed by ImageJ software to estimate the VEGF concentration in the wash buffer.

16. *In vitro* cell culture

HMSCs isolated from the iliac crest of normal adult donors were obtained from the NIH-funded Tulane Cancer Research Centre. These cells were cultured in α MEM (minimum essential medium) (Gibco) supplemented with 20% fetal bovine serum (Gibco), 200 mM L-glutamine (Gibco), 1x Antibiotic-Antimycotic cocktail (Gibco) and incubated in a humidified, 5% CO₂ atmosphere at 37°C. When required, HMSCs stably expressing the GFP gene was used.

17. 2-D cell culture

For 2-D cell culture, a non-tissue culture 96 well plate was coated with different ratios of LZ-Control and LZ-RGDS proteins. Briefly, 5 μ M LZ protein solution with different ratios of LZ-Control and LZ-RGDS (100:0, 75:25, 50:50) or bovine serum albumin (BSA) in bicarbonate/carbonate buffer (100 mM) was used. 100 μ L of the mixture was placed in each well overnight at room temperature to allow protein adsorption on the plates. The next day plates were washed with PBS and HMSCs were seeded at concentrations of 1.5×10^4 cells/well suspended in 100 μ L media and cell growth media was used to cover the cells. Medium was changed every other day. HMSCs seeded on 96 well polystyrene tissue culture plates (TCPS) served as positive control.

18. 3-D cell culture

For 3-D cell culture, 7% w/v LZ hydrogel containing different ratios of LZ-Control and LZ-RGDS were used. The freeze-dried hydrogel was first rehydrated by incubating with the culture media at 37°C, and 5% CO₂ for 1 hr before use. The 1% w/v PuraMatrix hydrogel (BD Biosciences) was prepared according to the manufacture's protocol and served as positive control. 1.5x10⁴ HMSCs were seeded on to the preformed LZ hydrogel placed in 96 well plates and cultured for 3 weeks. The medium was changed every other day.

19. MTS cell proliferation assay

The MTS cell proliferation assay was carried out on both 2-D surface and within the 3-D hydrogel with HMSCs utilizing CellTiter 96® AQueous One Solution Cell Proliferation Assay (Promega) according to manufacturer's instructions. For 2-D cell proliferation assay, the cells were cultured for 1, 4, 7, 14, 21 days. At the end of the specified time points, 20 µL of proliferation assay reagent was mixed with 100µl of culture media and added to each well. The plate was then placed in a 37°C incubator for 60 minutes and the absorbance measured at 490 nm using a microplate reader (BioTek Synergy 2). For 3-D cell proliferation assay, the cells were cultured for 1, 4, 7, 14 and 21 days. The samples were washed twice with PBS and 100 µL of fresh media with 20 µL of proliferation assay reagent were added to each well. After 90 minutes of incubation in a humidified 37°C chamber, the gels were removed

and the absorbance was measured at 490 nm using a microplate reader (BioTek Synergy 2).

20. Time-lapse live cell imaging

The live HMSC images were captured using the Zeiss imaging system equipped with an incubator that maintains temperature and carbon dioxide levels. 1.5×10^4 of the GFP-HMSCs were seeded on the 7% w/v LZ-Control hydrogel. The LZ hydrogel was hydrated by the cell suspension media. The images were captured every 15 minutes per frame via GFP signal for 16 hours after initial seeding. The playback of the time-lapse video is 15 frames per second.

21. Live-dead cell assay

Live-dead cell assay was carried out on HMSCs cultured in 3-D LZ hydrogel matrix for up to 7 days. At 1 day, 4 days and 7 days post seeding, live and dead cells were analyzed in triplicates using the live-dead cell assay kit (Molecular Probes) as per the manufacturer's recommended protocol. The calcein AM and the ethidium homodimer concentration were 10 μ M each to indicate the live (green) and dead (red) cells respectively. The samples were imaged using a Zeiss Axio-Observer D1 fluorescent microscope equipped with the required filter sets. Five individual fields of view were imaged for each and the percentage of dead cells to live cells was calculated. The method is followed the previous publication from our lab [67].

22. Actin staining

HMSCs were cultured for 7, 14 & 21 days within the LZ hydrogels and then rinsed three times with PBS, fixed with 4% paraformaldehyde for 4 hr and permeabilized with 0.5% Triton X-100 in PBS. The LZ hydrogel was incubated with Phalloidin-TRITC (1:1000, Sigma) in PBS overnight at 4°C. The gels were then washed 3 times with PBS to remove nonspecific bound reagent. They were then viewed and z-stack images were captured using a Zeiss 710 LSM Meta confocal microscope.

23. *In vivo* subcutaneous implantation of the LZ hydrogel scaffold

7% w/v of LZ-Control and LZ-RGDS hydrogels were used *in vivo* subcutaneous implantation without cells. The hydrogels were implanted subcutaneously on the dorsal side of wild type C57BL6 mice (Charles River Laboratories) in the dehydrated form. After 1 and 2 weeks of implantation, the hydrogel scaffold samples were removed from the sacrificed animals. After fixing in 4% neutral buffered formalin and embedding in paraffin. The hydrogel scaffold samples then are sectioned into 5 µm thick sections for following histological evaluation.

7% w/v of LZ hydrogel as shown below were pre-seeded with HMSCs expressing GFP and used for *in vivo* subcutaneous implantation. The groups consisted of LZ-Control hydrogel, LZ-Control:LZ-RGDS hydrogel in the ratio 75:25, 50:50 and LZ-control: LZ-ESQES: LZ-QESQSEQDS in the ratio 1:1:1.

The last group was used as such or premineralized with buffer containing high concentrations of calcium and phosphate. The effect of growth factor release was studied using LZ-Control:LZ-MMPHEP hydrogel combined in 1:9 ratio and adsorbed with either TGF- β 1 or BMP-2. Cell suspensions were prepared at concentrations of 5×10^5 cells/ 20 μ L in culture media. The dry scaffolds were hydrated using the cell suspension buffer. The cell-impregnated hydrogel was then implanted subcutaneously on the dorsal side of athymic nude mice (Charles River Laboratories). After 2 weeks of implantation, the hydrogel scaffolds samples were removed from the sacrificed animals. After fixing in 4% neutral buffered formalin and embedding in paraffin. The hydrogel scaffold samples then are sectioned into 5 μ m thick sections for following histological evaluation.

All animal experiments in this study were performed as per the protocol approved by the UIC animal care committee (Assurance Number A-3460-01).

24. Histology and immunohistochemistry

All sections were deparaffinized in xylene, hydrated in graded ethanol solutions, and immunostained with peroxidase conjugated secondary antibodies or fluorescent probes according to published protocols [196, 199]. The following antibodies were used: rabbit anti-cluster of differentiation 68 (CD68) antibody (1/100, Abcam), rabbit anti- cluster of differentiation (CD31) antibody (1/100, Abcam), rabbit anti-fibronectin (FN) antibody (1/100, Sigma), rabbit anti-vascular endothelial growth factor (VEGF) antibody (1/100, Santa

Cruz Biotechnology), mouse anti-Dentin Matrix Protein 1 (DMP-1) antibody (1/2000, a gift from Dr. Chunlin Qin from Baylor College of Dentistry), rabbit anti-pigment epithelium-derived factor (PEDF) antibody (1/500, Millipore), mouse anti-von Willebrand factor (vWF) antibody (1/100, Santa Cruz Biotechnology), mouse anti-runt-related transcription factor 2 (RUNX2) antibody (1/100, abcam), mouse anti-osteocalcin (OC) antibody (1/1000, abcam), mouse anti-phosphoserine antibody (1/100, Sigma), rabbit anti-glucose-regulated protein 78 (GRP78) antibody (1/200, a gift from Dr. Sylvie Blond from University of Illinois at Chicago), rabbit anti-TGF- β receptor type II interacting protein (TRIP) antibody (1/100 Santa Cruz Biotechnology). Alizarin red staining to visualize calcium deposition was performed as per standard procedures. All fluorescently stained sections were imaged at the University of Illinois at Chicago Research Resource Center core imaging facility. Imaging was performed using a Zeiss LSM 710 confocal microscope equipped with Zen image analysis software and peroxidase stained sections were imaged using a Zeiss Axio-observer D1 microscope. All comparative fluorescence images were obtained using the same imaging conditions.

25. Alizarin red staining

All sections were deparaffinized in xylene, hydrated in graded ethanol solutions. 2% Alizarin Red solution (Sigma) was added to the sections and incubated for 30 min. The sections were then washed in acetone for 5 min and rinsed with distilled water and imaged.

26. RNA isolation and quantitative RT-PCR

The RNA was isolated using the TRIzol Reagent (In-vitrogen) from HMSCs seeded on 7% w/v LZ hydrogel for 1 and 2 weeks. The hydrogel scaffolds that were used to determine gene expression analysis were LZ-Control:LZ-ESQES:LZ-QESQSEQDS in the ratio 1:1:1 unmineralized or premineralized with buffer containing high concentrations of calcium and phosphate, and LZ-Control:LZ-MMPHEP in the ratio 1:9 bound with TGF- β 1 or BMP-2 according to the manufacturer's instructions. The total RNA was dissolved in RNase/DNase free water and stored at -80°C.

A total of 1 μ g of extracted total RNA from each sample was purified and cDNA was generated using RT² First Strand Kit (QIAGEN) following manufacturer's recommended protocol.

Quantitative reverse transcription RT-PCR was performed with FastStart Universal SYBR Green Master (Roche) using ABI StepOnePlus instrument. Expression of Alkaline phosphatase (ALP), OC, RUNX2, Phosphate regulating endopeptidase homolog X-linked (PHEX), Growth/differentiation factor (GDF), Osteopontin (OPN), Collagen-1 (Col-1), BMP-2, VEGF, TGF- β 1, DMP-1, Fibroblast growth factor-1 (FGF-1), and Glyceraldehyde 3-phosphate dehydrogenase (GAPDH) were transcripts that were analyzed by qPCR during its linear phase of amplification. The relative gene expression level was estimated by using the $2^{-\Delta\Delta C_T}$ method, where C_T value = log linear plot of PCR signal *versus* the cycle number. $\Delta C_T = C_T$ value

of target gene – C_T value of GAPDH. RT-PCR primer sequences are provided in Table I.

27. Statistical analysis

All experiments were performed in triplicate unless stated otherwise. Statistical comparisons were made using two-tailed Student's t-test. Experimental values are reported as the mean \pm standard deviation. Data were analyzed using Student's t-test and p-values less than 0.05 were considered statistically significant.

TABLE I
LIST OF REAL TIME PCR PRIMERS

Genes	Accession Number	Primer Sequences	
ALP	NM_000478.4	Forward	5'- ACTGGTACTCAGACAACGAGA -3'
		Reward	5'- ACGTCAATGTCCCTGATGTTATG -3'
OC	NM_000234.2	Forward	5'- CACTCCTCGCCCTATTGGC -3'
		Reward	5'- CCCTCCTGCTTGGACACAAAG -3'
RUNX2	NM_001024630.3	Forward	5'- TGGTTACTGTCATGGCGGGTA -3'
		Reward	5'- TCTCAGATCGTTGAACCTTGCTA -3'
Phex	NM_000444.5	Forward	5'- GAGGCACTCGAATTGCCCT -3'
		Reward	5'- ACTCCTGTTTAGCTTGGAGACTT -3'
GDF	NM_004962.3	Forward	5'- AGATCGTTCGTCCATCCAACC -3'
		Reward	5'- GGGAGTTCATCTTATCGGGAACA -3'
OPN	NM_001040058.1	Forward	5'- AAACCCTGACCCATCTCAGAAGCA -3'
		Reward	5'- TGGCTGTGAAATTCATGGCTGTGG -3'
Col-I	NM_000088.3	Forward	5'- GAGGGCCAAGACGAAGACATC -3'
		Reward	5'- CAGATCACGTCATCGCACAAAC -3'
BMP2	NM_001200.2	Forward	5'- ACTACCAGAAACGAGTGGGAA -3'
		Reward	5'- GCATCTGTTCTCGGAAAACCT -3'
VEGF	NM_001025366.2	Forward	5'- AGGGCAGAATCATCACGAAGT -3'
		Reward	5'- AGGGTCTCGATTGGATGGCA -3'
TGF-b1	NM_000660.5	Forward	5'- CAATTCCTGGCGATACCTCAG -3'
		Reward	5'- GCACAACTCCGGTGACATCAA -3'
DMP1	NM_004407.3	Forward	5'- CTCCGAGTTGGACGATGAGG -3'
		Reward	5'- TCATGCCTGCACTGTTCAATC -3'
FGF1	NM_000800.4	Forward	5'- ACACCGACGGGCTTTTATACG -3'
		Reward	5'- CCCATTCTTCTTGAGGCCAAC -3'
GAPDH	NM_002046.5	Forward	5'- ACAACTTTGGTATCGTGGAAGG -3'
		Reward	5'- GCCATCACGCCACAGTTTC -3'

III. RESULTS AND DISCUSSIONS

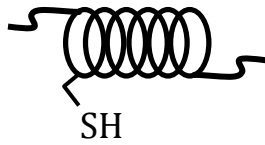
A. 3-D self-assembled leucine zipper hydrogel with tunable properties for tissue engineering

A.1. Synthesis of chimeric leucine zipper proteins

A series of chimeric LZ proteins were expressed from corresponding artificial genes in *E. coli*, purified via His-tag column, and analyzed by SDS-PAGE gel electrophoresis including LZ-Control, LZ-RGDS, LZ-ESQES, LZ-QESQSEQES, and LZ-MMPHEP. The corresponding chimeric LZ protein constructs and the peptide sequences are shown in Figure 1. In order to provide the covalent binding in the leucine zipper dimer and tetramer structure and prevent the dynamic re-assembly, the disulfide bonds were provided by the replacement of cysteine residuals in for the first amino acid in the first heptad of both the LZ domains in the construct. An extra cysteine residue was also introduced in the flexible random-coil tail of the LZ construct for the formation of a stable crosslinking network structure. This is inspired from the previous report [143] and the chimeric LZ construct was expected to form the self-assembled hydrogel as depicted in Figure 2. The molecular size of the LZ chimeric protein was ~37 kDa and the yield was about 80 mg per liter.

The cloning of the chimeric LZ proteins was designed to have the unique restriction enzyme digestion sites on the pQE9 vector at both ends of the biological signal motif site. This will allow easy manipulation in future LZ hydrogel studies and applications.

A Leucine Zipper Domain (S1C)



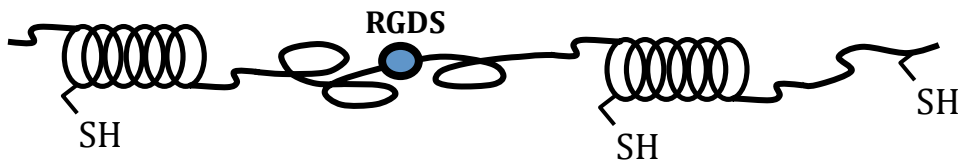
CGELENE VAQLERE VRSLEDE AAELEQK VSRLKNE IEDLKAE

B LZ-Control



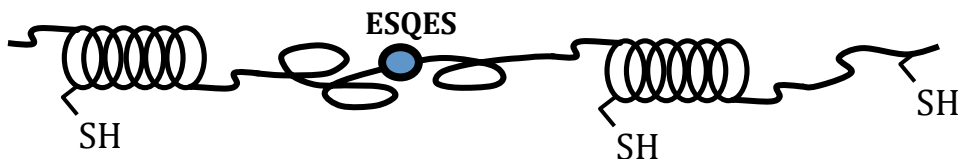
LQETHHHHHHSGSGS CGELENE VAQLERE VRSLEDE AAELEQK VSRLKNE IEDLKAE PGSEFTSPMG (AGAGAGPEG)₁₀ AMPLQLEGS CGELENE VAQLERE VRSLEDE AAELEQK VSRLKNE IEDLKAE PGSA(AGAGAGPEG)₂CAAAA

C LZ-RGDS



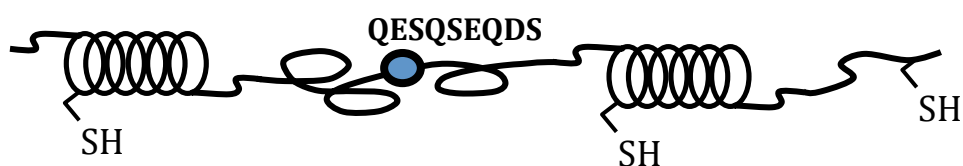
LQETHHHHHHSGSGS CGELENE VAQLERE VRSLEDE AAELEQK VSRLKNE IEDLKAE PGSEFTSPMG (AGAGAGPEG)₅ AMPLQKLRGDSRTSPMG (AGAGAGPEG)₅ AMPLQLEGS CGELENE VAQLERE VRSLEDE AAELEQK VSRLKNE IEDLKAE PGSA(AGAGAGPEG)₂CAAAA

D LZ-ESQES



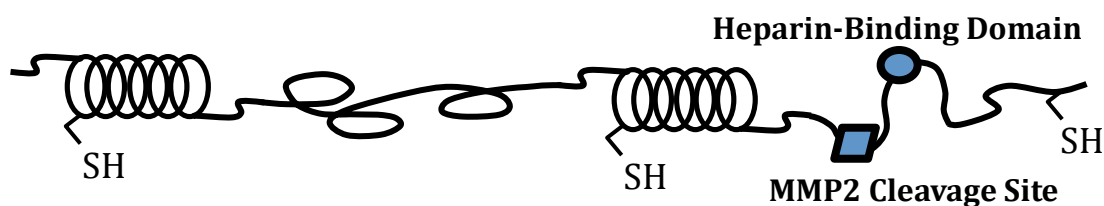
LQETHHHHHHSGSGS CGELENE VAQLERE VRSLEDE AAELEQK VSRLKNE IEDLKAE PGSEFTSPMG (AGAGAGPEG)₅ AMPLESQESPMG (AGAGAGPEG)₅ AMPLQLEGS CGELENE VAQLERE VRSLEDE AAELEQK VSRLKNE IEDLKAE PGSA(AGAGAGPEG)₂CAAAA

E LZ-QESQSEQDS



LQETHHHHHHSGSGS **CGELENE VAQLERE VRSLEDE AAELEQK VSRLKNE IEDLKAE** PGSEFTSPMG (AGAGAGPEG)₅ AMPLQESQSEQDSPMG (AGAGAGPEG)₅ AMPLQLEGS **CGELENE VAQLERE VRSLEDE AAELEQK VSRLKNE IEDLKAE** PGSA(AGAGAGPEG)₂CAAAA

F LZ-MMPHEP



LQETHHHHHHSGSGS **CGELENE VAQLERE VRSLEDE AAELEQK VSRLKNE IEDLKAE** PGSEFTSPMG (AGAGAGPEG)₁₀ AMPLQLEGS **CGELENE VAQLERE VRSLEDE AAELEQK VSRLKNE IEDLKAE** PGSAGAGAGPEG IPVSLRSG AGPEG **LRKKLGKA** (AGAGAGPEG)₂CAAAA

Figure 1. Schematic representation showing the peptide sequences used in the synthesis of the second generation chimeric leucine zipper protein.

(A) LZ motif. (B) LZ-Control. (C) LZ-RGDS. (D) LZ-ESQES. (E) LZ-QESQSEQDS. (F) LZ-MMPHEP. Note the heparin-binding domain and MMP2 cleavage site referred to in (F) represents the sequence LRKKLGKA and IPVSLRSG respectively.

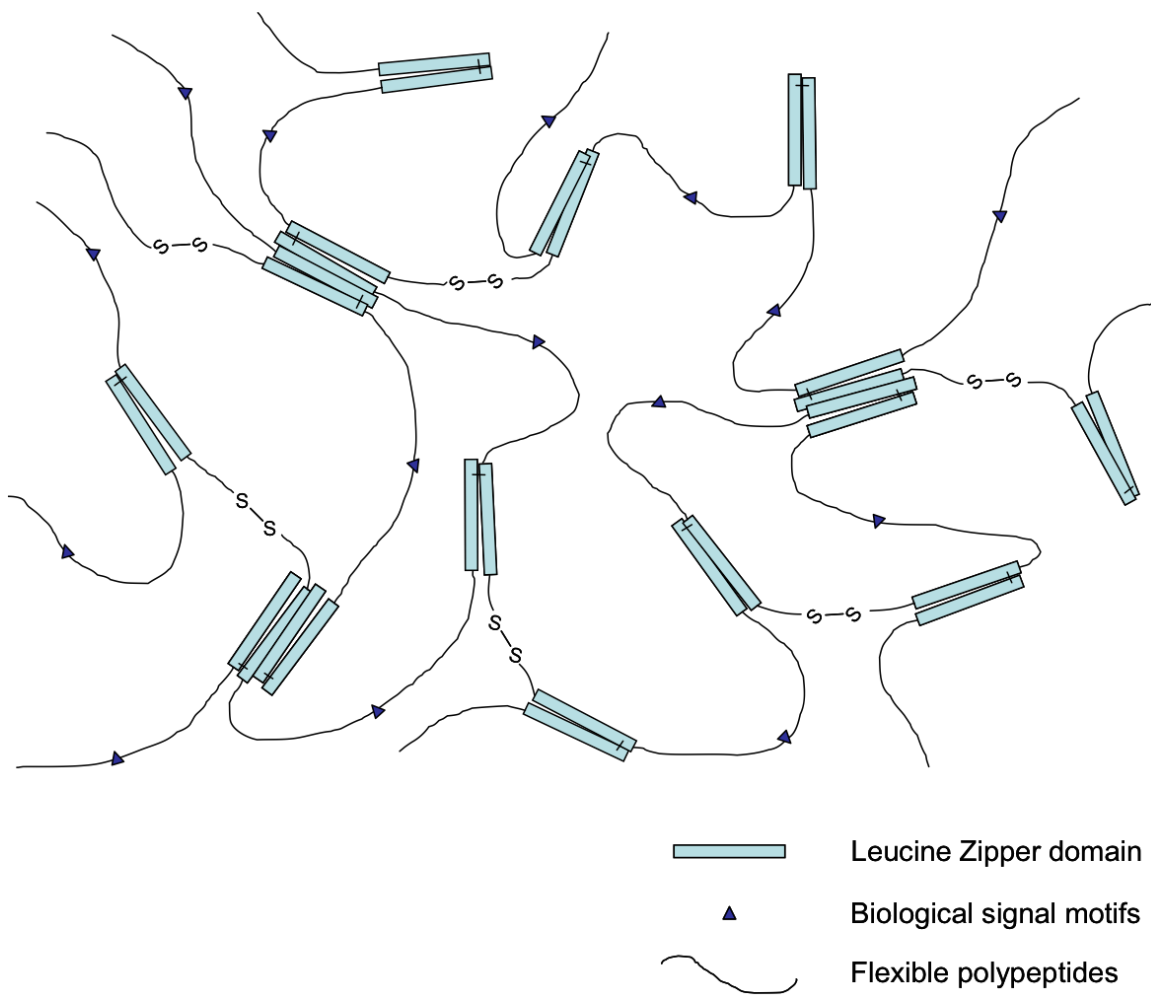


Figure 2. Schematic representation of the assembled hydrogel from chimeric leucine zipper protein construct.

A.2. Secondary structure of chimeric leucine zipper proteins

Circular dichroism spectroscopy was utilized to evaluate the folding of the chimeric LZ proteins. As expected, the molar ellipticity of the LZ-Control protein displayed minima at 208 and 222 nm implying that the alpha-helical structure is the predominant secondary structure at different pH (pH 4, pH 7.4 and pH 11) even in the presence of the disulfide bonds (Figure 3A). However, the signal intensity for the alpha helix was prominent at pH 4 and pH7.4, suggesting that stronger electrostatic interactions are capable of facilitating self-assembly of the alpha-helical peptides. Similar CD spectra displaying minima at 208 and 222 nm were also obtained for LZ-RGDS, LZ-ESQES, LZ-QESQSEQES, and LZ-MMPHEP at pH 7.4 (Figure 3B), indicating that the chimeric LZ proteins retained the alpha-helical structure even after incorporation of the biological signal motifs in the constructs. The alpha-helical structure is crucial to the LZ hydrogel self-assembly. This demonstrated that manipulating the sequence by addition of small signal motif sequence to the chimeric LZ construct is possible to tune its specific biological properties.

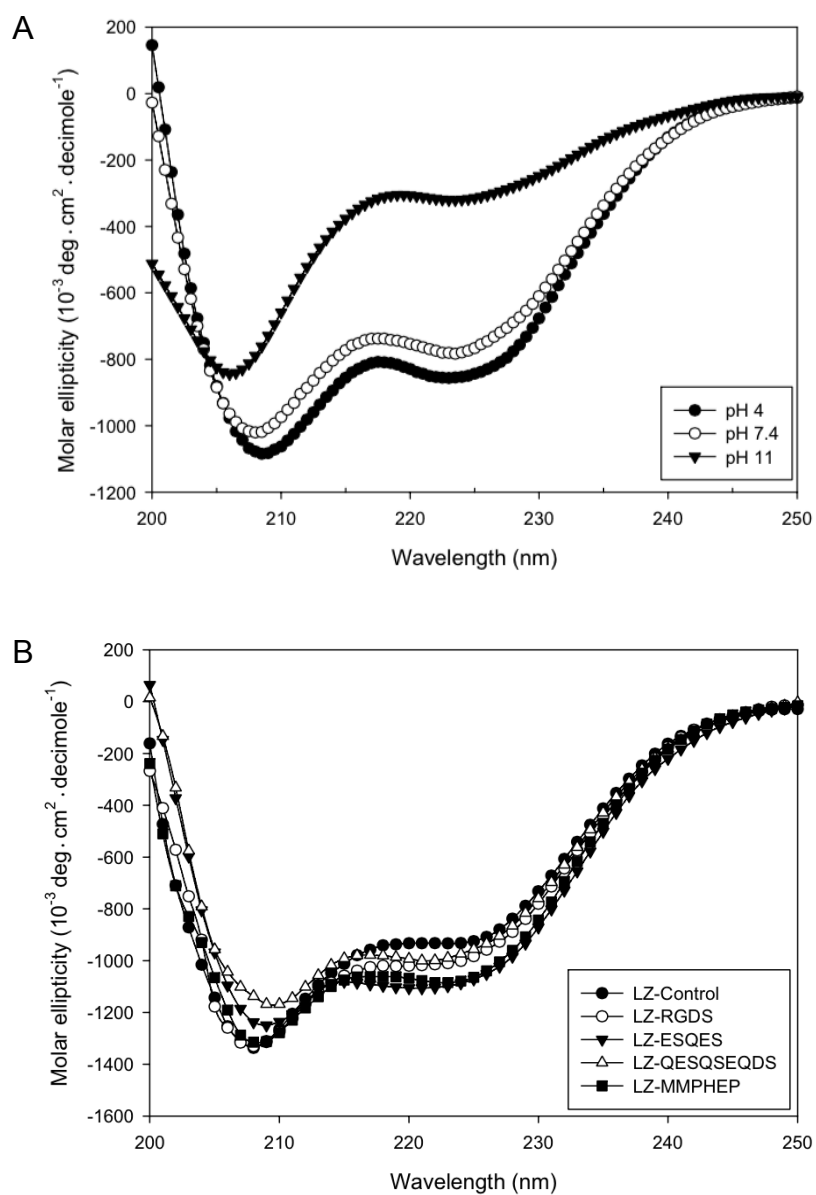


Figure 3. Secondary structure analyses of chimeric leucine zipper proteins by Circular Dichroism (CD).

(A) CD spectra of LZ-Control at pH=4 (●, 14 μM), pH=7.4 (○, 14 μM), pH=11 (▼, 14 μM) pH missing. (B) CD spectra of LZ-Control (●, 14 μM), LZ-RGDS (○, 14 μM), LZ-ESQES (▼, 14 μM), LZ-QESQSEQDS (△, 14 μM), and LZ-MMPHEP (■, 14 μM) at pH7.4. Spectra were recorded at 25°C in 100mM phosphate buffer.

A.3. Analysis of the surface characteristics and morphology of the leucine zipper hydrogels

The LZ hydrogels are stable and can be stored at room temperature under dehumidified environment for several months in its dried form after subjecting it to the dehydrothermal crosslinking method.

A cysteine was introduced at the beginning of the LZ motifs at the “a” position and also at the flexible tail domain at the end of the LZ protein construct. The cysteine residue was engineered as it contains a sulfur group that can facilitate in disulfide bonding. The disulfide bond is a covalent bond and was shown previous publications that this bonding improves the stability of the LZ hydrogel network. The presence of the disulfide bonds provide the physical association of the LZ motifs and can prevent the self-loop formation and also minimize the strand exchange resulting in formation of disengaged clusters [143]. The integrity of the LZ hydrogel was further strengthened by the dehydrothermal crosslinking treatment. Dehydrothermal crosslinking is a common method used for physical crosslinking of collagen fibers and during the blending of collagen with other polymers [200, 201]. It has been shown that the use of the dehydrothermal crosslinking treatment can improve the mechanical properties, and facilitate the cell attachment, proliferation, and migration [201]. Recently, dehydrothermal crosslinking treatment was also used for other natural material scaffolds for tissue engineering and drug delivery applications [202, 203]. By combining these two methodologies, we were able to fabricate a stable 3D LZ hydrogel.

Rehydration in PBS resulted in swelling of the LZ hydrogel to its original dimensions, and is flexible, soft and semi-transparent (Figure 4A). SEM images in Figure 4 depict the 3-D porous nature of the LZ hydrogel. The pore size measured from the SEM images ranged from about 100 μm in 7% w/v (Figure 4B), about 80 μm in 10% w/v (Figure 4C), and about 20 μm in 12% w/v (Figure 4D) respectively. This was calculated from the size of the scale bar in each image. Multiple images were used for calculating the pore size. Interconnectivity of the pores was also observed in all LZ hydrogels at different concentrations. These results indicate that it is possible to control the pore size by adjusting the composition of the hydrogel.

Cryo-TEM enables visualization of the LZ hydrogel network under cryogenic conditions, thereby preserving the *in situ* nanostructure. Dark areas in Figure 4E and 4F represent self-assembled hydrogel matrix while the gray areas represent vitrified water. Cryo-TEM images of 7% LZ hydrogel showed the presence of dense interconnected fibrillar microstructures resulting from the self-assembly process.

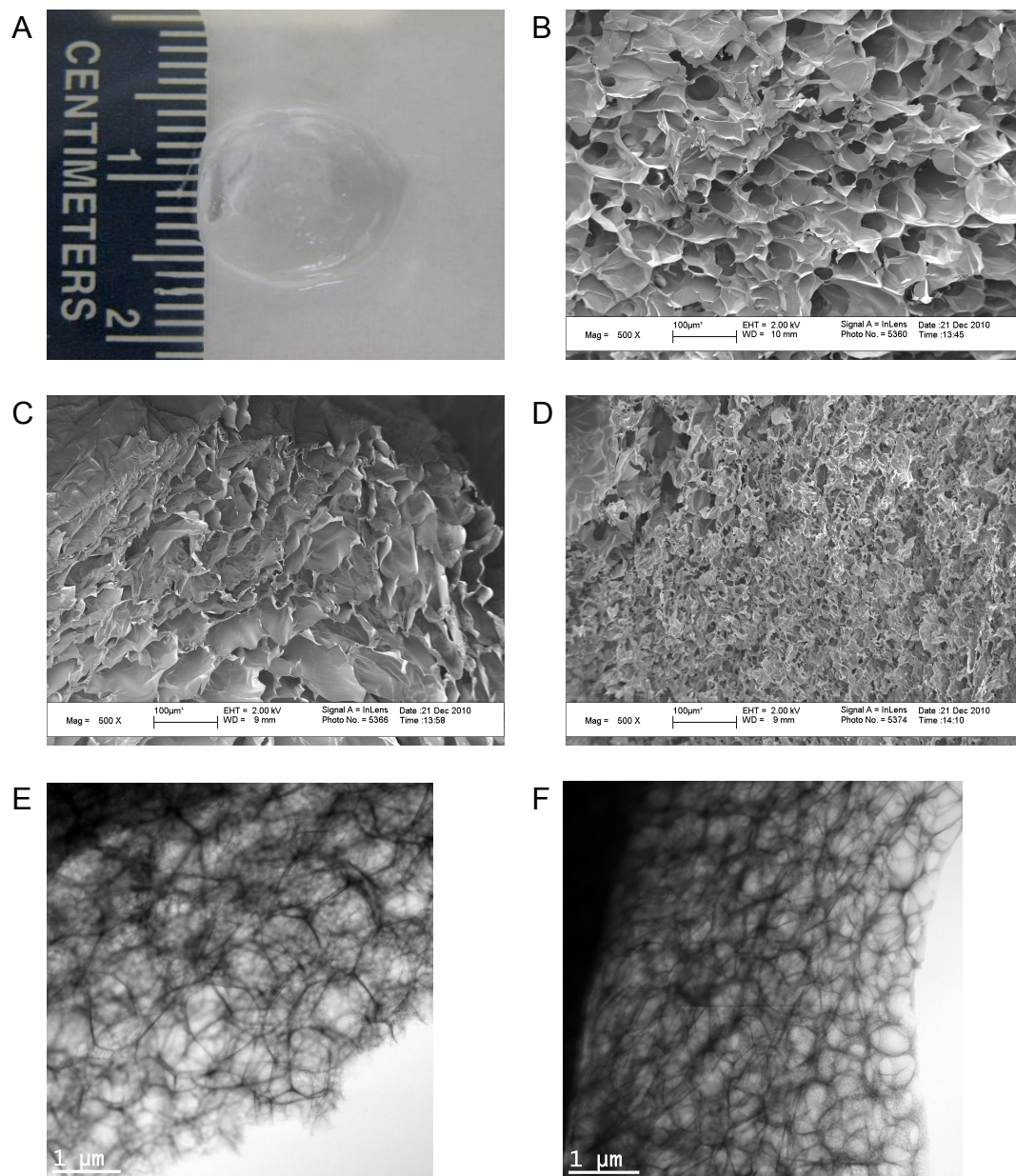


Figure 4. Microscopy-based characterization of the LZ hydrogel architecture.

Image of the hydrated 7% w/v LZ-Control hydrogel (A). Examination using SEM show the microstructure of the fractured surface of lyophilized 7% w/v LZ-Control (B), 10% w/v LZ-Control hydrogel (C), and 12% w/v LZ-Control hydrogel (D) in 100mM phosphate buffer. Scale bar for (B), (C) & (D) represents 100 μm . Examination of the microstructures using Cryo-TEM show the microstructure of self-assembled 7% w/v LZ-Control hydrogel (E) (F). Image shows interconnected dense network of the self-assembled hydrogel matrix (dark areas) surrounded by vitreous water (light areas). Scale bar represents 1 μm in (E) and (F).

A.4. Leucine zipper hydrogel mechanical properties

Hydrogels for tissue engineering applications must possess sufficient strength as cells sense and respond to their microenvironment [204, 205]. Therefore, we examined the material properties of the scaffolds using oscillatory sheer rheology.

Rheological studies conducted on 7, 10 and 12% w/v LZ hydrogels at frequency range from 0.01 to 1 Hz (Figure 5A) showed that the storage modulus (or elastic modulus, G') and the loss modulus (or viscous modulus, G'') increased with increasing concentrations of the hydrogel. The G' was greater than G'' by approximately an order of magnitude for all the samples studied and in fact the G' values were an order of magnitude higher than the previously reported values [143, 206]. For example, the average storage moduli (G') and loss moduli (G'') at 0.1 Hz were 2480 Pa and 203.2 Pa for 7% w/v, 4300 Pa and 302 Pa for 10% w/v, and 4390 Pa and 391.2 Pa for 12% w/v respectively. Additionally, there was no crossover point of G' and G'' at the frequencies used in this study. This behavior corroborates well with published reports of such hydrogels and demonstrates that the LZ hydrogel can assemble into a fairly rigid viscoelastic material with covalent crosslinking introduced by cysteine residues [207].

The loss tangent values represent the ratio between viscous and elastic properties and is the most sensitive indicator of various molecular motions within the material, $\tan \delta = G''/G'$. The loss tangent values were 0.082, 0.07, and 0.089 for 7%, 10% and 12% w/v LZ-Control hydrogel respectively. Similar

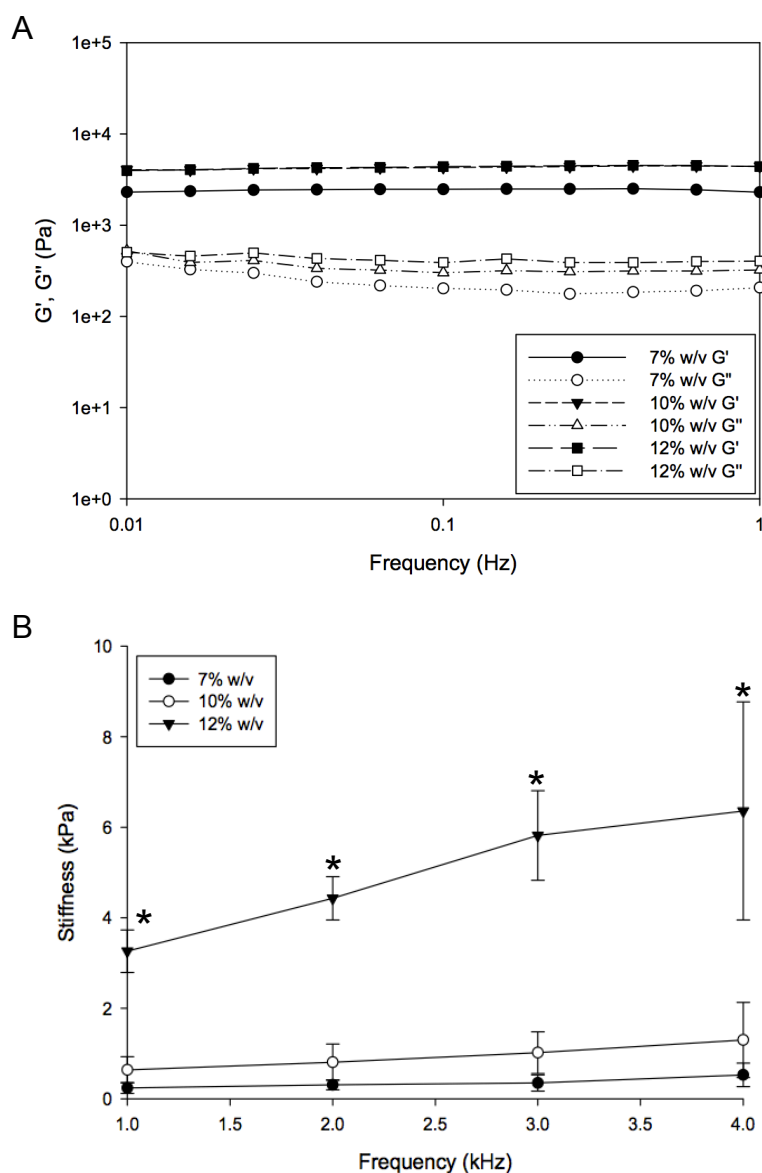


Figure 5. Viscoelasticity measurements of LZ-Control hydrogel.

(A) Graphical representation of the storage modulus G' (solid data points) and the relaxation modulus G'' (unfilled data points) with change in frequency. Together, the data represents the viscoelastic properties of the hydrogel. Note the increase in the G' and the G'' values with increase in the LZ concentration. (B) Shows changes in stiffness with frequency from magnetic resonance elastography. Shear stiffness was determined at all frequencies of vibration (1k, 2k, 3k and 4k Hz) with different concentrations of the LZ hydrogel (7%, 10%, 12% w/v). * represents statistical significance as determined by students t-test of the 12% hydrogel values with respect to both 10% and 7% hydrogels ($p < 0.05$ using students t-test)

$\tan \delta$ values with different concentrations of the hydrogel indicate a similar connectivity pattern. Further, a lower $\tan \delta$ value suggests a higher crosslink density [206]. However, the effects from microstructure stiffness and morphology may also change at the specific range of the oscillating frequency [208]. Thus, the results from the rheology experiments showed consistency between various concentrations of the LZ hydrogel including the oscillating frequency insensitivity and loss tangent values.

μ MRE was used to estimate the shear stiffness of the hydrogel at different concentrations (7%, 10% and 12% w/v) using different frequencies (1k, 2k, 3k and 4k Hz) as shown in Figure 5B. In the frequency range, the 12% w/v hydrogel showed significantly higher shear stiffness compared to 7% and 10% w/v LZ hydrogel. The higher shear stiffness implies greater fibrillar density [209, 210] due to increasing number of crosslinks present with higher hydrogel concentrations. Thus, the data from both the rheological and μ MRE studies show that the mechanical strength is tunable by adjusting the LZ hydrogel concentration.

A.5. *In vitro* degradation rate of the leucine zipper hydrogels

Directly related to the material stiffness property is the maintenance of the integrity of the hydrogel. Degradation rate of the hydrogel was determined *in vitro*. Result presented in Figure 6 shows that 7% w/v LZ hydrogel still retained 60% of its original weight at 30 days. We hypothesize that the integrity of the hydrogel is due to the presence of the 3 cysteines engineered into the construct. The integrity of the LZ hydrogel was further enhanced by the dehydrothermal treatment that provided additional crosslinks [211, 212]. In its absence the hydrogel was unstable, indicating the dehydrothermal treatment provided a sufficient structural reinforcement to the LZ hydrogel stability in 3-D. The most probable cause for degradation after four weeks could be due to the hydrolysis [213] of the peptide bonds. Thus, the introduction of cysteines and the thermal treatment provided integrity and mechanical strength to the hydrogel. Hence the hydrogel were stable in cell culture media and in vivo implantation experiments and were used in all experiments.

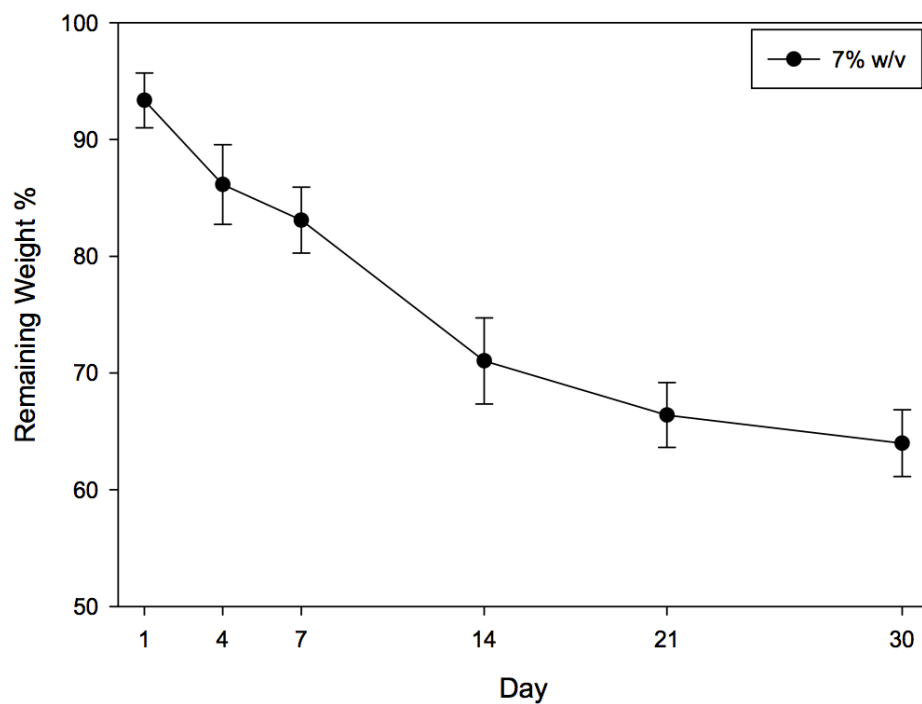


Figure 6. Stability of the LZ-Control hydrogel.

The graph represents drop in the weight (indicated as percentage of total weight) of the 7% w/v LZ- Control hydrogels immersed in PBS over time (in days). Results show that about 60% of the hydrogel weight still remained intact after 30 days indicating an approximate half-life of over a month.

A.6. Mesenchymal stem attachments on the leucine zipper hydrogels with RGDS motifs

Biomaterials can be designed to interact with cells by utilizing functional motifs found in native condition [2, 214]. Therefore, the LZ protein with and without the RGDS motif was tested for its ability to present a microenvironment that would support cell attachment. The MTS assay was used for this purpose. The reason for the choice of this assay was to quantitate the presence of metabolically active cells. The color change observed during this assay is possible only if metabolically active cells are present. Therefore, the results from this experiment can be used to gauge the ability of the LZ protein mixtures to favor cellular attachment and maintain cell functionality.

Results from the MTS assay (Figure 7A) showed that HMSCs on LZ substrate containing varying amounts of RGDS ligand showed faster cellular attachment when compared to LZ-Control. Specifically, at the four hour time point, the results indicate significantly higher number of metabolically active cells were attached to the plates coated with 25 and 50 percent LZ-Control:LZ-RGDS. However, at all the time points, the number of cells that attached to the plates were less when compared with tissue culture plates. Thus the presence of RGDS elicited the desired cellular responses.

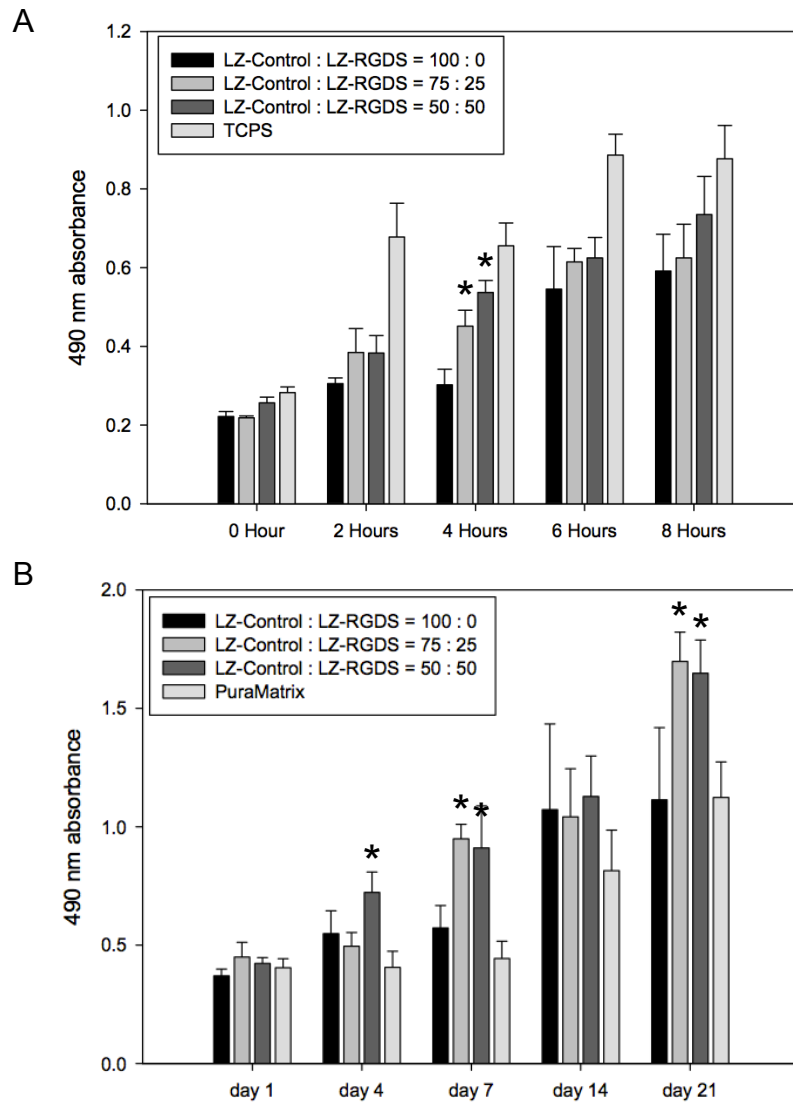


Figure 7. Attachment and Proliferation of HMSCs cultured on 2-D coated surfaces and 3-D LZ hydrogels with RGDS.

(A) Represents attachment of HMSCs on protein coated surfaces shown as change in absorbance at 490 following treatment with MTS assay reagent in 2-D cell culture system. Cells grown in tissue culture plastic served as positive control. LZ-RGDS motifs containing various combinations with the LZ control showed increase in number of attached cells. * Represents statistical significance ($p < 0.05$ using students t-test) with respect to LZ-Control. (B) Represents proliferation of HMSCs in 3-D hydrogels containing the indicated combinations of LZ-Control and LZ-RGDS motifs. * Represents statistical significance ($p < 0.05$ using students t-test) with respect to PuraMatrix. Note that the LZ hydrogels behaved significantly better than PuraMatrix.

A.7. Mesenchymal stem cell proliferation test on leucine zipper hydrogels with RGDS motifs

The LZ hydrogels were also tested for their ability to promote proliferation of HMSCs in 3-D culture conditions. 7% w/v hydrogel prepared with varying amounts of LZ-RGDS (100:0 or 75:25 or 50:50 LZ-control: LZ-RGDS) were examined for proliferation at 4, 7, 10, 14 and 21 days post cell seeding (Figure 7B). Interestingly, all conditions favored cell adhesion. At days 4 and 7 higher absorbance values were observed for a mixture containing higher amount of RGDS (LZ-Control: LZ-RGDS, 50:50). Even though the LZ-Control favored cell proliferation, it did so after 14 days. This suggests that the presence and density of the RGDS ligand might be the driving force for initial cell adhesion and proliferation on the hydrogel. Commercially, available PuraMatrixTM, was used as a positive control. PuraMatrixTM is a fully synthetic and absorbable hydrogel composed of repeating amino acids sequence of RADA. Such repeated RADA sequence self-assembles into nano-fiber structure when presenting in the salt under physiological condition. However, the LZ hydrogels proved to be significantly better in promoting cell viability and proliferation when compared to PuraMatrixTM indicating its superior properties in terms of cellular compatibility (Figure 7B).

A.8. Cell viability within the leucine zipper hydrogels with RGDS motifs

Figure 8 shows the live-dead cell assay for up to 7 days after seeding HMSCs on the LZ hydrogel. Green staining in the images represents live cells and red staining represent dead cells. From the images it is clear that while the LZ-Control hydrogel promoted cell viability, the morphology of the cells were rounded at day 1 (Figure 8A1). In contrast, cells on the higher RGDS containing scaffold (50:50 LZ-Control: LZ-RGDS, Figure 8A3) demonstrated good cell adhesion and had distinct spindle shaped morphology with long processes. Templates with lower amount of RGDS (LZ-Control: LZ-RGDS, 75:25) showed the least cell attachment (Figure 8A2) suggesting that the density of the RGDS motif is important for initial attachment. After 4 days, cells within all the LZ hydrogel types proliferated well and exhibited distinct 3-D cellular network (Figure 8B1, 8B2 and 8B3), however templates with none or lower amount of RGDS showed higher number of dead cells at the same time point (compare 8B1 and 8B2 with 8B3). From these results, we can conclude that although the presence of the RGDS motif is beneficial for initial cell attachment, over a longer time period, the cell viability is not greatly affected. On the other hand, because of reduced initial attachment, the total number of cells present in the hydrogel at a specific time point may be lesser in the LZ-Control hydrogels and the LZ hydrogels with reduced RGD motif (LZ-Control: LZ-RGDS 75:25).

Based on this data we opted to use LZ hydrogels with higher amount of RGDS for *in vivo* experiments.

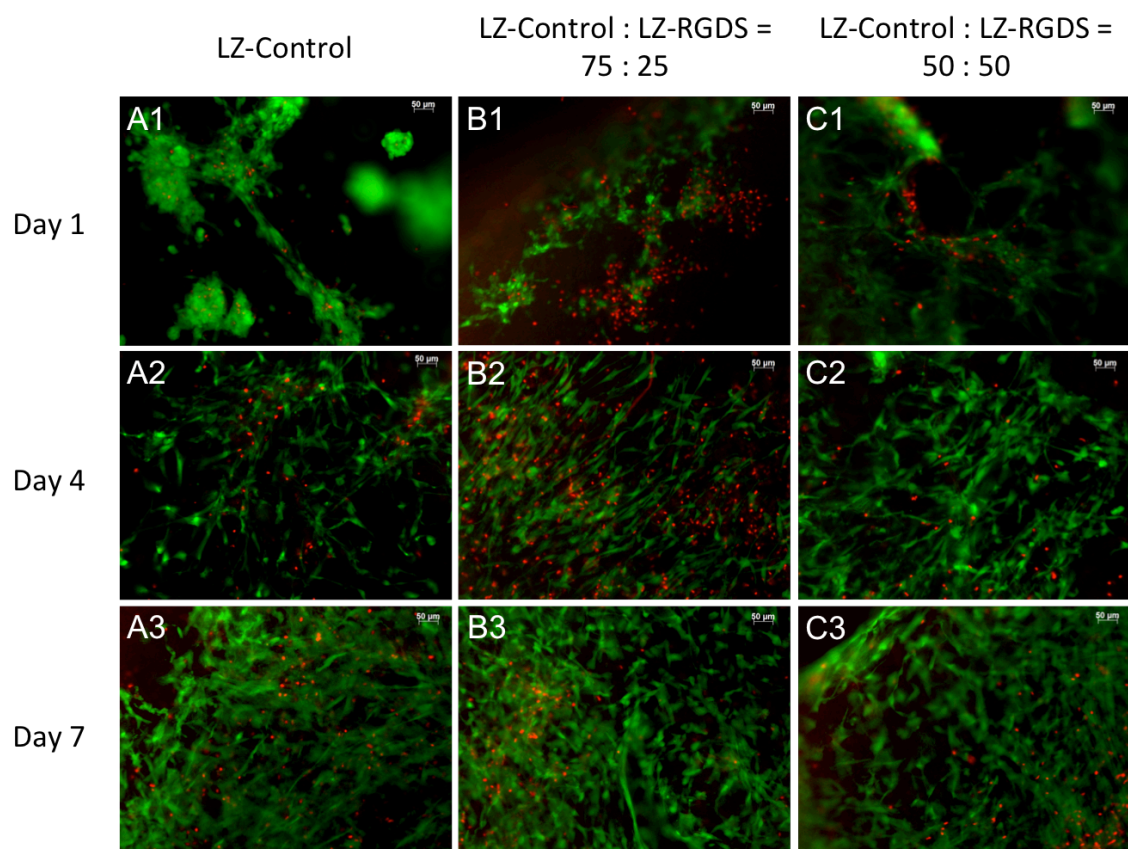


Figure 8. Live-dead cell assay of LZ hydrogel with RGDS.

The live-dead cell assay was performed on HMSCs seeded on 7% w/v LZ-Control (Group A), LZ-Control: LZ-RGDS = 75:25 (Group B), or LZ-Control: LZ- RGDS = 50:50 (Group C) for 1, 4 and 7 days. “Green” stain represents live cells and “red” stain represents dead cells. Scale bar represents 50μm for all images.

A.9. Cell migration in 3-D leucine zipper hydrogel culture system

Next we investigated the migration of GFP-HMSCs during the proliferative phase in 3-D LZ-Control hydrogel for 7, 14 and 21 days. As the cell viability and proliferation of HMSCs were similar after 7 days in culture irrespective of the presence or absence of RGDS, we opted to use only the LZ-Control hydrogel for this experiment. At the end of each time point the HMSCs were stained with actin and observed with confocal microscopy.

Results in Figure 9 show cell viability and the color-coding scheme depicts the depth of cell migration (green represents the top and blue represents the bottom of the hydrogel). Examination of the cell morphology showed long elongated polarized cells with well-developed actin-fiber bundles. Results in Figure 9A showed that by 1 week, cells from the surface had migrated within the gel. At 14 days (Figure 9B) the cells had migrated to a depth of 20 μm as indicated by the green color. At 21 days (Figure 9C) the cells still remained viable and migrated to about 100 μm within the LZ hydrogel as indicated by the blue color. Limitations with the confocal microscopy technique prevented measuring distances greater than 100 μm .

Time-lapse observation also revealed that the cells migrated by extending processes towards other cells in the matrix. Thus, HMSCs traveled long distances within the LZ-RGDS hydrogel due to a combination of favorable properties of the microenvironment.

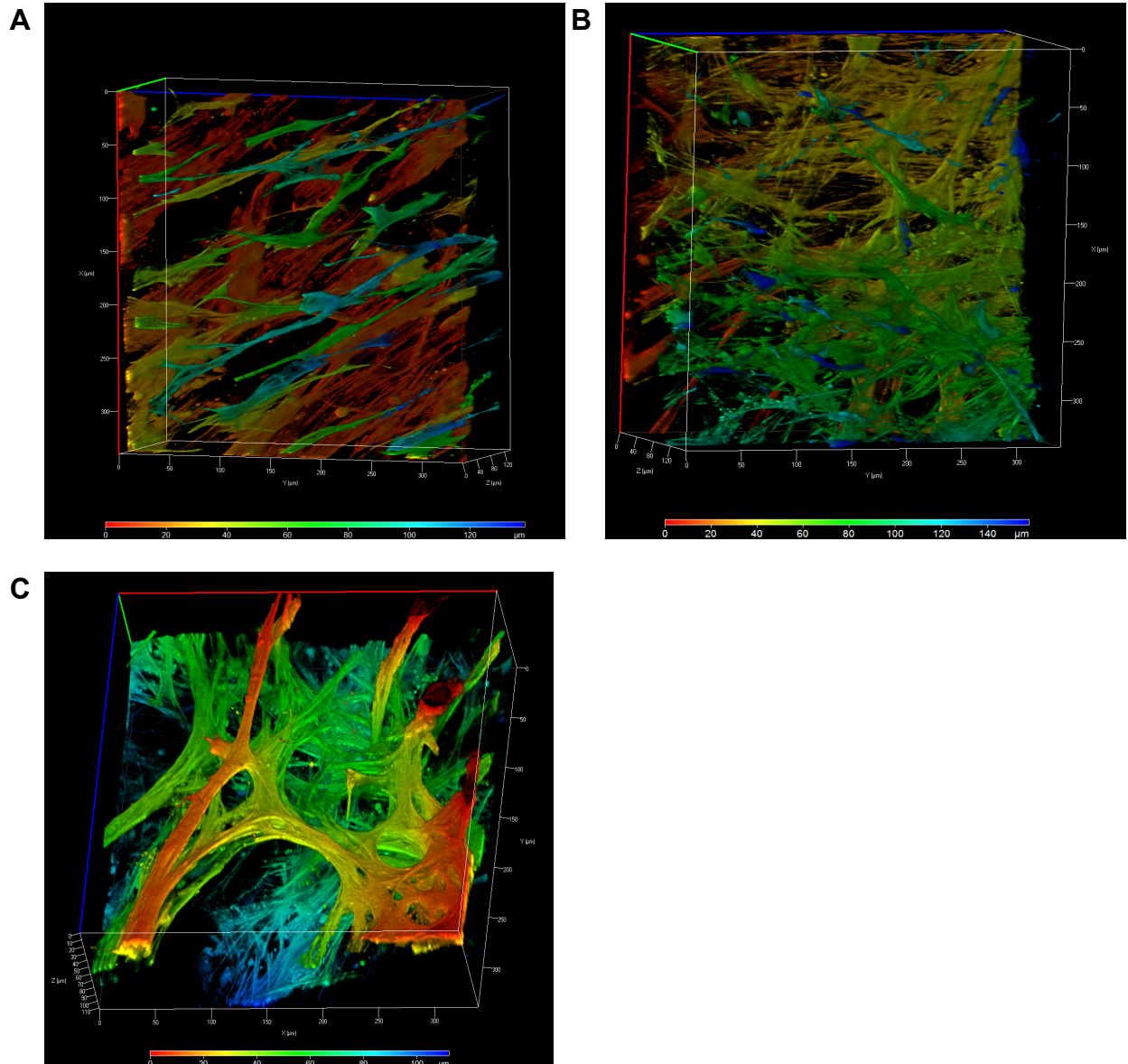


Figure 9. Z-stack confocal microscopy of HMSC seeded LZ-Control hydrogel.

3-D reconstructed images of HMSC cultured on 7% w/v LZ-Control hydrogel after 7 days (A), 14 days (B), and 21 days (C) and stained with TRITC-phalloidin staining for actin. Color-coding represents the depth profile from the surface red to blue at a depth of 150 μm . Phalloidin stains actin filament and shows the cytoskeletal organization of HMSCs within the LZ hydrogels.

A.10. Foreign body response to leucine zipper hydrogels

The LZ hydrogels were implanted subcutaneously in wild type mice to observe if there was a host generated foreign body response to the hydrogels. The scaffolds were implanted for a period of 1 and 2 weeks and explant sections were examined by immunohistochemistry.

CD68, a macrophage marker was used Immunohistochemical analysis for CD68 positive cells showed no staining at one week (Figure 10A1, 10B1) indicating the absence of foreign body reaction. After 2 weeks of implantation, positive staining for CD68 was observed at the periphery of the hydrogel in both the samples; however, they were not multi-nucleated macrophages (Figure 10A3 and 10B3). Multi-nucleated macrophages are the hallmark of adverse foreign body response. The absence of such macrophages after 2 weeks of implantation indicated that the LZ scaffolds were not subjected to foreign body reaction *in vivo*.

CD68 is a broad-spectrum macrophage marker. Therefore, the positive mono nucleated cells could be macrophage cells present in the blood due to the neovascularization in the LZ hydrogels after 2 weeks.

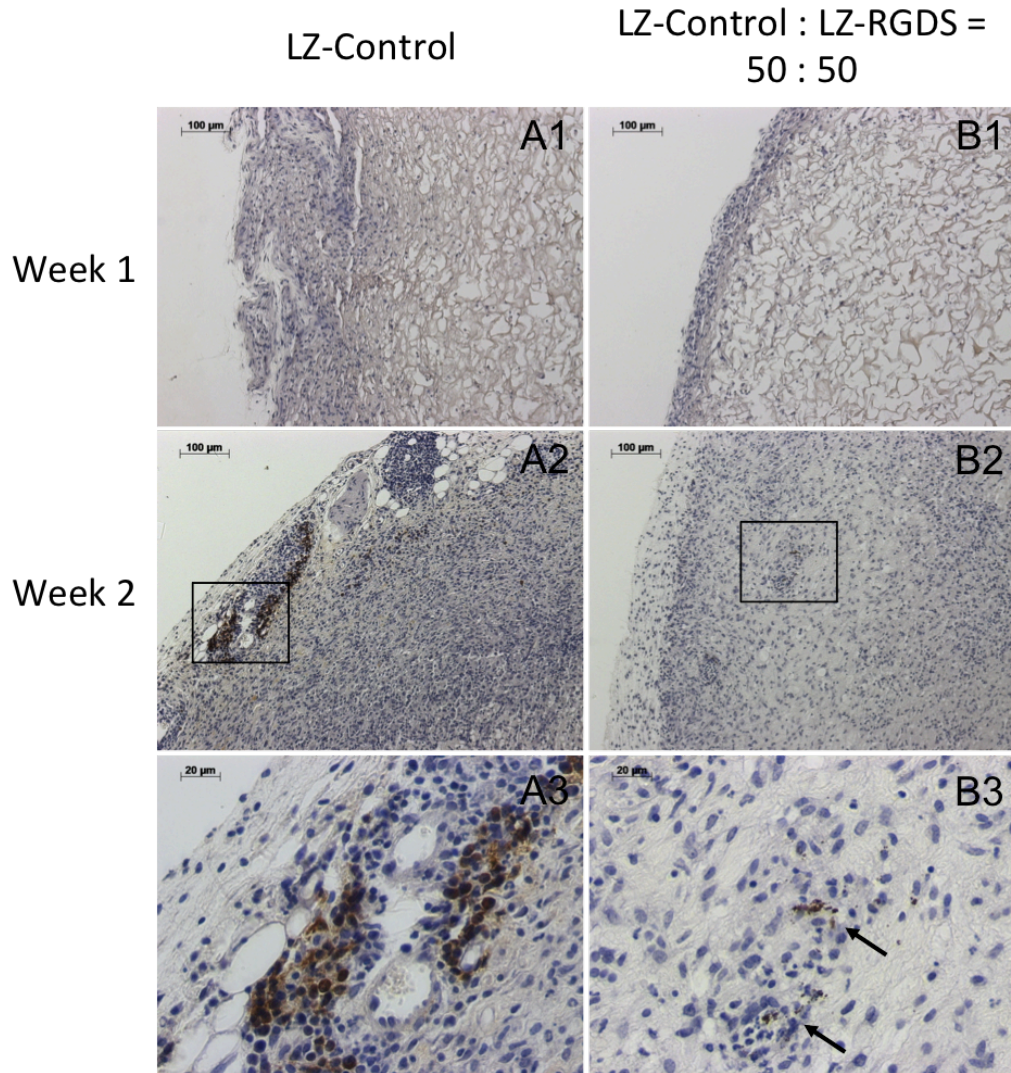


Figure 10. CD68 Immunohistochemistry of LZ hydrogel with RGDS.

Images represent CD68 stained sections of LZ-Control (A1, A2 and A3) and LZ-RGDS (50:50) (B1, B2 and B3) scaffolds implanted subcutaneously in wild type mice for 1 week (A1 and B1) and 2 weeks (A2, A3 and B2, B3) respectively. Note the absence of CD68 positive cells in A1 and B1 indicating the absence of macrophages after 1 week. At 2 weeks macrophages were observed (A2 and B2) positive staining. The boxed areas in A2 and B2 are shown in higher magnification in A3 and B3 respectively. These images show the presence of macrophages and also absence of multi-nucleated foreign body giant cells indicating the absence of adverse foreign body reaction.

A.11. Host cell response to LZ hydrogels

Hematoxylin staining in Figure 10 shows that the LZ gels supported colonization by host cells. To analyze if the colonized host cells were able to secrete a matrix and promote vascularization, a series of markers was used for immunohistochemical analysis.

Staining for fibronectin, the predominant ECM protein was particularly interesting. Intense staining of fibronectin in the ECM was observed with cells recruited to the LZ-RGDS scaffold (Figure 11B1-11B4) when compared with the control (Figure 11A1-11A4). Similar staining pattern was observed for DMP-1 (Dentin Matrix Protein 1) a regulatory protein in osteogenesis (Figure 11B1-11B4). This suggested that the presence of RGDS was critical for the initial colonization and matrix production by host cells. In order to determine if the LZ scaffold created a microenvironment for neovascularization, staining for VEGF (vascular endothelial growth factor) was performed. Results indicated that more VEGF staining was predominant at 1 week and reduced amounts were observed at 2 weeks (Figure 11C1-11C4). This staining pattern corroborated well with the levels of PEDF (Pigment-Epithelium Derived Factor). PEDF is one of the most potent anti-angiogenic factors and its expression increased at 2 weeks (Figure 11D1-11D4).

These results imply that the LZ scaffolds can provide an environment that can trigger favorable host cell response by enabling deposition of the host cell ECM and permitting host cell-mediated vascularization.

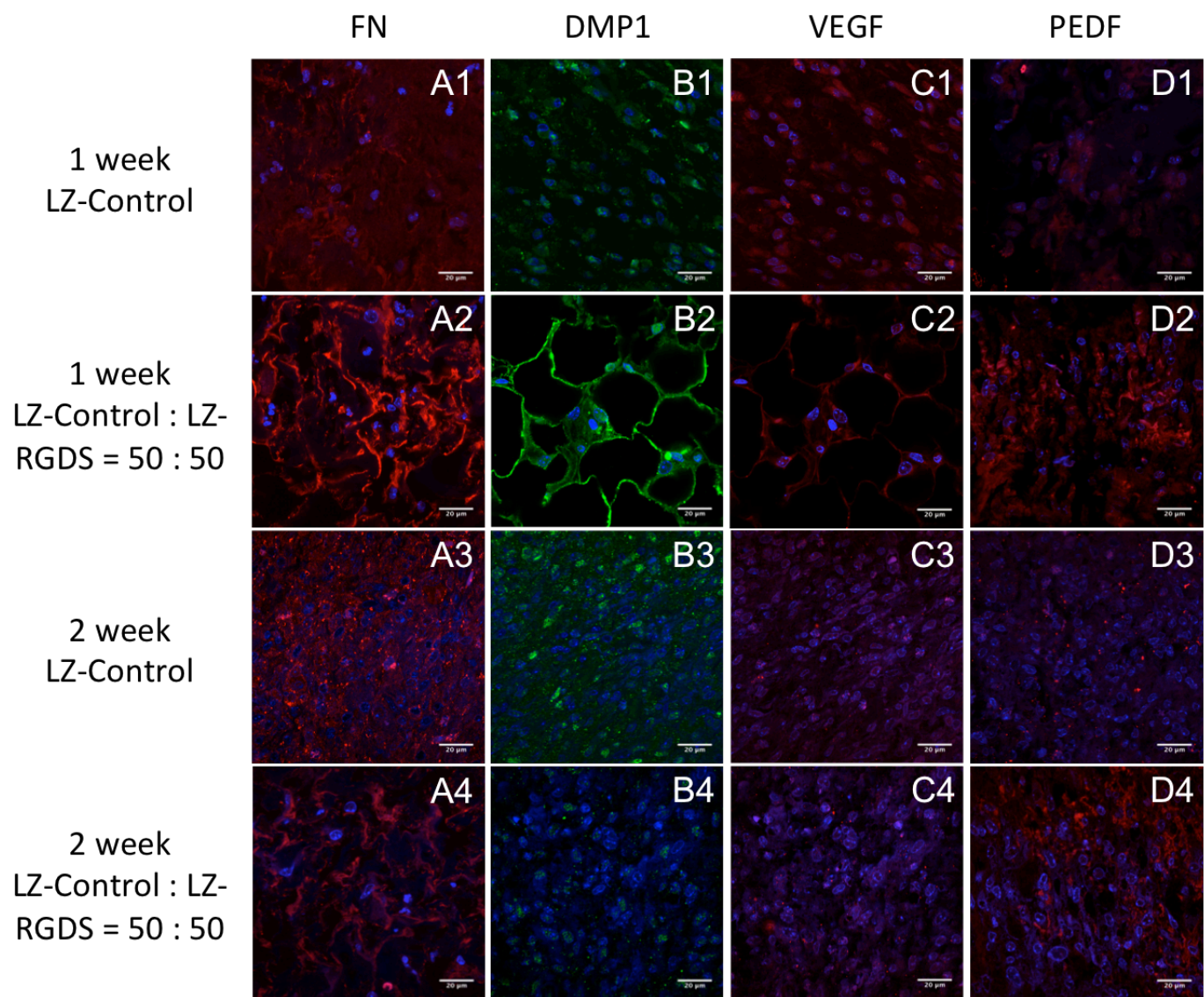


Figure 11. Immunofluorescence staining of scaffold sections from LZ hydrogel implanted in wild type mice.

Images are representative confocal micrographs showing the immunohistochemical localization of Fibronectin (A1, A2, A3 and A4), DMP-1 (B1, B2, B3 and B4), VEGF (C1, C2, C3 and C4) and PEDF (D1, D2, D3 and D4) in LZ-Control (A1-D1, A3-D3) and 50:50 LZ-Control: LZ-RGDS (A2- D2, A4-D4) after 1 and 2 weeks of subcutaneous implantation in wild type mice. Scale bar represents 20 μm for all images.

A.12. *In vivo* response of leucine zipper hydrogels pre-seeded with HMSCs

The LZ hydrogels provided an excellent microenvironment for host cell colonization and proliferation without triggering foreign body response. Our next step was to ascertain if LZ scaffolds seeded with mesenchymal stem cells were able to support the survival and proliferation of these cells *in vivo*. Although we seeded cells transfected with GFP, after post processing and section, the inherent GFP fluorescence was lost. Therefore, the sections were stained using a GFP antibody to visualize the implanted cells.

At the end of 2 weeks, staining for GFP showed the presence of GFP-positive cells within the scaffold (Figure 12A1, 12A2). As before, the ECM synthesized by the HMSCs seeded on the LZ-RGDS showed predominant staining for fibronectin (Figure 12B1, 12B2) and DMP-1 (Figure 12C1, 12C2). H&E staining of the tissues showed the presence of numerous RBCs indicating the presence of active blood flow within the scaffolds. Neovascularization was observed originating from the surface of the hydrogel to the interior by H&E staining (Figure 12F1, 12F2). Higher vessel density was observed with LZ-RGDS scaffold (Figure 12F2). Both VEGF and PEDF were expressed by the HMSCs in the control and the RGDS hydrogels indicating control over the process of angiogenesis. Presence of endothelial cells was further confirmed by observing the immunohistochemical localization of vWF (von Willebrand factor) (Figure 12G1, 12G2) and CD31 markers for endothelial cells (Figure 12H1, 12H2).

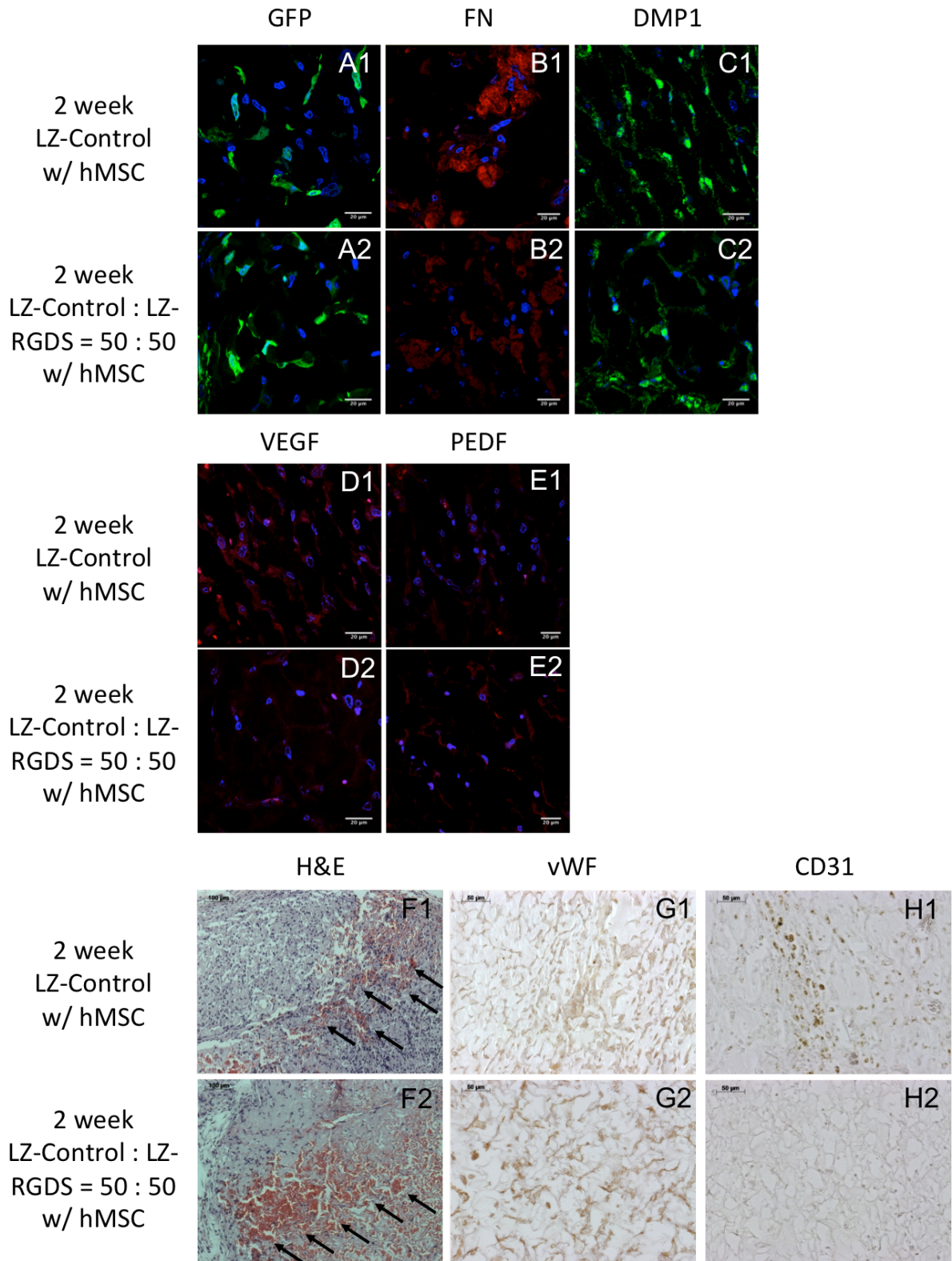


Figure 12. Histology and immunofluorescence staining of HMSC seeded LZ-scaffolds implanted in immunocompromised mice.

(A1-E1) represent immunohistochemical localization of GFP, fibronectin (FN), DMP-1, VEGF and PEDF in sections of LZ-Control scaffolds implanted subcutaneously in immunocompromised mice for 2 weeks. (A2-E2) are representative images showing the same from 50:50 LZ-Control:LZ-RGDS scaffolds. (F1, F2) are representative images of H&E stained sections of the two types of implanted scaffolds containing HMSCs. Note arrows indicate red blood cells. (G1, G2) are representative images showing the immunohistochemical localization of vWF and (H1, H2) show CD31 in the two types of scaffold.

Results from these experiments showed that the HMSCs seeded within the LZ-Control and LZ-RGDS scaffolds were able to proliferate and secrete an active ECM that favors vascularization.

B. Stable leucine zipper hydrogels with calcium-binding properties for hard tissue engineering

B.1. *In vitro* nucleation of calcium phosphate polymorphs under physiological concentrations of calcium and phosphate ions by leucine zipper hydrogels containing the DMP-1 calcium-binding motif

Calcium plays an important role in human physiology and is highly regulated. About 99% of the calcium is stored in the bone as the mineral in the form of calcium phosphate. In the cells, the concentration of intracellular calcium ion is around 100 nM but can increase up to 10~100 fold depending on the cellular functionality. During bone mineral formation, it is known that the calcium ion concentration is higher than the systemic level. The calcium ion concentration in the ECM of bone matrix is even higher which can be up to about 12,000 fold. Thus, the calcium ion concentration of about 1 mM can be considered as systemic or physiological level [215]. In this study, we tested the mineralization potential of the LZ hydrogel with the calcium binding domains derived from DMP-1 at physiological level of calcium and phosphate concentration and also at high concentrations. The use of physiological level concentration can provide the scenario whether the LZ hydrogel is capable to mineralize under normal conditions. The high concentrations of 1M of calcium and phosphate ions used in this study was to saturate the calcium binding sites in the LZ hydrogel scaffold.

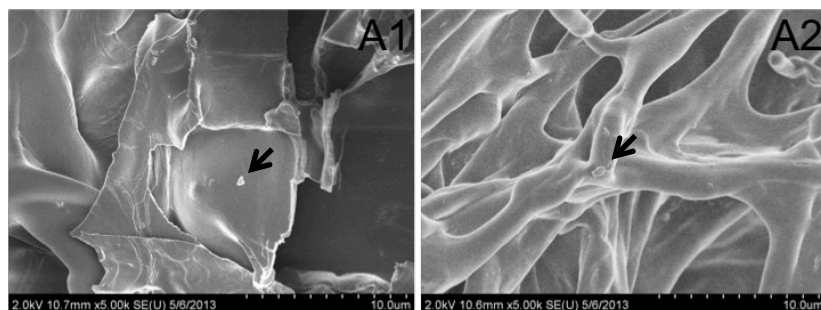
The idea behind the use of calcium-binding motifs is to facilitate nucleation of crystalline calcium phosphate. In order to verify the calcium ion binding abilities of the two incorporated calcium-binding motifs derived from DMP-1, we

performed an *in vitro* calcium phosphate nucleation assay. The hydrogels, containing either of the calcium-binding motifs (LZ-Control:LZ-ESQES:LZ-QESQSEQDS, 2:1:0 or 2:0:1) or both of them (LZ-Control:LZ-ESQES:LZ-QESQSEQDS 1:1:1) were placed in a nucleation chamber containing physiological concentrations of calcium and phosphate ions for two weeks. With the physiological levels, we show proof of concept that even in the presence of low amounts of calcium and phosphorus, the LZ hydrogel can nucleate CaP.

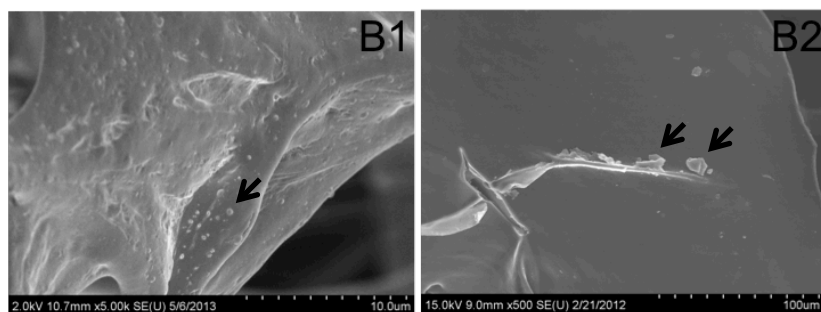
Figure 13 shows the SEM images of the LZ hydrogel surface after *in vitro* mineralization under physiological conditions for two weeks. All of the image showed mineral deposits. The SEM images show that there are no significant differences for mineral deposition across all of the three LZ hydrogel samples with respect to the size and quantity, except the LZ-Control:LZ-ESQES:LZ-QESQSEQDS 2:0:1 showed some mineral deposits up to 10 μm (Figure 13B2). However, the LZ- Control hydrogel did not initiate deposition of calcium phosphate salts and no detectable peaks for calcium and phosphorus were obtained with EDX analysis.

The results presented show the ability of the LZ hydrogel with DMP-1 derived calcium-binding domains to initiate calcium phosphate nucleation irrespective of the calcium-binding motif used. Initiation of nucleation was observed even when the calcium and phosphate concentrations were as low as the physiological level indicating the strong calcium-binding ability of the LZ

LZ-Control : LZ-ESQES : LZ-QESQSEQDS = 2:1:0



LZ-Control : LZ-ESQES : LZ-QESQSEQDS = 2:0:1



LZ-Control : LZ-ESQES : LZ-QESQSEQDS = 1:1:1

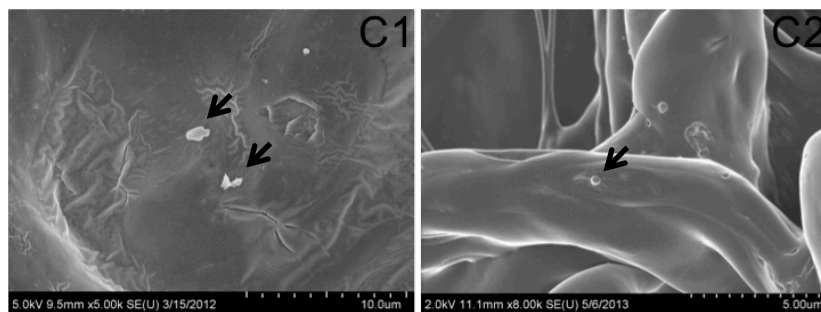


Figure 13. *In vitro* mineralization of the LZ hydrogel with different combinations of DMP-1 calcium-binding domains (LZ-ESQES and LZ-QESQSEQDS) under physiological concentrations of calcium and phosphahte.

The scanning electron microscopy (SEM) images show deposition of the mineral on the LZ hydrogel with varying ratios of the LZ-containing DMP-1 motives 2:1:0 LZ-Control:LZ-ESQES:LZ-QESQSEQDS (A), 2:0:1 LZ-Control:LZ-ESQES:LZ-QESQSEQDS(B), or 1:1:1 LZ-Control:LZ-ESQES:LZ-QESQSEQDS = (C).

hydrogel. During bone mineralization, the local calcium and phosphate concentration are much higher than the physiological concentrations used in this study [216]. Although the use of LZ-QESQSEQDS alone may be capable of greater mineral deposition, this property was not exhibited when it was used in combination with LZ-ESQES. The combined use of these two calcium-binding motifs, LZ-ESQES and LZ-QESQSEQDS provided a potential strategy for tuning the LZ hydrogel properties with respect to mineral nucleation rates as the two peptides have different properties with respect to mineral nucleation.

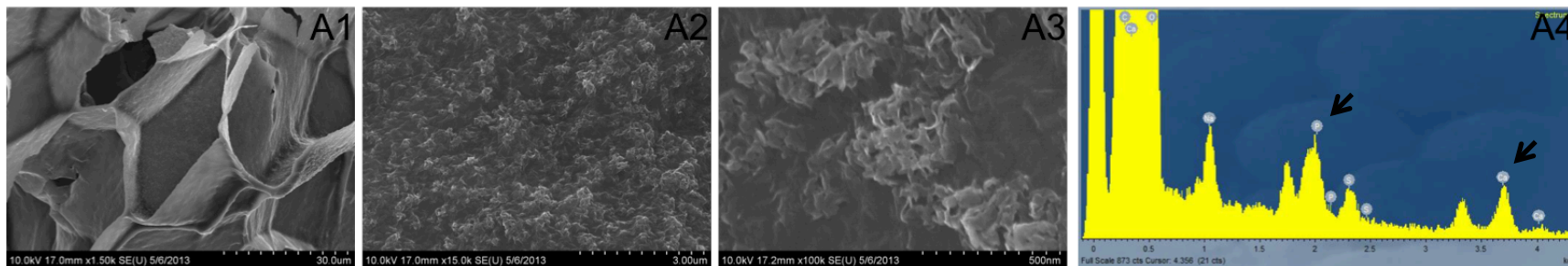
B.2. *In vitro* nucleation of calcium phosphate under high concentrations of calcium and phosphate ions by leucine zipper hydrogels containing the DMP-1 calcium-binding motifs

The second step of *in vitro* calcium phosphate nucleation test was conducted by incubating the LZ hydrogels in buffers containing 1M calcium chloride and 1M sodium phosphate

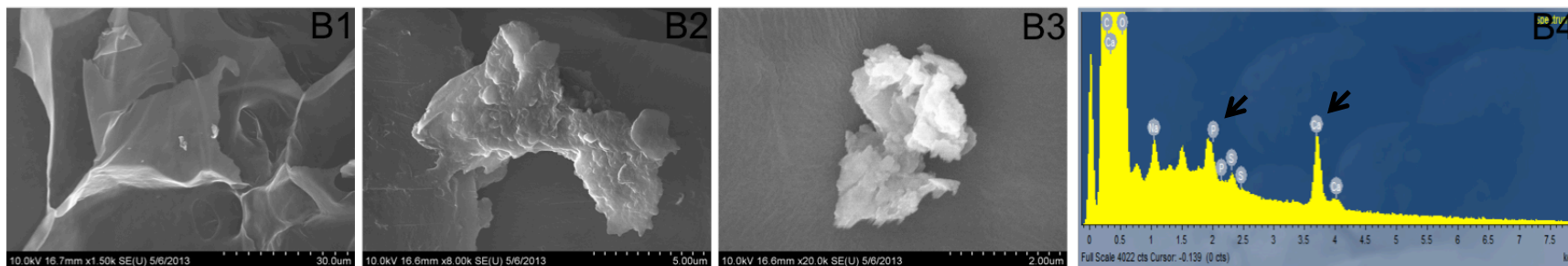
The SEM images of these LZ hydrogel fractured surfaces containing different ratios of the calcium-binding domains including 2:1:0, 2:0:1, and 1:1:1 of LZ-Control:LZ-ESQES:LZ-QESQSEQDS are shown in Figure 14A1-A3, B1-B3, and C1-C3 respectively, and the respective EDX analysis spectrums are shown in Figure 14A4, B4, and C4. In the 2:0:1 LZ-Control:LZ-ESQES:LZ-QESQSEQDS LZ hydrogel, the calcium phosphate nucleation only showed several bulky deposits up to 10 μm on the surface (Figure 14B1-B3). However, the SEM images show both 2:1:0 and 1:1:1 LZ-Control:LZ-ESQES:LZ-QESQSEQDS showed a thin layer deposition of calcium phosphate (Figure 14A1 and C1) and the microstructure showed the plate-shaped deposition especially in the 1:1:1 LZ-Control:LZ-ESQES:LZ-QESQSEQDS hydrogel (Figure 14A3 and C3).

The EDX analysis show the peaks of both calcium and phosphorus in all the LZ hydrogel samples (Figure 14A1, B1, and C1). Specifically, the spectra revealed that the Ca/P ratio was 1.63, 1.21, and 1.59 for 2:1:0, 2:0:1, and 1:1:1 LZ-Control:LZ-ESQES:LZ-QESQSEQDS LZ hydrogel samples respectively indicating the likelihood of the calcium phosphate deposits to be hydroxyapatite

LZ-Control : LZ-ESQES : LZ-QESQSEQDS = 2:1:0



LZ-Control : LZ-ESQES : LZ-QESQSEQDS = 2:0:1



LZ-Control : LZ-ESQES : LZ-QESQSEQDS = 1:1:1

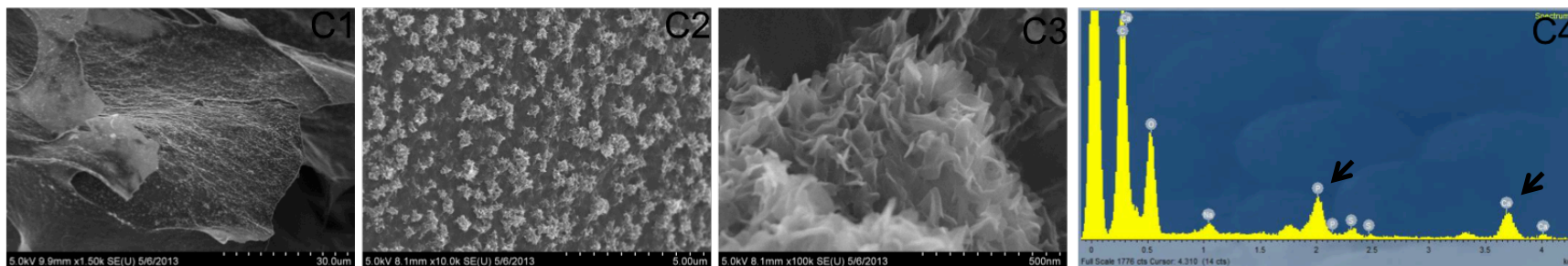


Figure 14. *In vitro* mineralization on LZ hydrogel with different combinations of DMP-1 calcium-binding domains (LZ-ESQES and LZ-QESQSEQDS) under high concentrations of calcium and phosphate.

(A1-A3) represent SEM analysis of the mineral deposits on the scaffolds containing 2:1:0 LZ-Control:LZ-ESQES:LZ-QESQSEQDS. These deposits were partially crystalline calcium phosphate and (A4) shows the energy dispersive X-ray (EDX) analysis indicating the presence of Ca and P and the Ca to P ratio. (B1-B3) represents the SEM image of mineral deposits on the 2:0:1 LZ-Control:LZ-ESQES:LZ-QESQSEQDS scaffold. The deposits were characterized as amorphous calcium phosphate and (B4) shows the EDX analysis indicating the presence of calcium and phosphorus along with the Ca to P ratio. (C1-C3) represents SEM images of mineral deposits present on the 1:1:1 LZ-Control:LZ-ESQES:LZ-QESQSEQDS. The deposits were characterized as crystalline hydroxyapatite and (C4) shows the EDX analysis indicating the presence of calcium and phosphorus along with its Ca to P ratio. Note different scale in (B3) was due to the overall sparse deposits in the LZ hydrogel.

in the 2:1:0 and the 1:1:1 hydrogels. The Ca/P ratio of 1.21 in the 2:0:1 LZ-Control:LZ-ESQES:LZ-QESQSEQDS LZ hydrogel indicates the presence of amorphous calcium phosphate. On the other hand, in the 2:1:0 and 1:1:1 LZ-Control:LZ-ESQES:LZ-QESQSEQDS LZ hydrogels, the calcium to phosphate ratios were that of hydroxyapatite similar to native bone that has a Ca/P ratio of 1.50–1.667 [217]. Again, the LZ-Control hydrogel didn't show any calcium phosphate mineral deposition under SEM imaging and there were no indications for the presence of calcium and phosphorus in the EDX analysis.

The crystallinity of the nucleated calcium phosphate polymorphs were analyzed using TEM followed by SAD. Figure 15 shows representative TEM (Figure 15A1-B1) and SAD images (Figure 15A2-B2) of 1:1:1 LZ-Control:LZ-ESQES:LZ-QESQSEQDS LZ hydrogel after nucleation with high concentrations of calcium and phosphate. The TEM images show the presence of both single crystal (Figure 15A1) and multi-crystal formations (Figure 15B1) of calcium phosphate. The SAD images further confirmed the crystallinity of these mineral deposits. Figure 15A2 shows a set of two SAD phases indicating a single crystal; Figure 15B2 shows multiple sets of SAD phases indicating a multi-crystal structure.

The physiological levels of calcium and phosphate ions used in the first part represent systemic levels and do not depict the amount of calcium and phosphorus present in the mineralizing niche. However, mineralization at high concentrations is an attempt to look at the ability of the gel to nucleate in a scenario where they are exposed to an inorganic environment that resembles the

LZ-Control : LZ-ESQES : LZ-QESQSEQDS = 1:1:1

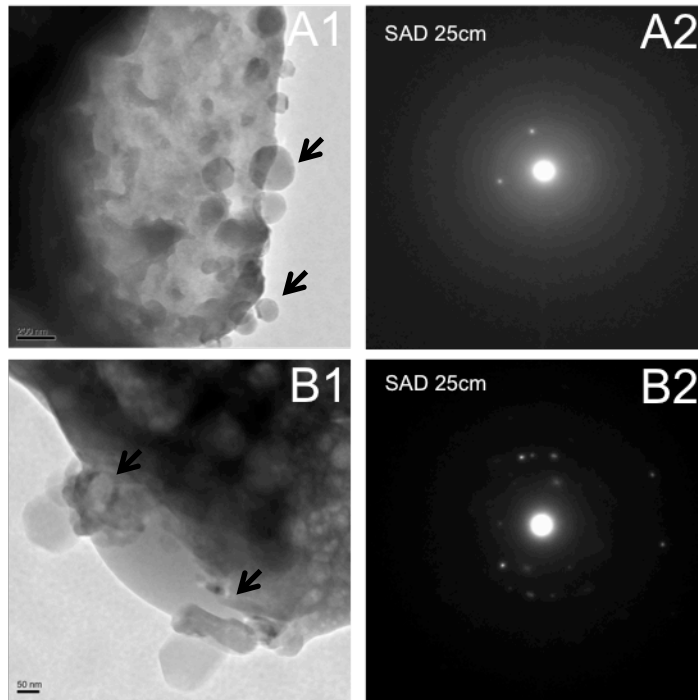


Figure 15. *In vitro* mineralization on the LZ hydrogel with DMP-1 calcium-binding domains under high concentrations of calcium and phosphate.

A1 and B1 represent the SEM micrograph images showing the plate-like structure of the mineralized calcium phosphate in the LZ hydrogel with DMP-1 calcium-binding domains (1:1:1 LZ-Control:LZ-ESQES:LZ-QESQSEQDS), A2 and B2 show the selected area electron diffraction (SAED) data from the mineralized LZ scaffold indicating the presence of crystalline hydroxyapatite.

mineralizing niche. Results from this study confirm that the DMP1-derived calcium-binding peptides can indeed bind calcium and initiate the process of crystal nucleation and growth. Such peptides have the added advantage of controlling the spatial deposition of CaPs. Further different combinations of the two DMP-1 derived calcium-binding motifs can affect the degree and quality of calcium phosphate deposition. Thus the choice and the ratio of the motifs can be used as a tunable factor for different applications.

B.3. Mechanical properties of the leucine zipper hydrogel with DMP-1 calcium-binding motifs after mineralization in high concentrations of calcium and phosphate buffer

The major purpose of introducing the DMP-1 calcium-binding motifs in the chimeric LZ protein construct is to reinforce and strengthen the mechanical properties of the hydrogel, as well as to create a biomimetic scaffold that can be used for the regeneration of hard tissues such as bone and dentin. Such approaches have been reported previously using pHEMA hydrogels [218, 219], and gelatin hydrogels [220].

We examined the viscoelastic properties of the LZ hydrogel with DMP-1 calcium-binding motifs after mineralization under high salt concentrations using oscillatory shear rheology. Rheological studies conducted on the 2:1:0, 2:0:1, and 1:1:1 LZ-Control:LZ-ESQES:LZ-QESQSEQDS LZ hydrogel at a frequency range from 0.01 to 1 Hz showed that storage moduli (G' , Figure 16A) and loss moduli (G'' , Figure 16B) changed with different combinations of DMP-1 calcium-binding motifs. The G' was greater than the G'' by approximately an order of magnitude for all the samples examined here. The average G' at 0.1 Hz were 4.4 kPa and 305.2 Pa, 33.5 kPa and 3.2 kPa, 244 kPa and 39.3 kPa, and 326 kPa and 128 kPa for LZ-Control and 2:1:0, 2:0:1, and 1:1:1 LZ-Control:LZ-ESQES:LZ-QESQSEQDS, LZ hydrogel respectively. Also similar to the previous test on the LZ-Control hydrogel without any modification, there are no crossover point of G' and G'' at the frequencies used in this study showing that the LZ hydrogels are fairly rigid viscoelastic materials with covalent crosslinking.

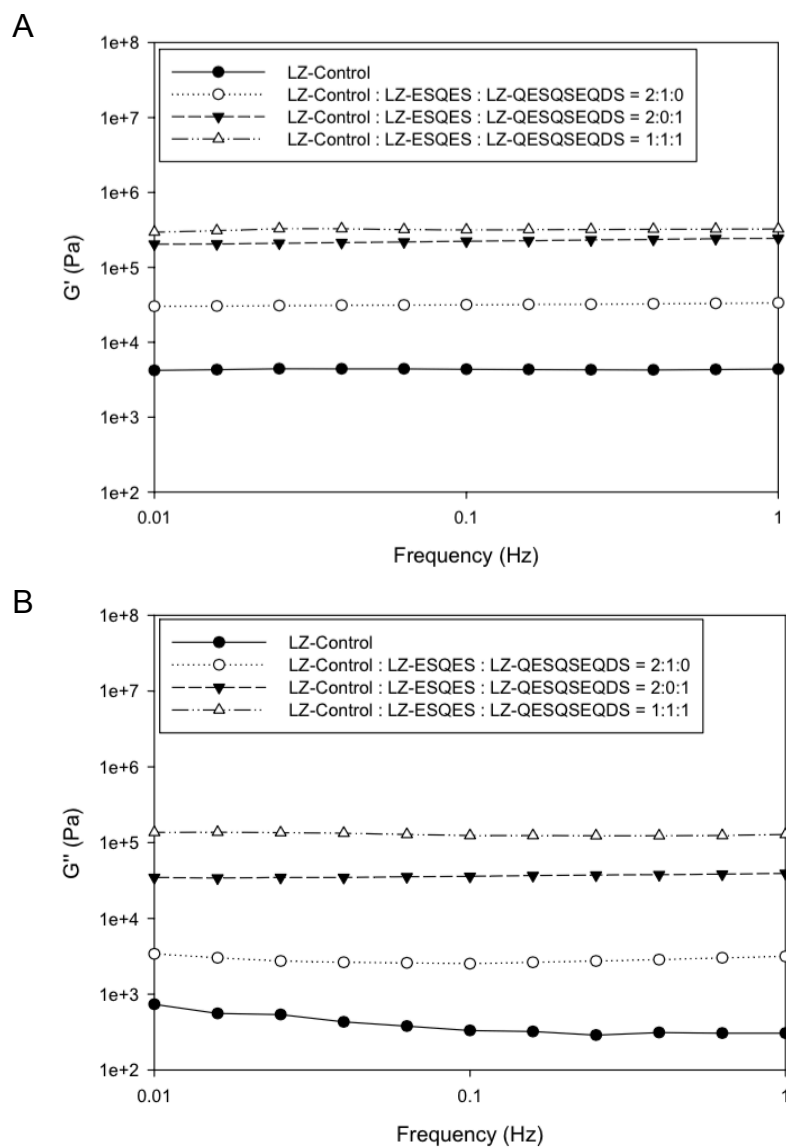


Figure 16. Viscoelasticity measurements of LZ hydrogel with different combinations of LZ-ESQES and LZ-QESQSEQDS under high concentrations of calcium and phosphate.

Graphical representation of the storage modulus G' (A) and the relaxation modulus G'' (B) with change in frequency. Note the change of G' and G'' values with the different combinations of DMP-1 calcium-binding motifs. The 1:1:1 LZ-Control:LZ-ESQES:LZ- QESQSEQDS showed a higher value.

Comparing the highest G' here from 1:1:1 LZ-Control:LZ-ESQES:LZ-QESQSEQDS LZ hydrogel, it is about 130 times higher than the LZ-Control hydrogel without any treatments. Also note that the G' and G'' values for LZ-Control hydrogel didn't show a big change (by only about two folds) with and without high calcium and phosphate concentration based nucleation showing that there was minimal amount of non-specific calcium ion binding on the hydrogel.

The loss tangent, $\tan \delta = G''/G'$, values at 0.1 Hz in this experiment were 0.07, 0.09, 0.16, and 0.39 for LZ-Control, 2:1:0, 2:0:1, and 1:1:1 LZ-Control:LZ-ESQES:LZ-QESQSEQDS hydrogel respectively. The loss tangent value of mineralized LZ-Control hydrogel was comparable with the value obtained without mineralization. This shows no intrinsic connectivity change between them. The 2:1:0 LZ-Control:LZ-ESQES:LZ-QESQSEQDS hydrogel did not show significant change in its connectivity as the loss tangent remained close to the LZ-Control hydrogel. However, the loss tangent value increased significantly in the 2:0:1, and especially in the 1:1:1 LZ-Control:LZ-ESQES:LZ-QESQSEQDS,LZ hydrogel. This loss tangent value increase suggests the presence of large amounts of calcium phosphate mineral deposition within the hydrogel. The dissipation of energy is higher for the hydrogel which contains deposits of calcium phosphate than for the hydrogel containing water [221].

The results from the rheology experiments shows the changes in the LZ hydrogels that are brought about by the incorporation of DMP-1 calcium-binding motifs and nucleation at high concentrations of calcium and phosphate. Based on the data, the 1:1:1 LZ-Control:LZ-ESQES:LZ-QESQSEQDS LZ hydrogel exhibits

the best yield for the mineral deposits , therefore we selected this combination for the preparation of LZ hydrogel with equal composition of LZ-ESQES and LZ-QESQSEQDS for *in vivo* subcutaneous experiments.. We anticipate that such a mineralized LZ hydrogel would improve the mechanical properties and can be used in tissue engineering applications for bone regeneration.

B.4. Mesenchymal stem cell adhesion to the leucine zipper hydrogels with DMP-1 calcium-binding motifs after mineralization

The 1:1:1 LZ-Control:LZ-ESQES:LZ-QESQSEQDS LZ hydrogels was mineralized and tested for their ability to facilitate cell attachment and promote the proliferation of HMSCs under 3-D cell culture conditions. The proliferation experiments were performed over a period of 21 days with time points at 1, 4, 7, 14, and 21 days. The result (Figure 17) shows that the total HMSCs cell number showed no significant difference in the first seven days. However, at days 14 and 21, the LZ hydrogels with DMP-1 derived calcium-binding motifs showed a tendency to promote increased cell proliferation (statistically significant change as determined by student t-test). This suggests that the calcium phosphate mineral deposited on the hydrogel deposition did not impede cell growth in the LZ hydrogel and even promoted cell proliferation when cultured for a long term.

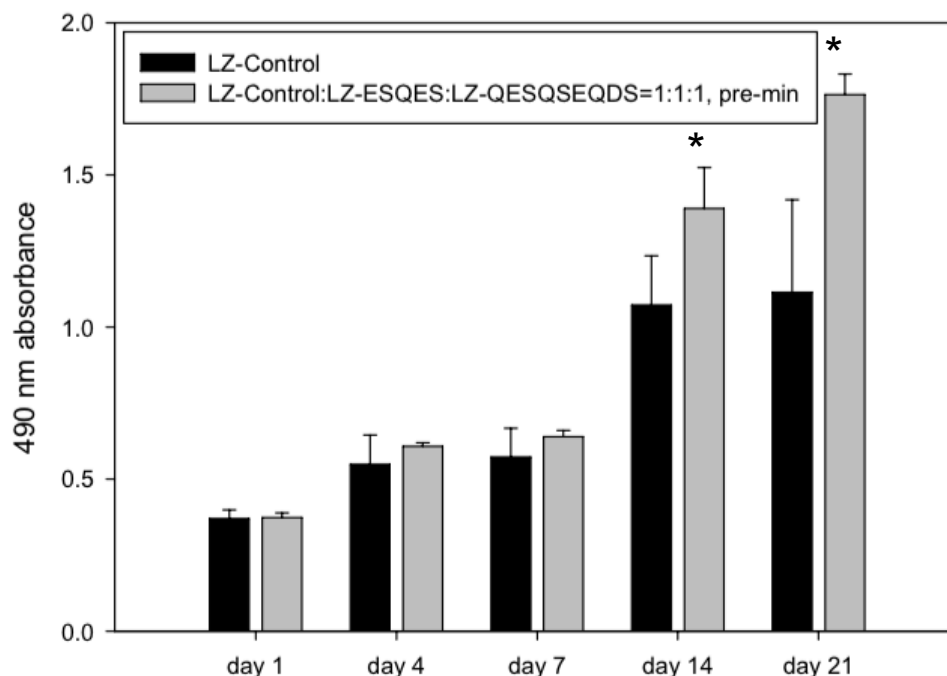


Figure 17. Proliferation rate of HMSCs cultured on 3-D LZ mineralized scaffold. LZ scaffold was subjected to mineralization under high concentrations of calcium and phosphate and used for culturing HMSCs.

The MTT assay indicate the proliferation of HMSCs on mineralized 3-D LZ scaffolds with DMP-1 calcium-binding motifs (1:1:1 LZ-Control:LZ-ESQES:LZ-QESQSEQDS) * represents statistical significance ($p < 0.05$ using students t-test) with respect to LZ-Control hydrogel.

B.5. Leucine zipper hydrogels containing DMP-1 calcium-binding motifs facilitated vascularization

The mineralized LZ scaffold had a positive effect not only on the mechanical property, but also facilitated cell proliferation. The next step was to characterize the scaffold in *in vivo* implantation experiments. We performed subcutaneous implantation in the athymic nude mice to understand the host responses of the pre-seeded HMSCs response on the unmineralized and mineralized LZ scaffolds containing DMP-1 calcium-binding motifs. Two characteristic properties that were investigated were angiogenesis and osteogenic differentiation.

As formally mentioned, vascularization of the scaffold indicates angiogenesis, and angiogenesis is known to facilitate osteogenic differentiation. For angiogenesis, CD31, vWF, VEGF and PEDF are the major markers used to detect endothelial cells and vascularization.

The angiogenesis related markers were used to analyze if the colonized host cells were able to secrete a matrix that promoted vascularization. The staining represented in Figure 18 shows H&E staining (A1-D1), CD31 (A2-D2), and vWF (A3-D3) of the implanted 1:1:1 LZ-Control:LZ-ESQES:LZ-QESQSEQDS LZ hydrogels with and without mineralization and implanted for 2 and 4 weeks.. The H&E staining at 2 weeks show the absence of microvessels in the control LZ hydrogel but a homogeneous distribution of the seeded-cells was observed (Figure 18A1); the mineralized LZ hydrogel also did not show microvessel formation, but interestingly showed some huge matrix channe

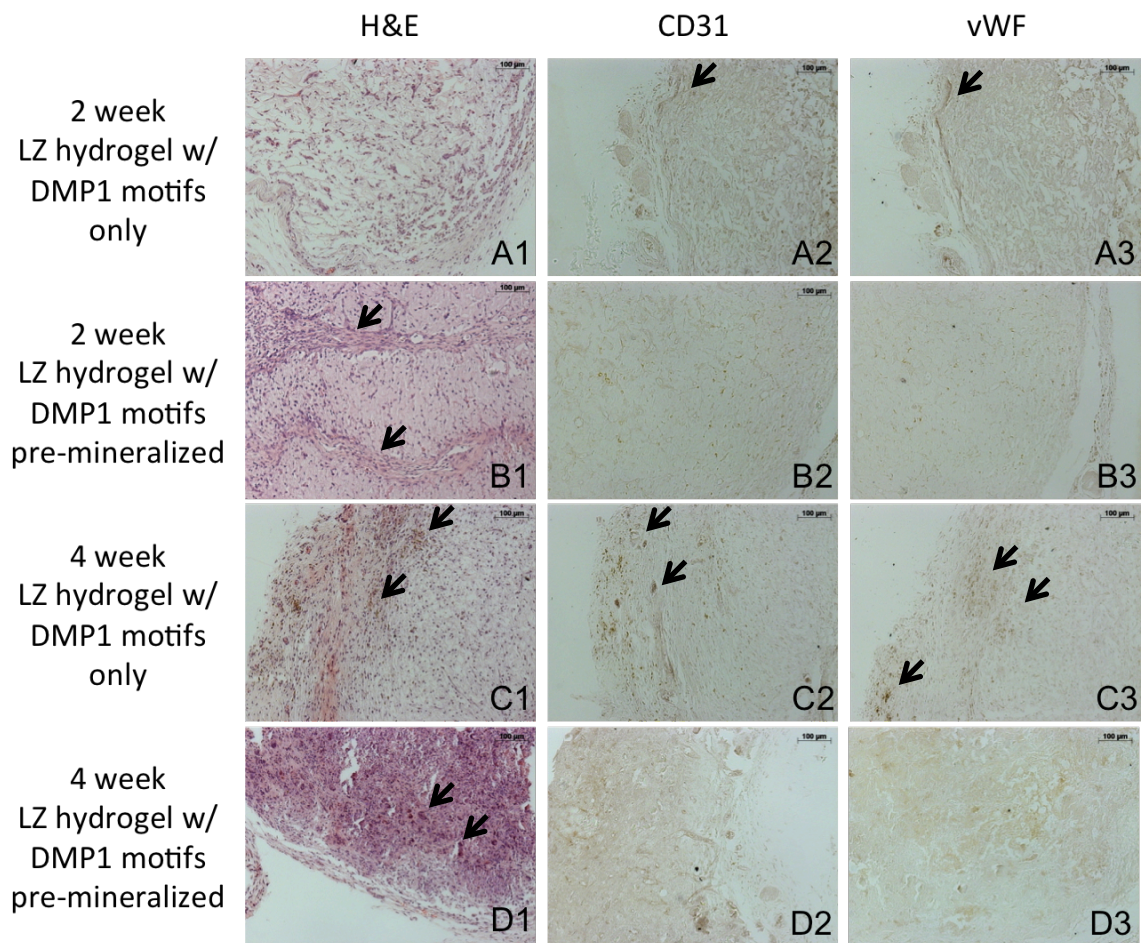


Figure 18. Histological staining and immunohistochemical analysis of angiogenic markers performed on HMSC-seeded LZ scaffolds with DMP-1 calcium-binding motifs before and after mineralization, implanted in immunocompromised mice.

(A1-D1) are representative H & E images of implanted LZ hydrogel scaffolds with DMP-1 calcium-binding motifs (1:1:1 LZ- Control:LZ-ESQES:LZ-QESQSEQDS) which were either mineralized or unmineralized implanted with HMSCs and harvested after 2 or 4 weeks. Note the pink hematoxylin staining which indicates ECM deposition in the pre- mineralized LZ hydrogel scaffold (arrows in B1 and overall pink staining in D1) and the red blood cells (arrows in C1 and D1). (A2-D2 and A3-D3) are representative images showing the immunohistochemical localization of CD31 (A2-D2) and vWF (A3-D3) in the harvested scaffolds in both the LZ hydrogel scaffolds with and without mineralization (1:1:1 LZ-Control:LZ-ESQES:LZ- QESQSEQDS) containing HMSCs after 2 and 4 weeks.

within the hydrogel (Figure 18B1). At 4 weeks, some neovasculature was observed in the peripheral region of the unmineralized LZ hydrogel (Figure 18C1); the mineralized LZ hydrogel still remained non-vascularized but showed great cell density with heavily deposited ECM (Figure 18D1).

The immunohistochemical localization of CD31 and vWF which are both markers for endothelial cells show the same trend. The unmineralized LZ hydrogel stained for both CD31 and vWF in the peripheral region of the hydrogel section indicating neovascularization at 2 weeks of implantation. This process remained active even at 4 weeks of implantation. On the other hand, mineralized LZ hydrogel showed only dispersed staining for CD31 and vWF within the hydrogel at both 2 weeks and 4 weeks indicating a slower response to neovascularization.

The immunofluorescence staining of VEGF and PEDF in the implanted 1:1:1 LZ-Control:LZ-ESQES:LZ-QESQSEQDS LZ hydrogel with and without mineralization after 2 and 4 weeks of implantation is shown in Figure 19. At 2 weeks, the LZ hydrogel with DMP-1 calcium-binding motif only, showed no staining of VEGF but a few areas stained positive for PEDF (Figure 19A1-A2). When compared with the VEGF and PEDF activity in Figure 11 in LZ-Control hydrogel, we can speculate that the VEGF signaling may occur as early as 1 week after implantation (Figure 11C1) and decrease at 2 weeks with PEDF signaling being predominant as it is a regulator of angiogenesis (Figure 11C3 and 11D3). This is further supported by immunohistochemical analysis of CD31 and vWF that was observed at 2 weeks (Figure 18A2-A3). At 4 weeks, the VEGF

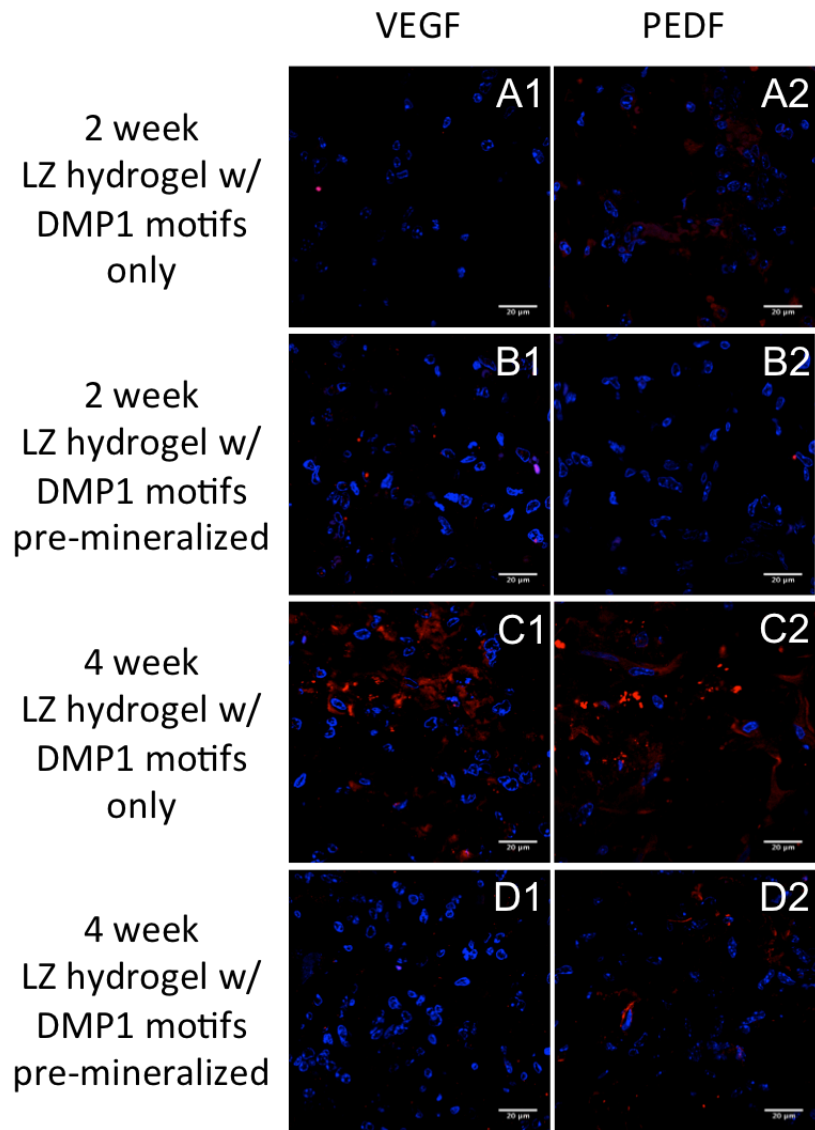


Figure 19. Immunofluorescence staining for angiogenic markers expressed by HMSC-seeded LZ scaffolds with DMP-1 calcium-binding motifs when implanted in immunocompromised mice.

(A1-A2) represent immunohistochemical localization of VEGF and PEDF in sections of LZ hydrogel scaffolds with DMP-1 calcium-binding motifs (1:1:1 LZ-Control:LZ-ESQES:LZ-QESQSEQDS) without mineralization and implanted subcutaneously in immunocompromised mice for 2 weeks, (C1-C2) are representative images showing the expression of the angiogenic markers after 4 weeks of implantation. (B1-B2) represent the expression of the above mentioned factors on sections obtained from LZ hydrogel scaffolds with DMP-1 calcium-binding motifs subjected to mineralization under high calcium and phosphate concentrations and then implanted subcutaneously in immunocompromised mice for 2 weeks, (D1-D2) are representative images showing the expression levels from sections obtained after 4 weeks of implantation.

and PEDF presence was high as shown in Figure 19C1 and 19C2 indicating an active vascularization process. On the other hand, the mineralized LZ hydrogel did not show the presence of VEGF and PEDF at 2 weeks of implantation (Figure 19B1-B2). At 4 weeks, PEDF was observed when VEGF was still absent indicating that vasculogenesis may have been initiated between 2 weeks and 4 weeks (Figure 19D1-D2). Overall, these results indicate that the mineralized matrix delays the process of vasculogenesis.

B.6. Evaluation of osteogenic differentiation of HMSCs seeded on premineralized leucine zipper hydrogels with DMP-1 calcium-binding motifs

The presence of calcium phosphate has been shown to induce osteogenic differentiation of stem cells [222, 223]. Therefore, we evaluated the ability of premineralized LZ hydrogel scaffold to promote osteogenic differentiation in vivo in a subcutaneous model. The immunofluorescence staining was performed to look for markers of osteogenesis like DMP-1, GRP-78, RUNX2, and phosphoserine in the control and premineralized experimental sections of 1:1:1 LZ-Control:LZ-ESQES:LZ-QESQSEQDS LZ hydrogels. Sections from 2 and 4 weeks implantation time points were analyzed. Figure 20 shows the results from these experiments.

RUNX2 is a key transcription factor and essential for osteogenic differentiation and bone formation [224, 225]. DMP-1 plays an important role in mineralization, ossification, cell attachment, and differentiation and is expressed in cartilage, bone, and dentin [226-229]. In the control 1:1:1 LZ-Control:LZ-ESQES:LZ-QESQSEQDS LZ hydrogel at 2 weeks of implantation, the seeded HMSCs show low levels of RUNX2 (Figure 20A1). At 4 weeks, the expression level of RUNX2 increased (Figure 20C1). This result indicates that the seeded HMSCs could undergo osteogenic differentiation. Osteogenic differentiation of HMSCs were also confirmed by DMP-1 immunofluorescence. Results show that DMP-1 expression levels were upregulated at 4 weeks of implantation when compared to 2 weeks (Figure 20A2 and 20C2).

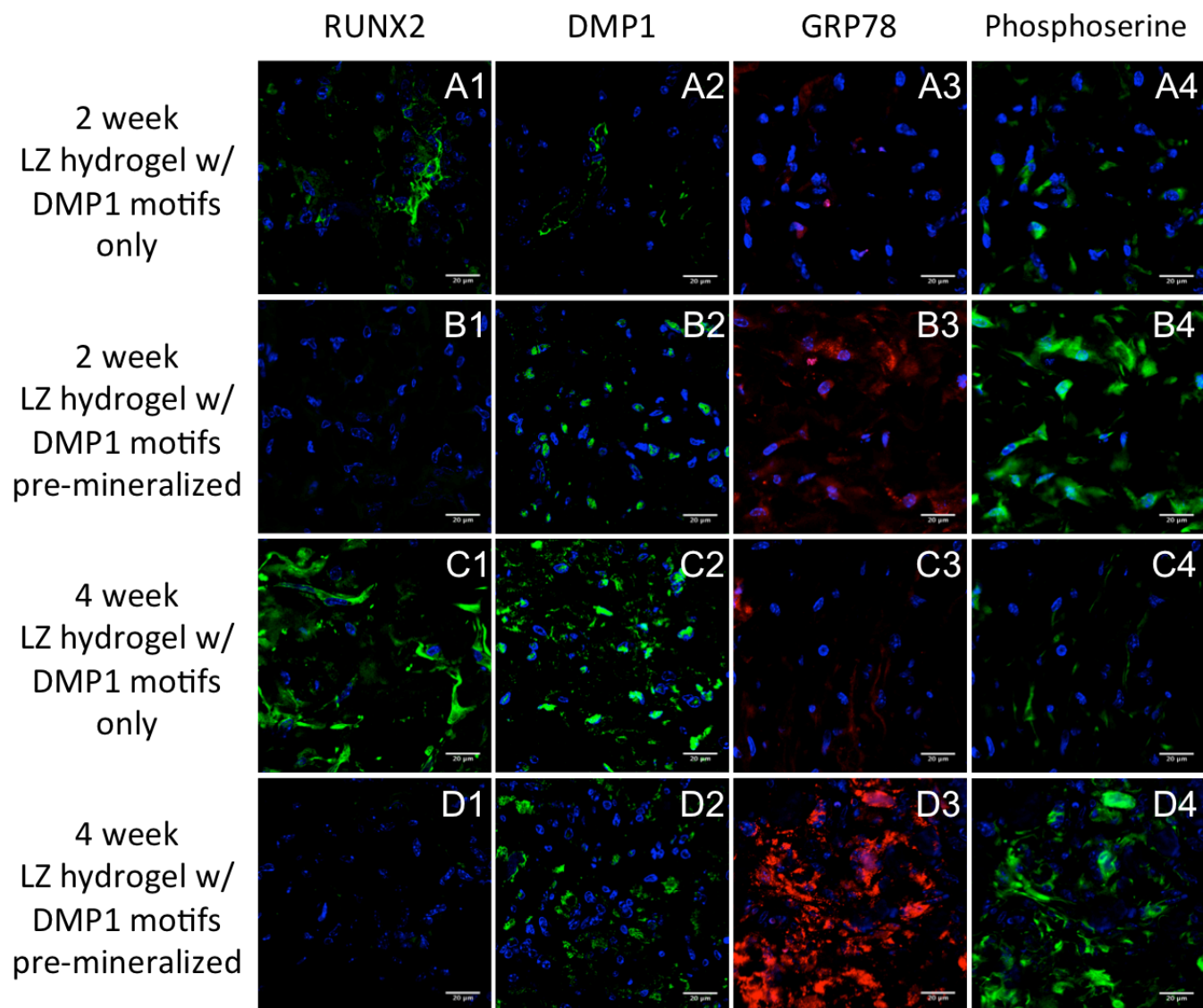


Figure 20. Immunofluorescence staining for osteogenic markers. HMSC-seeded LZ scaffolds with DMP-1 calcium-binding motifs were implanted in immunocompromised mice.

(A1-A4) represent localization of RUNX2, DMP-1, GRP78, and phosphoserine in sections of LZ hydrogel scaffolds with DMP-1 calcium-binding motifs (1:1:1 LZ-Control:LZ-ESQES:LZ-QESQSEQDS) without pre-mineralization and implanted subcutaneously in immunocompromised mice for 2 weeks. (C1-C4) are representative images showing the same from the hydrogel implanted for 4 weeks. (B1-B4) represent immunohistochemical localization of same set of protein markers in sections of LZ hydrogel scaffolds with DMP-1 calcium-binding motifs subjected to mineralization with high calcium and phosphate concentrations and implanted subcutaneously in immunocompromised mice for 2 weeks, (D1-D4) are representative images showing the same from the hydrogel implanted for 4 weeks.

GRP-78 is well known for its major intracellular function as a molecular chaperone for protein folding, endoplasmic reticulum (ER) calcium-binding, or regulation of the ER stress sensors [230]. Recently, it has been shown to serve as a receptor for DMP-1 mediated signaling events and also as a facilitator of biomineralization [231]. Presence of GRP78 is necessary for osteoblast differentiation and matrix mineralization [232]. Therefore it can be treated as an osteogenic marker.

During biomineralization, phosphorylated proteins serve as source of phosphorus for calcium phosphate nucleation. Therefore, the increased presence of phosphorylated proteins can be an indicator for mineralized matrix formation [233, 234]. The phosphoserine antibody stains all proteins with phosphoserine residues and was used as a marker for mineralization read out..

In the control 1:1:1 LZ-Control:LZ-ESQES:LZ-QESQSEQDS LZ hydrogel after 2 and 4 weeks, the expression of GRP78 and phosphoserine were both low (Figure 20A3-A4 and C3-C4). This result is consistent with that of the RUNX2 and DMP-1 staining indicating that the seeded HMSCs were still in the osteogenic differentiation stage.

On the other hand, the HMSCs didn't express RUNX2 in the 1:1:1 LZ-Control:LZ-ESQES:LZ-QESQSEQDS mineralized LZ hydrogel after 2 and 4 weeks of implantation (Figure 20B1 and 20D1). At the same time DMP-1 expression level did not change from 2 weeks to 4 weeks time point (Figure 20B2 and 20D2). This indicates that the pre-seeded HMSCs were not in the osteogenic differentiation stage. Examination of GRP78 immunofluorescence staining,

however, showed expression at 2 weeks and the intensity increased from 2 to 4 weeks time point (Figure 20B3 and 20D3); the phosphoserine staining also showed an abundance of phosphorylated proteins in the LZ hydrogel at both 2 and 4 weeks (Figure 20B4 and 20D4).

These results indicated that the pre-seeded HMSCs embedded cells initiated osteogenic differentiation at the 2 weeks time point. Multiple studies have shown that the stiffer cell culture substrates might promote stem cell differentiation [235-238]. Therefore, our results agree with published reports.

B.7. Calcified matrix formation in *in vivo* implanted 1:1:1 leucine zipper scaffold with calcium-binding DMP-1 motifs

In order to identify calcified matrix formation in the subcutaneous implanted LZ hydrogels, alizarin red staining was performed. The alizarin red staining is primarily used to indicate the presence of calcium in the tissue. Polarized light microscopy was also used to confirm the presence of calcium phosphate deposits. The calcium phosphate mineral will show birefringence under the polarized light.

In Figure 21, we stained the 1:1:1 LZ-Control:LZ-ESQES:LZ-QESQSEQDS LZ hydrogel with and without mineralization after 2 and 4 weeks of subcutaneous implantation with alizarin red (Figure 21A1-21D1) and also imaged the slides under polarized light (Figure 21A2-21D2). In the implanted LZ hydrogel without mineralization, we observed some granular aggregation of mineral deposits in the peripheral region after 2 weeks of implantation (Figure 21A1) and the mineral deposit was also verified by the birefringence under the polarized light (Figure 21A2). After 4 weeks, the granular aggregations were reduced and instead formed a constant and homogeneous distribution of mineral deposition in the peripheral areas (Figure 21C1). This result suggests that the pre-seeded HMSCs were undergoing osteogenic differentiation and forming a calcified matrix. At longer time points, the CaP deposition was spread throughout the scaffold. The implanted premineralized 1:1:1 LZ-Control:LZ-ESQES:LZ-QESQSEQDS LZ hydrogel showed positive staining for alizarin as it already contained calcium deposits (Figure 21B1). This was also confirmed by polarized

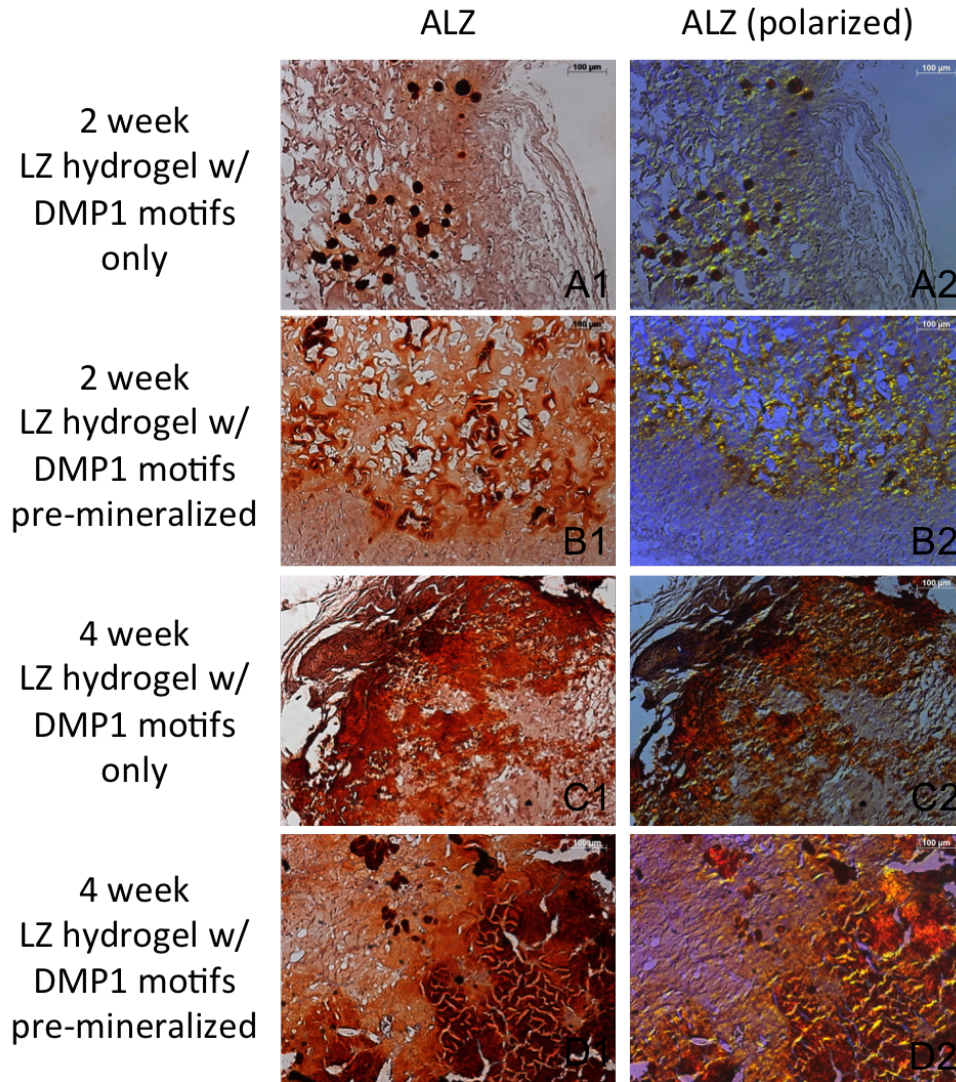


Figure 21. Histology staining of HMSC-seeded LZ scaffolds with DMP-1 calcium-binding motifs implanted in immunocompromised mice.

(A1-D1) are representative images of alizarin red (ALZ) stained sections of implanted scaffolds LZ hydrogel with DMP-1 calcium-binding motifs (1:1:1 LZ-Control:LZ-ESQES:LZ-QESQSEQDS) subjected to with and without pre-mineralization and seeded with HMSCs and implanted for 2 and 4 weeks. (A2-D2) are the polarized-light micrographs in the implanted scaffolds including with and without pre-mineralization treatment LZ hydrogel with DMP-1 calcium-binding motifs (1:1:1 LZ-Control:LZ-ESQES:LZ-QESQSEQDS) containing HMSCs after 2 and 4 weeks. Note the birefringence is relative to mineral density.

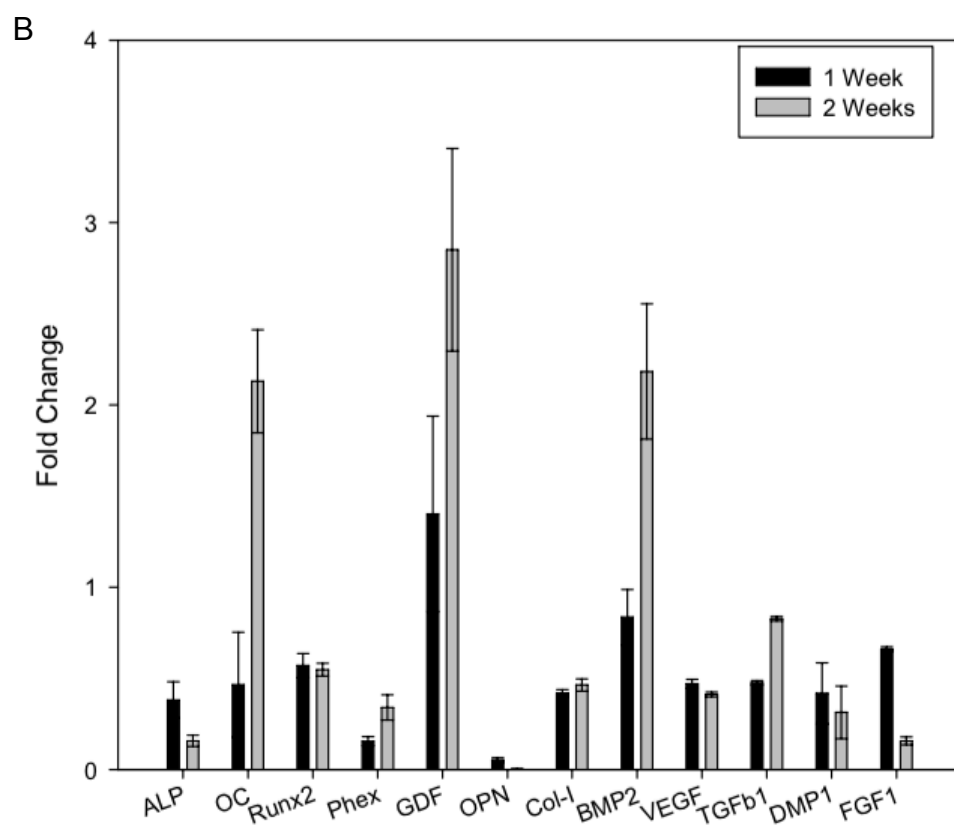
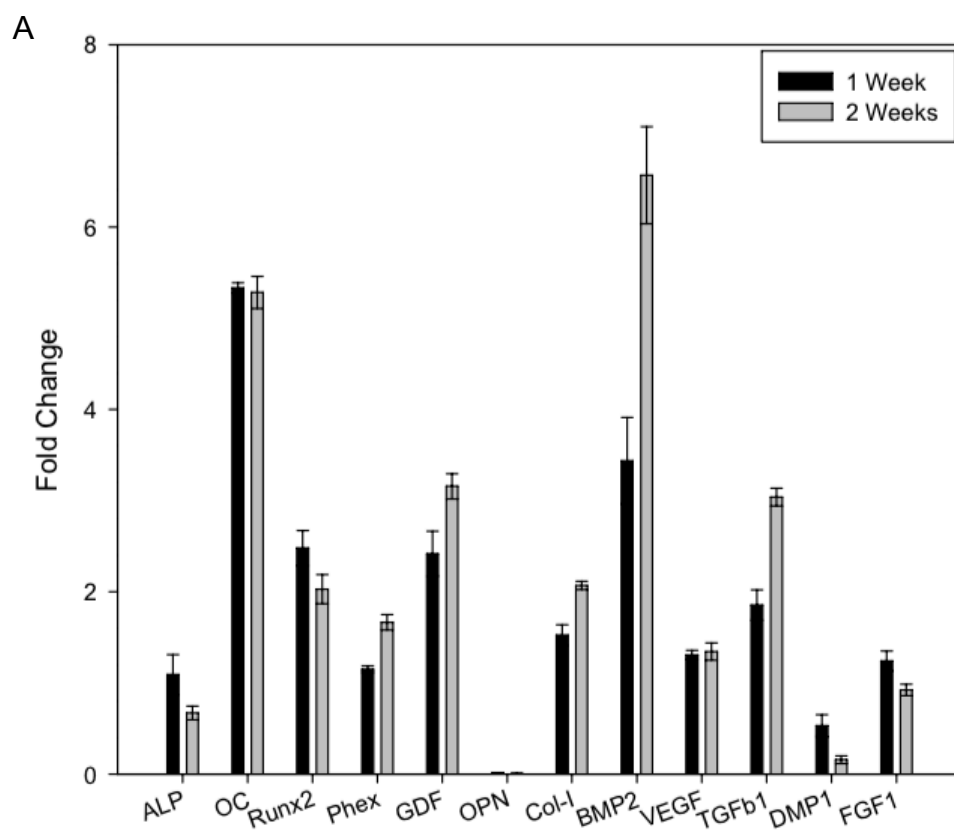
light microscopy (Figure 21B2). After 4 weeks of implantation, the LZ hydrogel shows stronger alizarin red staining (Figure 21D1) as well as stronger birefringence under the polarized light (Figure 21D2). The change in intensity of alizarin red staining between 2 and 4 weeks suggests increased mineral deposition. This supports our previous hypothesis that a stiffer substrate promotes faster osteogenic differentiation of HMSCs.

B.8. Evaluation of osteogenic gene expression in leucine zipper hydrogel with DMP-1 motifs

Gene regulation studies were conducted for HMSCs isolated from LZ hydrogels cultured under *in vitro* conditions. HMSCs were seeded on LZ hydrogels including LZ-Control hydrogel, 1:1:1 LZ-Control:LZ-ESQES:LZ-QESQSEQDS hydrogel with or without mineralization treatment for up to 2 weeks. The expression of the key osteogenic differentiation and mineralization related markers were evaluated and the results are shown in Figure 22.

Figure 22A shows the fold change in gene expression of HMSCs cultured on the LZ hydrogel with DMP-1 calcium-binding domains without mineralization treatment and compared with HMSCs cultured on LZ-Control hydrogel. The result shows that most of the osteogenic differentiation markers like RUNX2 and OC were up regulated in the LZ hydrogel scaffold containing DMP-1 calcium-binding motifs when compared with the LZ-Control hydrogel. DMP-1 is well known to function as a signaling molecule in osteogenic differentiation [239]. This result suggests that the calcium-binding domains derived from DMP-1 might play a regulatory role in regulating osteogenic differentiation through specific signaling mechanism.

Figure 22B shows the fold change in gene expression of HMSCs cultured on the LZ hydrogel with DMP-1 calcium-binding domains with mineralization treatment when compared with HMSCs cultured on the LZ-Control hydrogel without any treatment. The result shows high expression level of OC, GDF and



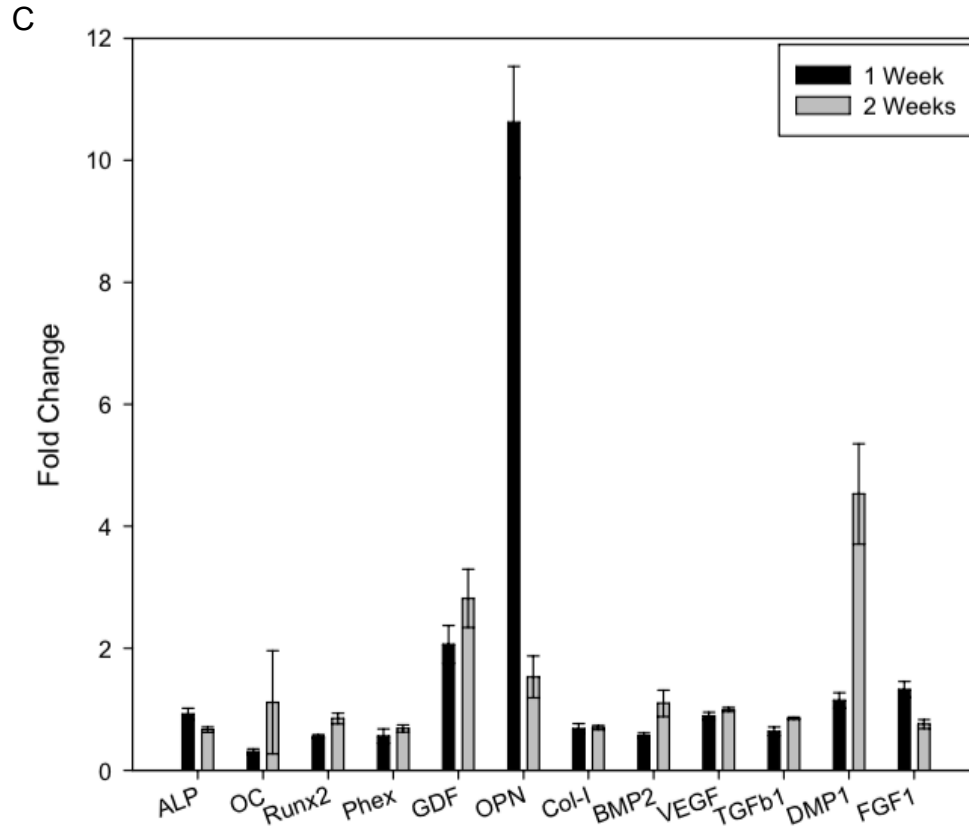


Figure 22. *In vitro* quantitative RT-PCR analysis was performed to determine osteogenic related gene expression levels on HMSCs seeded on LZ hydrogels.

(A) represents the gene expression levels obtained from HMSC seeded LZ hydrogel scaffolds with DMP-1 calcium-binding motifs (1:1:1 LZ-Control:LZ-ESQES:LZ-QESQSEQDS) without pre-mineralization and implanted for 1 and 2 weeks. The fold changes are respective to LZ-Control hydrogel without any treatment. (B) represents the gene regulation of premineralized LZ hydrogel scaffolds with DMP-1 calcium-binding motifs (1:1:1 LZ-Control:LZ-ESQES:LZ-QESQSEQDS) seeded with HMSCs and implanted for 1 and 2 weeks. The fold changes are respective to LZ-Control hydrogel without any treatment. (C) represents the gene regulation of premineralized LZ hydrogel scaffolds with DMP-1 calcium-binding motifs (1:1:1 LZ-Control:LZ-ESQES:LZ-QESQSEQDS) seeded with HMSCs and implanted for 1 and 2 weeks. The fold changes are respective to LZ hydrogel scaffolds with DMP-1 calcium-binding motifs without pre-mineralization. Note 1 fold change was considered as the baseline of control.

BMP-2 at 2 weeks. This suggests that DMP-1 mediated mineralized scaffolds facilitate osteogenic differentiation. It is well established that DMP-1 plays a critical role to regulate the calcification of the ECM [226] and is involved in bone and dentin formation [240]. GDF gene was significantly up regulated at 1 and 2 weeks. GDF is also known as BMP-3B and is involved in the bone formation and craniofacial skeletogenesis [241, 242], and maintains high level of expression during osteogenesis [243]. The up regulation of GDF and BMP-2 indicate pro-osteogenic differentiation of the HMSCs. It suggests this could be contributed to the stiffer LZ hydrogel coated with calcium phosphate deposits. This result is consistent with previous studies demonstrate that the HMSCs differentiation can be controlled by the stiffness of the hydrogel [168]. Furthermore, it is possible that the calcium phosphate deposits might provide a sufficient source of calcium ions to the HMSCs and hence facilitate osteogenic differentiation. The increased concentration of calcium ions may also affect cell behavior and morphology facilitating cell-cell or cell-matrix interaction. Published studies have also indicated that high concentrations of calcium ions can enhance osteogenic differentiation and mineralization potential of mesenchymal cells [244]. Hence, the mineralized LZ hydrogel matrix may provide a suitable microenvironment to mimic bone matrix.

Figure 22C shows the gene expression fold changes of the HMSCs cultured on LZ hydrogel with DMP-1 motifs mineralized or unmineralized. The result shows high expression level of GDF, OPN and DMP-1. OPN is a phosphorylated glycoprotein with different functions and is found in several

different cell types including osteoblast. During the bone development, OPN is secreted by osteoblasts at the earlier stage. This has been suggested to promote the osteoblasts adhesion to the ECM [245]. OPN is also involved in regulating cell adhesion through the integrin ligand [246]. The up regulation of GDF, OPN and DMP-1 indicate the tendency of HMSC to undergo osteogenic differentiation when cultured on mineralized LZ hydrogel scaffold is higher than unmineralized LZ hydrogel. This implies the effect of osteogenic differentiation from the mechanical cues due to stiffer matrix may be higher than the signaling cues achieved by the unmineralized LZ hydrogel scaffold.

Based on these results, it could be concluded that the cells respond to osteogenic differentiation based on the microenvironment. The mineralized hydrogel scaffold might be osteoconductive and promote expression of both early and late markers for osteogenic differentiation are observed.

C. Synthesis of leucine zipper hydrogels with growth factor releasing properties for hard tissue engineering

C.1. The LZ-MMPHEP hydrogel can bind heparin and heparin-binding growth factors

The chimeric LZ-MMPHEP protein construct is shown in Figure 1F. The LZ-MMPHEP contains the heparin-binding sequence LRKKLGKA selected from a previously published study [124]. The heparin-binding domain was inserted to aid the tethering of heparin-binding growth factors such as VEGF, TGF- β 1, and BMP-2. A cleavage site IPVSLRSG [247] was placed between the LZ protein backbone and the heparin-binding domain to facilitate proteolytic cleavage in vivo and thereby release the bound growth factors.

The LZ-MMPHEP hydrogel used in this study was a 1:9 mixture of LZ-MMPHEP:LZ-Control 7% w/v hydrogel. In order to verify the growth factor binding ability of the LZ-MMPHEP hydrogel, immunofluorescence imaging was carried out after both of the LZ-Control and the LZ-MMPHEP hydrogel were used for heparin followed by VEGF binding. The results from the confocal microscopy images are shown in Figure 23. After excessive wash to negate the non-specific binding, the LZ-MMPHEP hydrogel showed homogenous distribution of TRITC tagged VEGF (Figure 23B) while LZ-Control only showed minimal non-specific signals (Figure 23A). This experiment provided validation of the concept of using LZ hydrogel as a growth factor reservoir by means of heparin-binding.

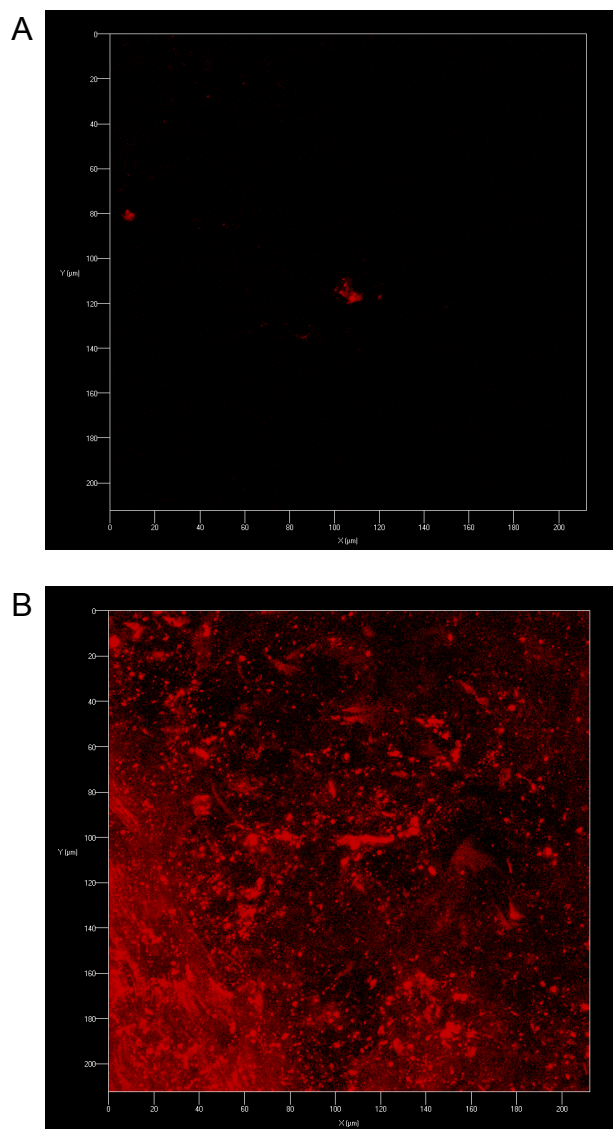


Figure 23. Functionality of the heparin-binding domain on the LZ-MMPHEP hydrogel.

Binding experiments were performed by premixing recombinant VEGF with heparin in PBS and soaking the hydrogels in the mixture, followed by extensive washing and treatment with TRITC secondary. Shown here are 3-D reconstruction of z-stack confocal images obtained from LZ-Control hydrogel (A), or LZ-MMPHEP hydrogel (LZ-Control:LZ-MMPHEP = 9:1) (B).

C.2. Growth factor binding efficiency of the LZ-MMPHEP hydrogel

A series of *in vitro* LZ-MMPHEP hydrogel characterization was carried out including the testing of the efficiency of binding of heparin-binding growth factor. The LZ-MMPHEP hydrogels were incubated with heparin and VEGF as described in materials and methods section. The remaining heparin and VEGF mixture and the wash PBS solution were then collected. The amount of unbound VEGF was analyzed using dot-blots. The intensity of each sample (dot) was compared and converted to VEGF quantity using a standard curve (Figure 24A).

Two concentrations of 10 ng and 20 ng VEGF were used in the initial heparin and VEGF mixture in PBS for both LZ-Control and LZ-MMPHEP hydrogel binding efficiency test. The binding efficiency results are shown in Figure 24B. The results show that in the LZ-MMPHEP hydrogel, the loaded VEGF amounts were about 70% for both 10 ng and 20 ng VEGF in the initial loading (Figure 24B). In contrast, only about 10% and 30% of VEGF bound to LZ-Control hydrogel.

It is worth noting the mole ratio of the VEGF to the heparin-binding domain quantity, as 20 ng of VEGF is about 952 fmole; the moles of heparin-binding domain in the LZ hydrogel is about 3.62 nmole showing around 3800 fold more available heparin-binding capacity compared to VEGF assuming a 1:1 binding stoichiometry.

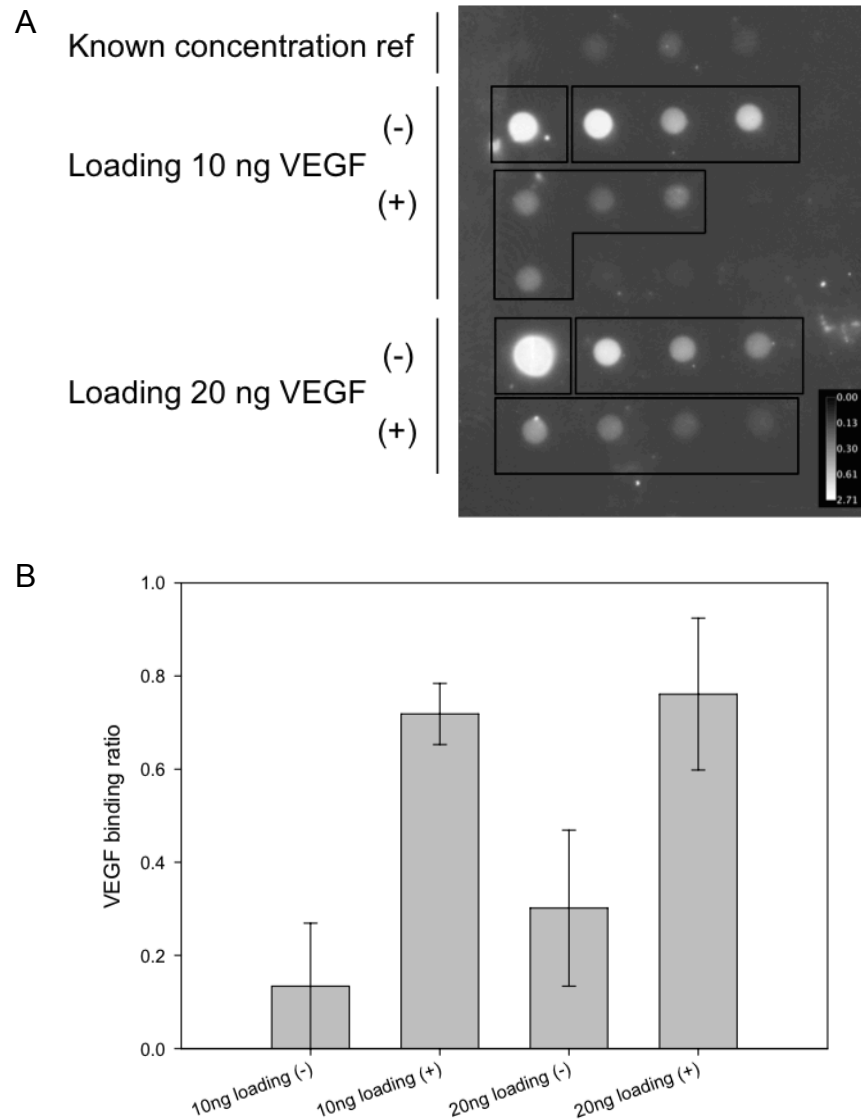


Figure 24. Growth factor binding efficiency of the LZ-MMPHEP hydrogel.

VEGF was mixed with heparin in varying amounts (10 ng and 20 ng) in PBS, and the LZ- Control hydrogel (-) or LZ-MMPHEP hydrogel (LZ-Control:LZ-MMPHEP = 9:1) (+) were soaked in this mixture. The loaded VEGF was determined by analyzing the density of the spots on the dot-blot (A). The LZ-MMPHEP hydrogel loaded VEGF at approximately 70% of efficiency. Higher VEGF concentration was shown to increase non-specific binding in LZ-control hydrogel (B).

C.3. Growth factor release profile from the LZ-MMPHEP hydrogel

The heparin-binding growth factor release profile was also carried out by using the dot-blot to determine the released growth factor quantity. The initial loading of VEGF was 20 ng. Different amount of MMP-2 (20 ng or 50 ng) was added during the incubation. The results are shown in Figure 25. The LZ-MMPHEP hydrogel released about 60% of its loaded VEGF over a period of 11 days without the presence of MMP-2. This self-releasing behavior might partially be due to the degradation of the LZ hydrogel by hydrolysis [213] that was shown in Figure 6.

Both MMP-2 concentrations showed significant increase in the rate of VEGF release at all time points after day 1 compared to the absence of MMP-. When comparing the difference between the two concentrations of MMP-2 used, although a higher (50 ng) MMP-2 amount showed more VEGF release in the first 5 days, it was not significantly high compared to lower (20 ng) MMP-2 amount. After 5 days of release, no significant change was observed between the two amounts of MMP-2. We predict that the MMP-2 to cleavage site ratio was so low (i.e. more sites without growth factors) that it negated the effect of a small change in concentration. Note the moles of MMP-2 was about 281.69 fmole for 20 ng and 704.23 fmole for 50 ng.

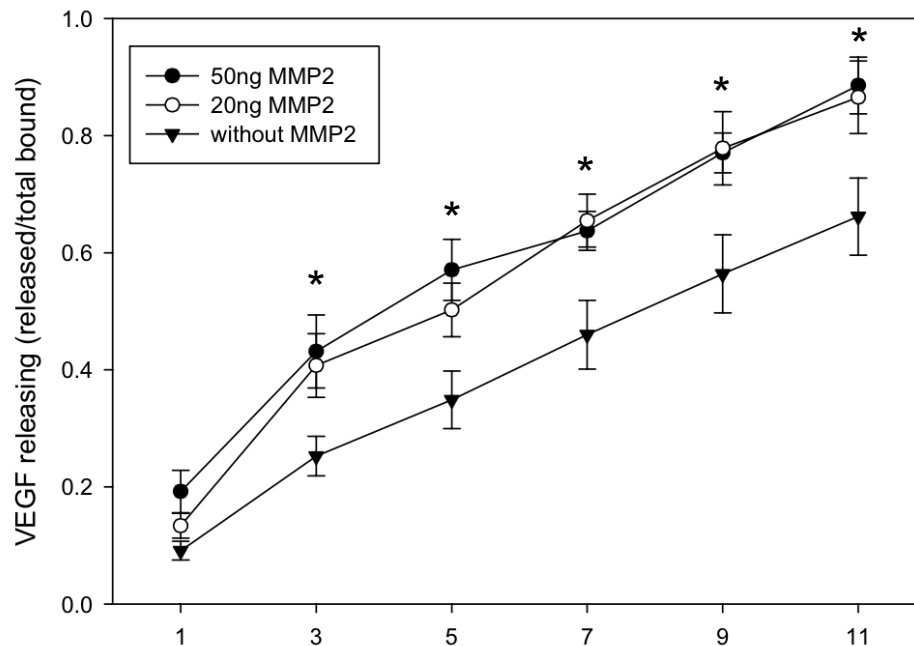


Figure 25. Release profile of VEGF loaded from the LZ-MMPHEP hydrogel in the presence of varying amounts of MMP-2.

The VEGF loaded LZ-MMPHEP hydrogel were incubated in PBS with or without presence of MMP-2 for over 11 days. Without MMP-2, the VEGF was released in a linear manner. Lack of burst effect demonstrates the self-degradation of the LZ hydrogel. In the presence of MMP-2, higher VEGF release was observed within 3 to 5 days. * represents statistical significance ($p < 0.05$ using students t-test) with respect to release without MMP-2.

C.4. Angiogenesis in the growth factor loaded LZ-MMPHEP hydrogels

To study the *in vivo* behavior of the growth factor-loaded LZ hydrogels, we performed subcutaneous implantation in nude mice. Two growth factors were tested. They are TGF- β 1 and BMP-2. 20 ng of both growth factors was loaded onto the hydrogel right before implantation. Figure 26 shows a photograph of the LZ-Control and LZ-MMPHEP hydrogel explants after 1 and 2 weeks. We can observe angiogenesis and neovascularization in both of the LZ control hydrogels after 1 and 2 weeks (Figure 26A1-26A2). On the other hand, LZ-MMPHEP hydrogel with either TGF- β 1 or BMP-2 were smaller and degraded faster than the control hydrogel during the first week. They did not change much between 1 and 2 weeks (Figure 26B1-26B2 and 26C1-26C2). This result suggests that the loaded growth factors increased cellular activity and thereby increased the rate of LZ hydrogel degradation possibly due to increased MMP-2 production (Figure 26B1-26B2 and 26C1-26C2).

Figure 27 shows immunohistochemical analysis including H&E staining, and staining for angiogenesis markers CD31 and vWF. Figure 28 shows the immunofluorescence staining for VEGF and PEDF that were performed on the LZ hydrogel explant sections.

Utilizing H&E staining, the LZ-MMPHEP hydrogel loaded with TGF- β 1 and HMSCs showed ECM deposition after 1 week of implantation (Figure 27A1) and the ECM formation increased intensively after 2 weeks as the eosin staining turned much brighter (Figure 27B1). The CD31 and vWF immunohistochemical localization showed the same trend. At 1 week, there was positive staining for

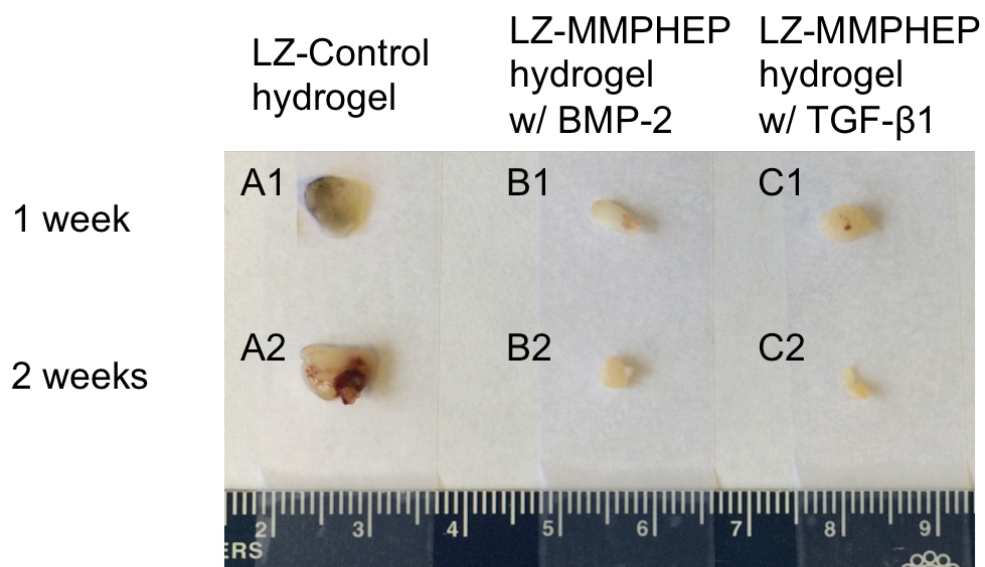


Figure 26. Images of the HMSC-seeded LZ scaffolds with heparin-binding domain and loaded with growth factors in immunocompromised mice.

Photo Images represent the LZ-Control hydrogel scaffolds (A1-A2), LZ hydrogel scaffolds with heparin-binding domain (9:1 LZ-Control:LZ-MMPHEP) and loaded with BMP-2 (B1-B2), and TGF- β 1 (C1-C2) and implanted subcutaneously in immunocompromised mice for 1 and 2 weeks

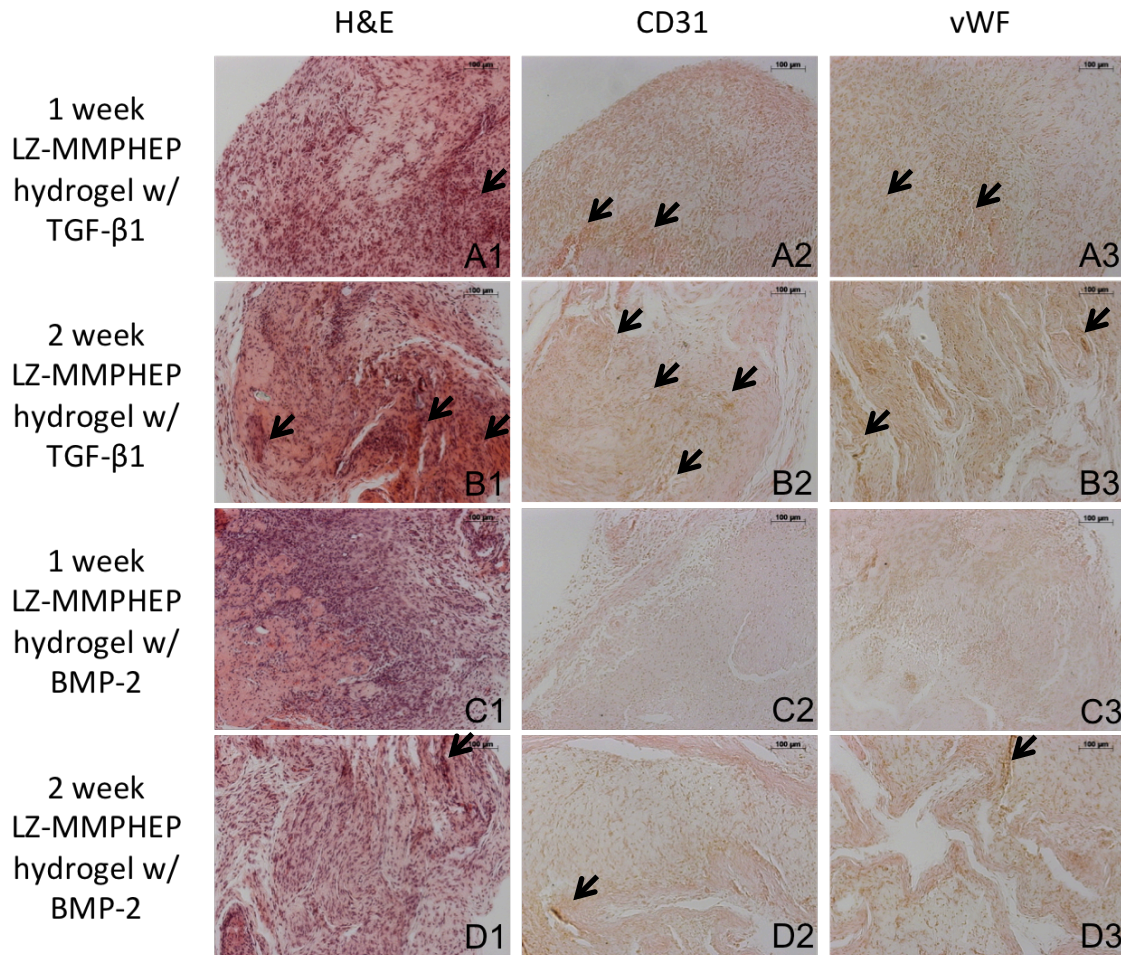


Figure 27. Histology staining and immunohistochemical analysis of HMSC-seeded LZ hydrogel scaffolds with heparin-binding domain loaded with growth factors and implanted in immunocompromised mice.

(A1-D1) are representative images of H&E stained sections of implanted LZ hydrogel scaffolds with heparin-binding domain (9:1 LZ-Control:LZ-MMPHEP) and loaded with TGF- β 1 or BMP-2 containing HMSCs after 1 and 2 weeks. (A2-D2 and A3- D3) are representative images showing the immunohistochemical localization of CD31 (A2-D2) and vWF (A3-D3) in the implanted LZ hydrogel scaffolds with heparin-binding domain (9:1 LZ-Control:LZ-MMPHEP) and loaded with TGF- β 1 or BMP-2 containing HMSCs after 1 and 2 weeks.

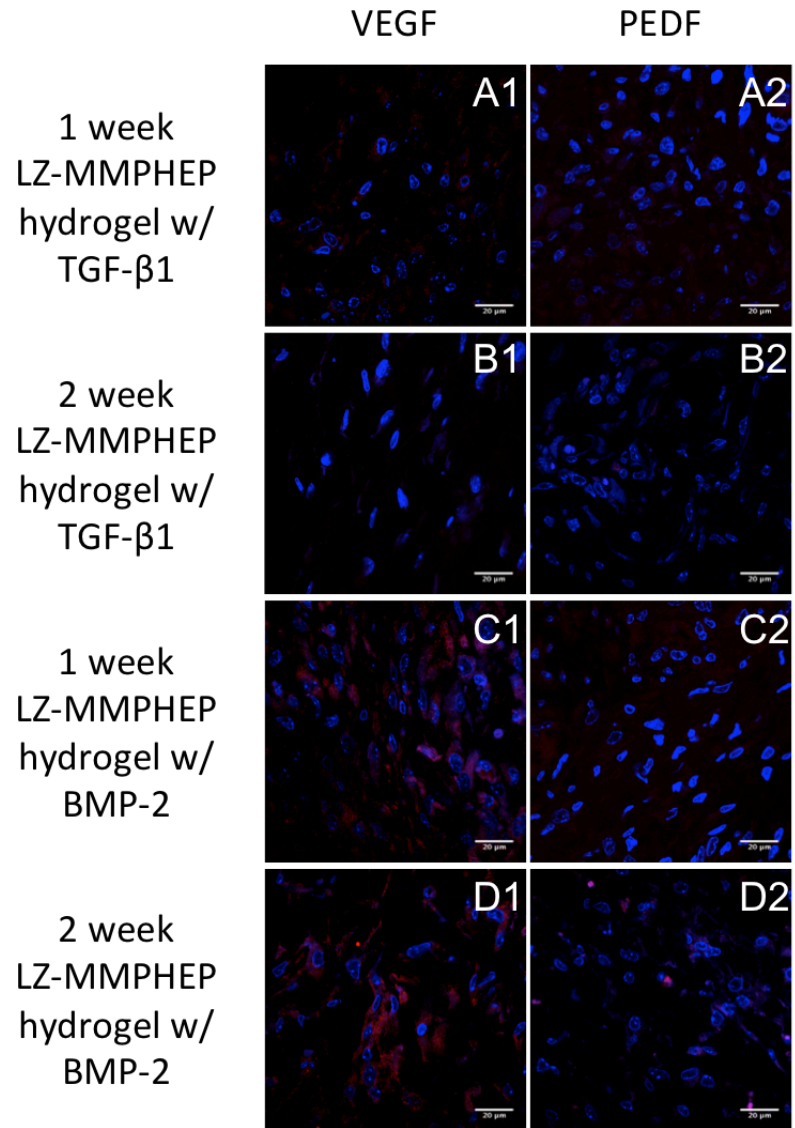


Figure 28. Immunofluorescence staining for angiogenesis markers of HMSC-seeded LZ scaffolds with heparin-binding domain loaded with growth factors and implanted in immunocompromised mice.

(A1-A2) represent immunohistochemical localization of VEGF and PEDF in sections of LZ hydrogel scaffolds with heparin-binding domain (9:1 LZ-Control:LZ-MMPHEP) and loaded with TGF- β 1 and implanted subcutaneously in immunocompromised mice for 1 week, (B1-B2) are representative images showing the same from the hydrogel implanted for 2 weeks. (C1-C2) represent immunohistochemical localization of same set of protein markers in sections of LZ hydrogel scaffolds with heparin-binding domain (9:1 LZ-Control:LZ-MMPHEP) and loaded with BMP-2 and implanted subcutaneously in immunocompromised mice for 1 week. (D1-D2) are representative images showing the same from the hydrogel implanted for 4 weeks.

CD31 and vWF in the peripheral region of the LZ hydrogel section (arrows in Figure 27A2 and 27A3) but the expression became more homogenous at 2 weeks (arrows in Figure 27B2 and 27B3). The expression of CD31 and vWF indicates the presence of endothelial cells in the hydrogel. In fact when examining the photographic image of the implanted LZ hydrogel, some vascularization could be seen (Figure 26C1) after 1 week of implantation. The immunofluorescence staining was consistent with the immunohistochemical staining for CD31 and vWF, and showed VEGF localization at 1 week of implantation (Figure 28A1) but downregulated at 2 weeks (Figure 28B1). This indicates that angiogenesis was initiated before the 1 week time point. PEDF did not show any localization at both 1 and 2 weeks for LZ-MMPHEP hydrogel loaded with TGF- β 1 (Figure 28A2 and 28B2).

The LZ-MMPHEP hydrogel loaded with BMP-2 and HMSCs showed high cell density at 1 week (Figure 27C1) and angiogenesis was observed at 2 weeks (arrow in Figure 27D1). The CD31 and vWF immunohistochemical staining indicated no expression at 1 week (Figure 27C2-27C3) and its absence in the peripheral region of the hydrogel section (Figure 27D2-27D3). At 2 weeks immunofluorescence staining, showed the presence of VEGF at both 1 and 2 weeks (Figure 28C1-28C2). No PEDF expression was observed at both time points (28D1-28D2). These results suggest that the LZ-MMPHEP hydrogel with BMP-2 and HMSCs showed angiogenesis but at a slower pace when compared with the TGF- β 1 loaded LZ-MMPHEP hydrogel.

C.5. Osteogenic differentiation of HMSCs in the growth factor loaded LZ-MMPHEP hydrogels in vivo

We examined the expression of osteogenic markers to track the *in vivo* response of the HMSCs to the growth factors (TGF- β 1 or BMP-2). The immunofluorescence staining images of RUNX2 and DMP-1 are shown in Figure 29.

At 1 week, the HMSCs in the LZ-MMPHEP hydrogel containing TGF- β 1 or BMP-2 showed expression of RUNX2 (Figure 29A1 and 29C1). We predict that this is due to both TGF- β 1 and BMP-2 being involved in the osteoblast differentiation pathway [248]. The immunofluorescence staining intensity was stronger in the BMP-2 loaded LZ-MMPHEP hydrogel indicating that the osteogenic potency of BMP-2 on HMSCs was higher. This was further confirmed by the DMP-1 staining in the BMP-2 loaded LZ-MMPHEP hydrogel that showed higher level of DMP-1 (Figure 29C2) expression compared to the TGF- β 1 loaded LZ-MMPHEP hydrogels (Figure 29A2).

RUNX2 expression level was muted in both TGF- β 1 and BMP-2 loaded hydrogels at 2 weeks (Figure 29B1 and 29D1). This could be attributed to the natural progression of the differentiation process. However, DMP-1 expression level remained consistent throughout the time points studied, confirming osteogenic differentiation (Figure 29B2 and 29D2).

The alizarin red staining is shown in Figure 30. The result shows calcium deposition and mineralization in the LZ-MMPHEP hydrogels loaded with TGF- β 1 and BMP-2. In comparison, both showed increased calcium accumulation from 1

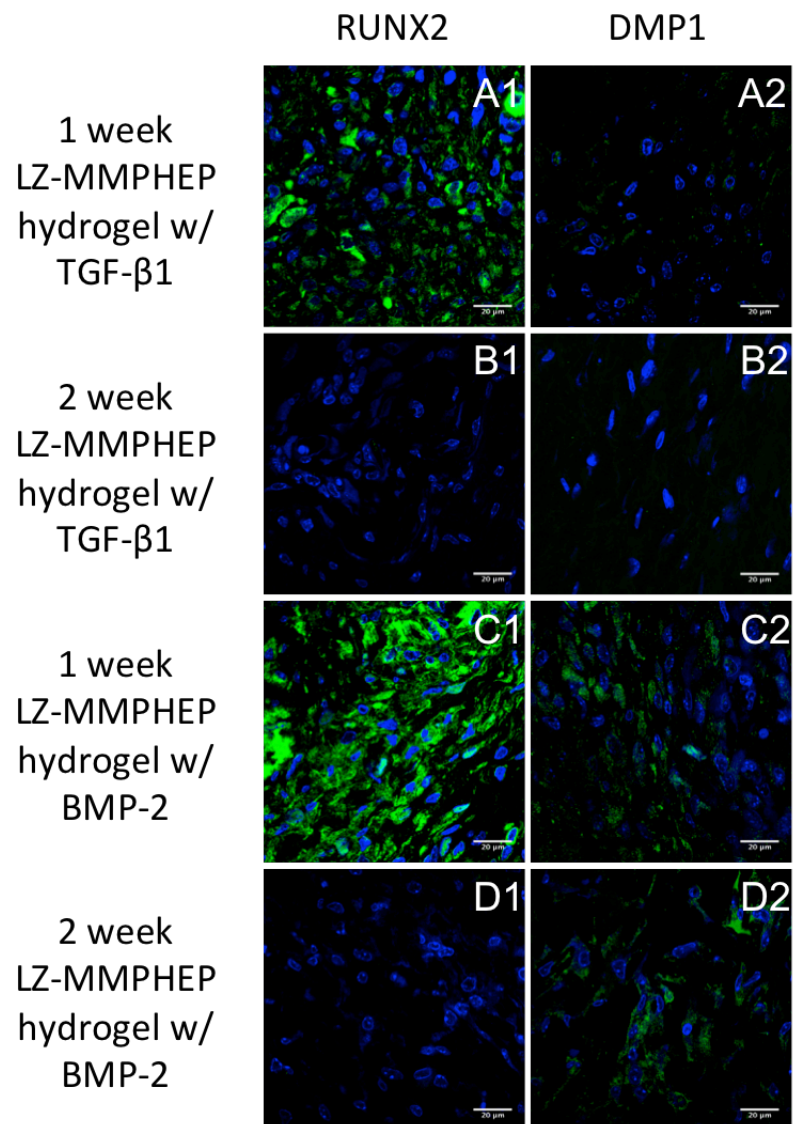


Figure 29. Immunofluorescence staining for osteogenic markers of HMSC-seeded LZ scaffolds with heparin-binding domain and loaded with growth factors and implanted in immunocompromised mice.

(A and B) represent immunohistochemical localization of RUNX2 and DMP-1 in sections of LZ hydrogel scaffolds with heparin-binding domain (9:1 LZ-Control:LZ-MMPHEP) and loaded with TGF- β 1 and implanted subcutaneously in immunocompromised mice for 1 week (A1-A2), and 2 weeks (B1-B2). (C and D) are representative images showing the same markers from LZ hydrogel scaffolds with heparin-binding domain (9:1 LZ-Control:LZ-MMPHEP) sections and loaded with BMP-2 and implanted subcutaneously in immunocompromised mice for 1 week (C1-C2), and 2 weeks (D1-D2)

week to 2 weeks (Figure 30A1-30D1). However, BMP-2 was more potent in inducing mineralization as the birefringence was observed as early as 1 week (Figure 30C2) indicating early onset of calcium deposition.

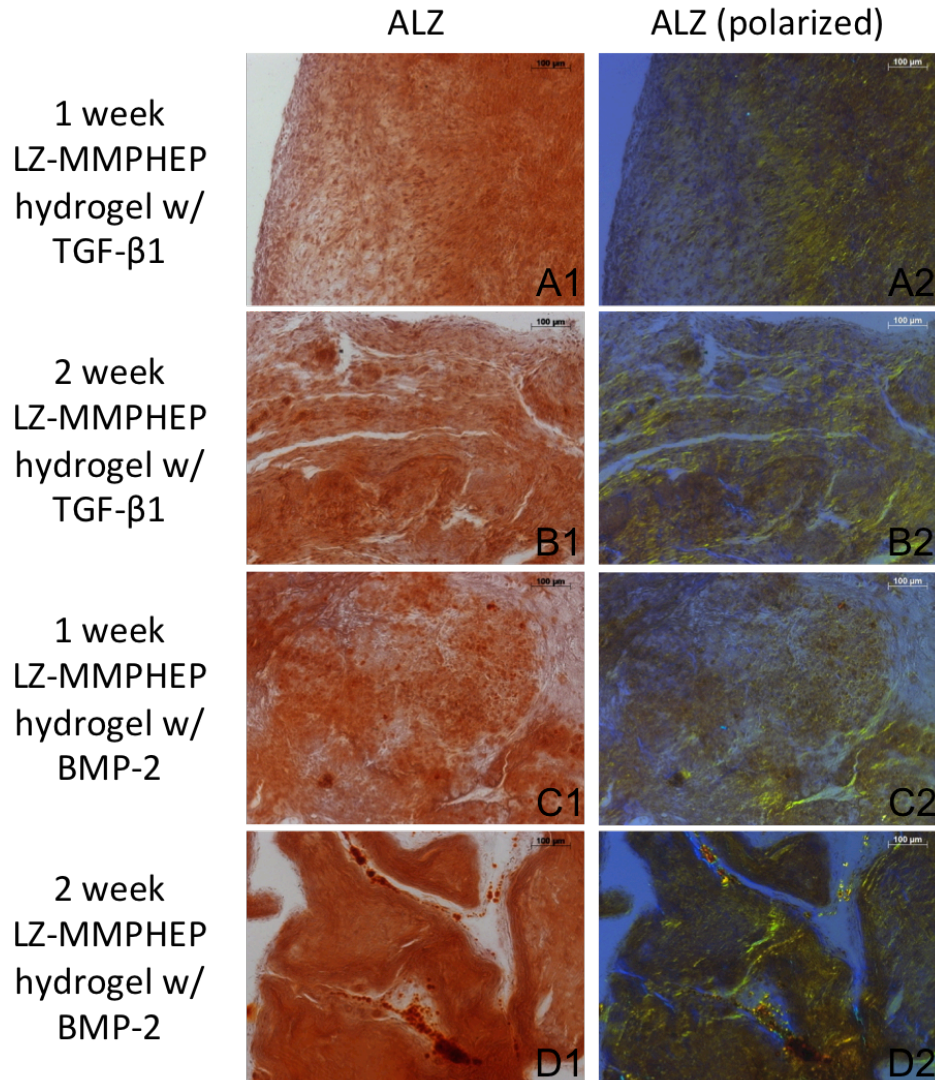


Figure 30. Histology staining and immunostaining for osteogenesis markers of HMSC-seeded LZ hydrogel scaffolds with heparin-binding domain and loaded with growth factors and implanted in immunocompromised mice.

(A and B) represent alizarin red (ALZ) staining and the polarized-light micrographs in sections of LZ hydrogel scaffolds with heparin-binding domain (9:1 LZ-Control:LZ-MMPHEP) and loaded with TGF- β 1 and implanted subcutaneously in immunocompromised mice for 1 week (A1-A2), and 2 weeks (B1-B2). (C and D) are representative images showing the same from the sections obtained from LZ hydrogel scaffolds with heparin-binding domain (9:1 LZ-Control:LZ-MMPHEP) and loaded with BMP-2 and implanted subcutaneously in immunocompromised mice for 1 week (C1-C2), and 2 weeks (D1-D2).

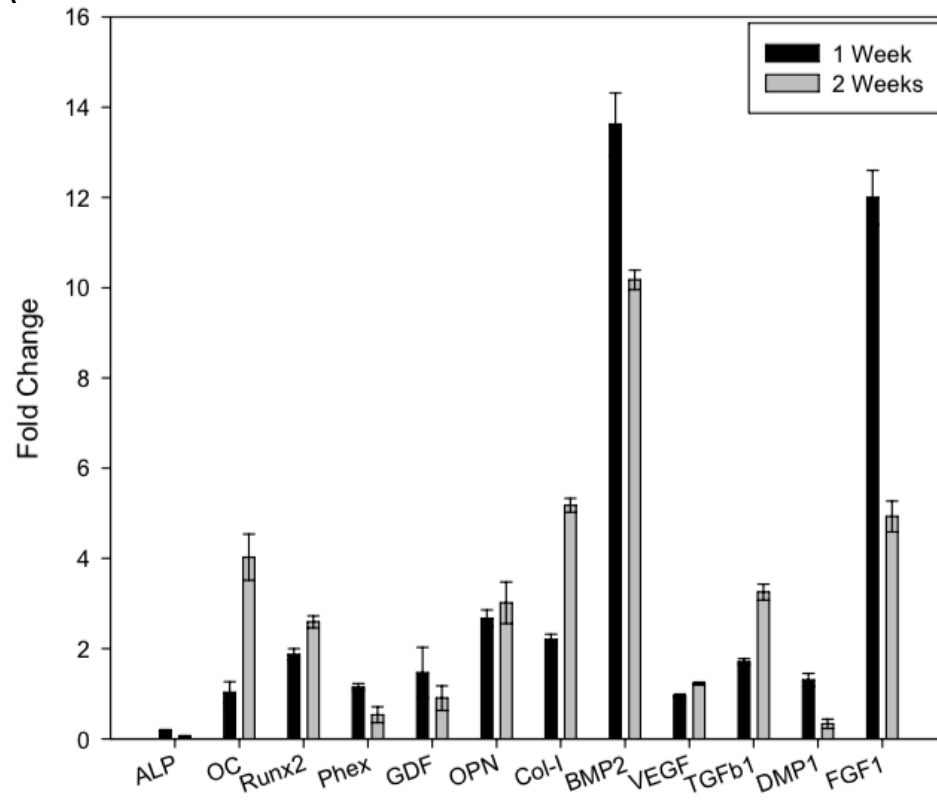
C.6. Regulation of osteogenic gene expression in LZ-MMPHEP hydrogels loaded with TGF- β 1 or BMP-1

Gene regulation studies were conducted on samples obtained from *in vitro* cell culture. HMSCs were seeded on LZ-Control hydrogel, 9:1 LZ-Control:LZ-MMPHEP hydrogel loaded with TGF- β 1 or BMP-2 for up to 2 weeks. The gene expression pattern of the key osteogenic differentiation and mineralization related markers were evaluated. The results are presented in Figure 31.

Figure 31A shows fold changes in gene expression of HMSCs in the TGF- β 1 loaded hydrogels with respect to controls (LZ hydrogels loading TGF- β 1). Results show that OC, RUNX2, OPN, TGF- β 1 expression was higher than control and increased between 1 and 2 weeks. BMP-2 and FGF1 showed the highest change. These results show that the TGF- β 1 tethered to the hydrogel is bioactive.

Figure 31B shows similar results for HMSC cultured on BMP-2 loaded hydrogels. In the presence of BMP-2, osteogenic markers were up regulated at 1 week. At 2 weeks, only OC was up regulated. Other genes either maintained same levels of expression or were down regulated. This change at 2 weeks could be related to the phenotypic changes of the cells as they differentiate to a functional mineralized matrix producing cell. In any event, the results show the feasibility of tethering growth factors to the hydrogel to influence cell fate.

A



B

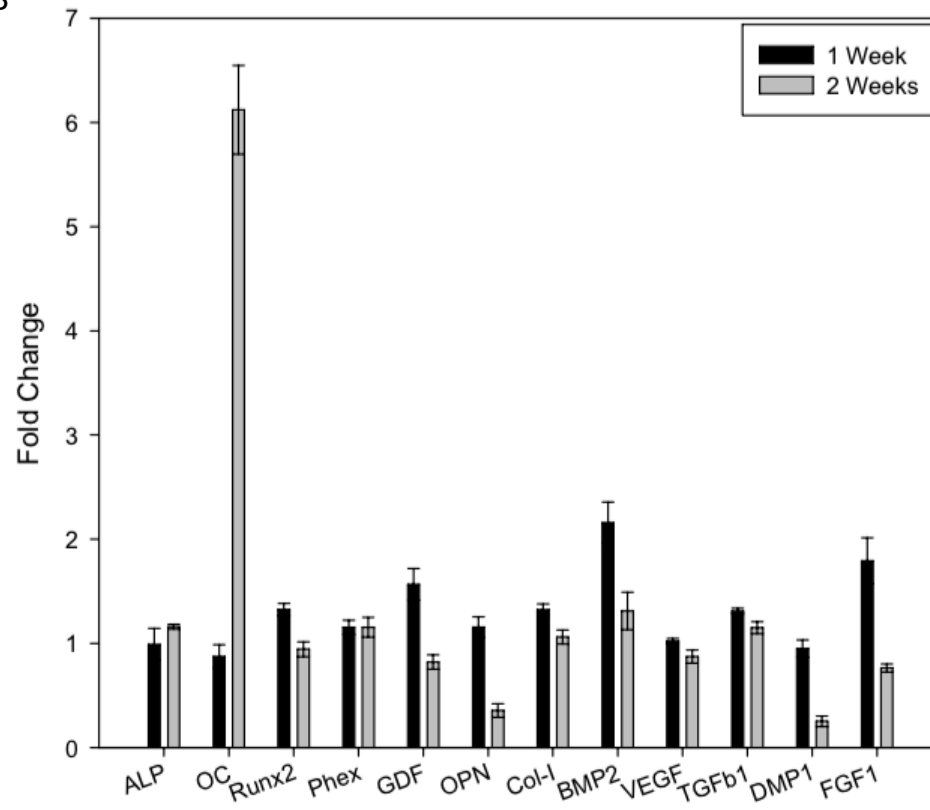


Figure 31. *In vitro* quantitative RT-PCR analysis of mRNA expression from HMSCs seeded on LZ hydrogel and implanted in immunocompromised mice.

(A) represents the gene expression levels of HMSCs obtained from LZ hydrogel scaffolds with heparin-binding domain (9:1 LZ-Control:LZ-MMPHEP) and loaded with TGF- β 1 and implanted subcutaneously in immunocompromised mice for 1 and 2 weeks. The fold changes are respective to LZ-Control hydrogel without any loading of growth factors. (B) represents gene expression levels of HMSCs obtained from LZ hydrogel scaffolds with heparin-binding domain (9:1 LZ-Control:LZ-MMPHEP) and loaded with BMP-2 and implanted subcutaneously in immunocompromised mice for 1 and 2 weeks. The fold changes were calculated with respect to LZ-Control hydrogel without any growth factors loaded.

IV. CONCLUSION

A. Synthesis and characteristic of a stable leucine zipper hydrogel; evaluation of the incorporated RGDS motif

In this study we have shown that leucine zipper, a self-assembling peptide can be utilized for the synthesis of a functional scaffold for tissue engineering. The engineered leucine zipper domain can facilitate the formation of physical and covalent crosslinks in hydrogel structures leading to the formation of interconnected pores of varying sizes and mechanical properties can be tuned by manipulating the peptide concentration. The LZ hydrogel can be further strengthened by dehydrothermal crosslinking treatment. This results in a stable hydrogel with delayed degradation rate. The biological functionality can also be achieved by incorporating various cell signaling domains. In this study we have used the integrin binding RGDS domain to be incorporated into the chimeric LZ protein backbone.

This is the first report on the development of a stable 3-D LZ hydrogel with tunable mechanical and biological properties. Increased cell adhesion, proliferation and migration of HMSCs within LZ-RGDS scaffolds suggest the potential use of this scaffold in various *in vivo* tissue engineering applications. *In vivo* experiments demonstrate that the LZ scaffolds do not trigger unfavorable foreign body response. This property is of significant advantage for tissue engineering applications. The unique ability of LZ scaffolds to permit neovascularization without the need for delivery of growth factors such as VEGF

creates new opportunities in tissue regeneration. Neovascularization ensures delivery of oxygen and nutrients during tissue regeneration.

Overall, the *de novo* synthesized LZ chimeric protein had better rheological properties; tunable pore size, permitted dynamic cellular interaction, host cell colonization and actively permitted vascularization making it a biologically active scaffold for tissue engineering.

B. Evaluation of the incorporated DMP-1 derived calcium binding motifs and the effect of high calcium and phosphate concentration on mineralization and cellular response of the leucine zipper hydrogel scaffold

The Dentin Matrix Protein-1 (DMP-1) derived calcium binding motifs, ESQES and QESQSEQDS, were used for being incorporated into the chimeric LZ protein backbone. The LZ hydrogel was cast with different combinations of these two calcium-binding motifs.

The results showed that the LZ hydrogel was able to adapt to the calcium binding function from the incorporated motifs. Subjecting the scaffold to *in vitro* nucleation test, showed that the 1:1:1 LZ-Control:LZ-ESQES:LZ-QESQSEQDS demonstrated higher amounts of calcium phosphate deposition under high calcium and phosphate concentrations but there was no significant advantage for nucleation under physiological concentrations of calcium and phosphate. This suggested that not only the LZ hydrogel was capable of initiating calcium phosphate deposition due to the calcium-binding motifs for trapping calcium ions, but also was capable to form crystalline hydroxyapatite structures when the 2

peptides containing LZ's were mixed in a defined ratio. This, further demonstrates that the LZ hydrogel is tunable and mineral deposition can increase the mechanical properties depending upon its use in tissue engineering applications. The *in vivo* subcutaneous implantation studies in nude mice also showed different response of the pre-seeded HMSCs on the LZ hydrogel with or without mineralized matrix. The HMSCs showed a slower pace for osteogenic differentiation after two weeks on the LZ hydrogel without mineralization treatment; whereas, the HMSCs produced a mineralized matrix as early as 1 week in the LZ with mineralization treatment.

Overall, by incorporating the DMP1 motives responsible for mineralization, it was shown that the properties of the LZ hydrogel were tunable. Premineralization of the scaffold provided the use of a stiffer matrix with osteoconductive properties, while the unmineralized scaffold could provide signaling cues for osteogenic differentiation. Both matrices have the potential for modification, in the future, to cater to different tissue engineering applications.

C. Evaluation of the incorporated heparin-binding domain and MMP-2 cleavage site for leucine zipper hydrogel growth factor release

Therapeutic strategies in tissue engineering often rely on the delivery of growth factors to stimulate cellular activities. Therefore, the potential of LZ hydrogel scaffold for the release of growth factors was tested. For this the LZ hydrogel was engineered with the MMP-2 cleavage site at the C-terminus followed by the heparin-binding domain at the end. This design allowed the

heparin-binding growth factors to bind to heparin which was bound to the LZ hydrogel. The release of the growth factor was activated by the MMP-2 cleavage site engineered into the LZ protein. The LZ hydrogel showed about 70% of growth factor binding efficiency with 10% to 30% of non-specific binding. About 70% of the bound growth factor were released within 11 days without the use of MMP-2 protease; while the release was 90% with the use of MMP-2. The release of the bound growth factor due to MMP-2 was observed early on within the first 3 days. The *in vivo* subcutaneous implantation studies in nude mice were conducted by using LZ hydrogel loaded with two kinds of growth factors. When loaded with TGF- β 1, the pre-seeded HMSCs LZ scaffold showed a potential towards angiogenesis, while the BMP2 growth factor showed a tendency toward osteogenic differentiation. Overall, the results showed LZ hydrogel could be designed for the release of growth factors. In this study heparin was used to load growth factors. However, by carefully designing the chimeric LZ protein, various biological functional motifs can be incorporated for loading other proteins. Multiple release mechanisms can also be designed and blended using different chimeric LZ proteins. This allows us to generate a potentially sophisticated release mechanism for stimulating cellular activities for specific tissue engineering applications. Together, the three different types of LZ-scaffolds have established proof-of-concept for cell-interactive matrices for tissue engineering and regeneration.

APPENDICES

Appendix A

All of the *in vivo* animal works in this study were conducted under the regulation of the Animal Care Committee (ACC) from University of Illinois at Chicago. The approved animal surgical protocol number is ACC 13-073.

The approval letter from UIC ACC for the animal surgical protocol is attached below.

Office of Animal Care and
Institutional Biosafety Committees (MC 672)
Office of the Vice Chancellor for Research
206 Administrative Office Building
1737 West Polk Street
Chicago, Illinois 60612-7227

July 2, 2013

Anne George
Oral Biology
M/C 690

Dear Dr. George:

The protocol indicated below was reviewed at a convened ACC meeting in accordance with the Animal Care Policies of the University of Illinois at Chicago on **5/21/2013**. *The protocol was not initiated until final clarifications were reviewed and approved on 7/1/2013. The protocol is approved for a period of 3 years with annual continuation.*

Title of Application: Biomimetic Scaffolds for Bone Tissue Regeneration

ACC Number: 13-073

Initial Approval Period: 7/1/2013 to 5/21/2014

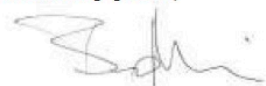
Current Funding: *Currently protocol NOT matched to specific funding source. Modification will need to be submitted prior to Just in time or acceptance of award to match protocol to external funding source. All animal work proposed in the funding application must be covered by an approved protocol.*

UIC is the only performance site currently approved for this protocol.

This institution has Animal Welfare Assurance Number A3460.01 on file with the Office of Laboratory Animal Welfare (OLAW), NIH. **This letter may only be provided as proof of IACUC approval for those specific funding sources listed above in which all portions of the funding proposal are matched to this ACC protocol.**

In addition, all investigators are responsible for ensuring compliance with all federal and institutional policies and regulations related to use of animals under this protocol and the funding sources listed on this protocol. Please use OLAW's "What Investigators Need to Know about the Use of Animals" (<http://grants.nih.gov/grants/olaw/InvestigatorsNeed2Know.pdf>) as a reference guide. Thank you for complying with the Animal Care Policies and Procedures of UIC.

Sincerely yours,



Bradley Merrill, PhD
Chair, Animal Care Committee
BM/ss

cc: BRL, ACC File, Sriram Ravindran, Chun Chieh Huang, Youbin Zhang

Appendix B

Published article listed below from *Biomaterials* (published by Elsevier) was reused for part of the thesis. We would like to express our fully acknowledgement to Elsevier for supporting of publication sharing, disseminating and maximizing the impact of the research achievements. Here we also include the published policy for author right of reusing the published article from Elsevier below.

CC Huang, S Ravindran, Z Yin, A George. 3-D self-assembling leucine zipper hydrogel with tunable properties for tissue engineering. *Biomaterials*. 2014; 35: 5316-5326. doi: 10.1016/j.biomaterials.2014.03.035

Author Rights

Elsevier supports the need for authors to share, disseminate and maximize the impact of their research. We take our responsibility as stewards of the online record seriously, and work to ensure our policies and procedures help to protect the integrity of scholarly works.

Author's rights to reuse and post their own articles published by Elsevier are defined by Elsevier's copyright policy. For our proprietary titles, the type of copyright agreement used depends on the author's choice of publication:

For subscription articles: These rights are determined by a copyright transfer, where authors retain scholarly rights to post and use their articles.

For open access articles: These rights are determined by an exclusive license agreement, which applies to all our open access content.






















In both cases, the fundamental rights needed to publish and distribute an article remain the same and Elsevier authors will be able to use their articles for a wide range of scholarly purposes.

Details on how authors can reuse and post their own articles are provided below.

Help and support

For reuse and posting not detailed below, please see our [posting policy](#), or for authors who would like to:

- Include material from other sources in your work being published by Elsevier, please visit: [Permission seeking guidelines for Elsevier authors](#).
- Obtain permission to re-use material from Elsevier books, journals, databases, or other products, please visit: [Obtaining permission to reuse Elsevier material](#)
- Or if you are an Elsevier author and are contacted by a requestor who wishes to re-use all or part of your article or chapter, please also refer them to our [Obtaining Permission to Re-Use Elsevier Material page](#).
- See our [FAQ on posting and copyright queries](#).
- Contact us directly, please email our [Permissions Help Desk](#).

Definitions	Author Posting	Author Use														
<h3>How authors can use their own journal articles</h3> <p>Authors can use their articles for a wide range of scholarly, non-commercial purposes as outlined below. These rights apply for all Elsevier authors who publish their article as either a subscription article or an open access article.</p> <p>We require that all Elsevier authors always include a full acknowledgement and, if appropriate, a link to the final published version hosted on Science Direct.</p> <p>For open access articles these rights are separate from how readers can reuse your article as defined by the author's choice of Creative Commons user license options.</p>																
<div>Authors can use either their accepted author manuscript or final published article for:</div> <table><tr><td></td><td>Use at a conference, meeting or for teaching purposes</td></tr><tr><td></td><td>Internal training by their company</td></tr><tr><td></td><td>Sharing individual articles with colleagues for their research use* (also known as 'scholarly sharing')</td></tr><tr><td></td><td>Use in a subsequent compilation of the author's works</td></tr><tr><td></td><td>Inclusion in a thesis or dissertation</td></tr><tr><td></td><td>Reuse of portions or extracts from the article in other works</td></tr><tr><td></td><td>Preparation of derivative works (other than for commercial purposes)</td></tr></table>				Use at a conference, meeting or for teaching purposes		Internal training by their company		Sharing individual articles with colleagues for their research use* (also known as 'scholarly sharing')		Use in a subsequent compilation of the author's works		Inclusion in a thesis or dissertation		Reuse of portions or extracts from the article in other works		Preparation of derivative works (other than for commercial purposes)
	Use at a conference, meeting or for teaching purposes															
	Internal training by their company															
	Sharing individual articles with colleagues for their research use* (also known as 'scholarly sharing')															
	Use in a subsequent compilation of the author's works															
	Inclusion in a thesis or dissertation															
	Reuse of portions or extracts from the article in other works															
	Preparation of derivative works (other than for commercial purposes)															
<p>*Please note this excludes any systematic or organized distribution of published articles.</p>																

CITED LITERATURES

- [1] Huang CC, Ravindran S, Yin Z, George A. 3-D self-assembling leucine zipper hydrogel with tunable properties for tissue engineering. *Biomaterials*. 2014;35:5316-26.
- [2] Seliktar D. Designing cell-compatible hydrogels for biomedical applications. *Science*. 2012;336:1124-8.
- [3] Tibbitt MW, Anseth KS. Hydrogels as extracellular matrix mimics for 3D cell culture. *Biotechnology and bioengineering*. 2009;103:655-63.
- [4] Slaughter BV, Khurshid SS, Fisher OZ, Khademhosseini A, Peppas NA. Hydrogels in regenerative medicine. *Advanced materials*. 2009;21:3307-29.
- [5] Malafaya PB, Silva GA, Reis RL. Natural-origin polymers as carriers and scaffolds for biomolecules and cell delivery in tissue engineering applications. *Advanced drug delivery reviews*. 2007;59:207-33.
- [6] Peppas NA, Bures P, Leobandung W, Ichikawa H. Hydrogels in pharmaceutical formulations. *European journal of pharmaceuticals and biopharmaceutics : official journal of Arbeitsgemeinschaft fur Pharmazeutische Verfahrenstechnik eV*. 2000;50:27-46.
- [7] Hoffman AS. Hydrogels for biomedical applications. *Advanced drug delivery reviews*. 2002;54:3-12.
- [8] Halper J, Kjaer M. Basic components of connective tissues and extracellular matrix: elastin, fibrillin, fibulins, fibrinogen, fibronectin, laminin, tenascins and thrombospondins. *Advances in experimental medicine and biology*. 2014;802:31-47.
- [9] Haycock JW. 3D cell culture: a review of current approaches and techniques. *Methods in molecular biology*. 2011;695:1-15.
- [10] Tanaka H, Murphy CL, Murphy C, Kimura M, Kawai S, Polak JM. Chondrogenic differentiation of murine embryonic stem cells: effects of culture conditions and dexamethasone. *Journal of cellular biochemistry*. 2004;93:454-62.
- [11] Gerecht S, Burdick JA, Ferreira LS, Townsend SA, Langer R, Vunjak-Novakovic G. Hyaluronic acid hydrogel for controlled self-renewal and differentiation of human embryonic stem cells. *Proceedings of the National Academy of Sciences of the United States of America*. 2007;104:11298-303.
- [12] Maltman DJ, Przyborski SA. Developments in three-dimensional cell culture technology aimed at improving the accuracy of in vitro analyses. *Biochemical Society transactions*. 2010;38:1072-5.
- [13] Bhadriraju K, Chen CS. Engineering cellular microenvironments to improve cell-based drug testing. *Drug discovery today*. 2002;7:612-20.
- [14] Burdick JA, Vunjak-Novakovic G. Engineered microenvironments for controlled stem cell differentiation. *Tissue engineering Part A*. 2009;15:205-19.
- [15] Rodríguez-Cabello JC, Reguera J, Girotti A, Alonso M, Testera AM. Developing functionality in elastin-like polymers by increasing their molecular complexity: the power of the genetic engineering approach. *Progress in polymer science*. 2005;30:1119-45.
- [16] Schmeichel KL, Bissell MJ. Modeling tissue-specific signaling and organ function in three dimensions. *Journal of cell science*. 2003;116:2377-88.

- [17] Sun T, Jackson S, Haycock JW, MacNeil S. Culture of skin cells in 3D rather than 2D improves their ability to survive exposure to cytotoxic agents. *Journal of biotechnology*. 2006;122:372-81.
- [18] Langer R, Tirrell DA. Designing materials for biology and medicine. *Nature*. 2004;428:487-92.
- [19] Nguyen KT, West JL. Photopolymerizable hydrogels for tissue engineering applications. *Biomaterials*. 2002;23:4307-14.
- [20] Sawhney AS, Pathak CP, van Rensburg JJ, Dunn RC, Hubbell JA. Optimization of photopolymerized bioerodible hydrogel properties for adhesion prevention. *Journal of biomedical materials research*. 1994;28:831-8.
- [21] Miyata T, Uragami T, Nakamae K. Biomolecule-sensitive hydrogels. *Advanced drug delivery reviews*. 2002;54:79-98.
- [22] Chang C, Duan B, Cai J, Zhang L. Superabsorbent hydrogels based on cellulose for smart swelling and controllable delivery. *European Polymer Journal*. 2010;46:92-100.
- [23] Swarbrick J. *Encyclopedia of Pharmaceutical Technology* 3ed. New York: CRC Press; 2006.
- [24] Williams DF. *Concise Encyclopedia of Medical & Dental Materials*. Oxford: Pergamon Press; 1990.
- [25] Langer R, Peppas NA. Advances in biomaterials, drug delivery, and bionanotechnology. *Bioengineering, Food and Natural Products*. 2003;49:2990-3006.
- [26] Gibas I, Janik H. Review: Synthetic Polymer Hydrogels for Biomedical Applications. *Chemistry and Chemical Technologies*. 2010;4:297-304.
- [27] Gunatillake PA, Adhikari R. Biodegradable synthetic polymers for tissue engineering. *European cells & materials*. 2003;5:1-16; discussion
- [28] Dhandayuthapani B, Yoshida Y, Maekawa T, Kumar DS. Polymeric Scaffolds in Tissue Engineering Application: A Review. *International Journal of Polymer Science*. 2011;2011:1-19.
- [29] Kubinova S, Horak D, Sykova E. Cholesterol-modified superporous poly(2-hydroxyethyl methacrylate) scaffolds for tissue engineering. *Biomaterials*. 2009;30:4601-9.
- [30] Lee KY, Mooney DJ. Hydrogels for Tissue Engineering. *Chemical Reviews*. 2001;101:1869-79.
- [31] Zhao X, Harris JM. Novel degradable poly(ethylene glycol) hydrogels for controlled release of protein. *Journal of pharmaceutical sciences*. 1998;87:1450-8.
- [32] Tan H, DeFail AJ, Rubin JP, Chu CR, Marra KG. Novel multiarm PEG-based hydrogels for tissue engineering. *Journal of biomedical materials research Part A*. 2010;92:979-87.
- [33] Zhu J. Bioactive modification of poly(ethylene glycol) hydrogels for tissue engineering. *Biomaterials*. 2010;31:4639-56.
- [34] Mikos AG, Sarakinos G, Leite SM, Vacanti JP, Langer R. Laminated three-dimensional biodegradable foams for use in tissue engineering. *Biomaterials*. 1993;14:323-30.
- [35] Temenoff JS, Mikos AG. Injectable biodegradable materials for orthopedic tissue engineering. *Biomaterials*. 2000;21:2405-12.

- [36] Schmedlen RH, Masters KS, West JL. Photocrosslinkable polyvinyl alcohol hydrogels that can be modified with cell adhesion peptides for use in tissue engineering. *Biomaterials*. 2002;23:4325-32.
- [37] Johnson T, Bahrampourian R, Patel A, Mequanint K. Fabrication of highly porous tissue-engineering scaffolds using selective spherical porogens. *Bio-medical materials and engineering*. 2010;20:107-18.
- [38] Sirova M, Van Vlierberghe S, Matyasova V, Rossmann P, Schacht E, Dubruel P, et al. Immunocompatibility evaluation of hydrogel-coated polyimide implants for applications in regenerative medicine. *Journal of biomedical materials research Part A*. 2014;102:1982-90.
- [39] Cloutier J, Blais AS, Moore K, Bolduc S. Prospective study using a new bulking agent for the treatment of vesicoureteral reflux: polyacrylamide hydrogel. *The Journal of urology*. 2013;190:1034-7.
- [40] Wittmann K, Storck K, Muhr C, Mayer H, Regn S, Staudenmaier R, et al. Development of volume-stable adipose tissue constructs using polycaprolactone-based polyurethane scaffolds and fibrin hydrogels. *Journal of tissue engineering and regenerative medicine*. 2013.
- [41] Lutolf MP, Hubbell JA. Synthetic biomaterials as instructive extracellular microenvironments for morphogenesis in tissue engineering. *Nature biotechnology*. 2005;23:47-55.
- [42] Wadea RJ, Burdick JA. Engineering ECM signals into biomaterials. *Mater Today*. 2012;15:454-9.
- [43] Zhong C, Wu J, Reinhart-King CA, Chu CC. Synthesis, characterization and cytotoxicity of photo-crosslinked maleic chitosan-polyethylene glycol diacrylate hybrid hydrogels. *Acta biomaterialia*. 2010;6:3908-18.
- [44] Buwalda SJ, Boere KW, Dijkstra PJ, Feijen J, Vermonden T, Hennink WE. Hydrogels in a historical perspective: From simple networks to smart materials. *Journal of controlled release : official journal of the Controlled Release Society*. 2014.
- [45] Griffin DR, Kasko AM. Photodegradable macromers and hydrogels for live cell encapsulation and release. *Journal of the American Chemical Society*. 2012;134:13103-7.
- [46] Li Y, Rodrigues J, Tomas H. Injectable and biodegradable hydrogels: gelation, biodegradation and biomedical applications. *Chemical Society reviews*. 2012;41:2193-221.
- [47] Wang C, Varshney RR, Wang DA. Therapeutic cell delivery and fate control in hydrogels and hydrogel hybrids. *Advanced drug delivery reviews*. 2010;62:699-710.
- [48] Xu XL, Lou J, Tang T, Ng KW, Zhang J, Yu C, et al. Evaluation of different scaffolds for BMP-2 genetic orthopedic tissue engineering. *Journal of biomedical materials research Part B, Applied biomaterials*. 2005;75:289-303.
- [49] Koch S, Yao C, Grieb G, Prevel P, Noah EM, Steffens GC. Enhancing angiogenesis in collagen matrices by covalent incorporation of VEGF. *Journal of materials science Materials in medicine*. 2006;17:735-41.
- [50] Sumita Y, Honda MJ, Ohara T, Tsuchiya S, Sagara H, Kagami H, et al. Performance of collagen sponge as a 3-D scaffold for tooth-tissue engineering. *Biomaterials*. 2006;27:3238-48.

- [51] Ikada Y, Tabata Y. Protein release from gelatin matrices. *Advanced drug delivery reviews*. 1998;31:287-301.
- [52] Young S, Wong M, Tabata Y, Mikos AG. Gelatin as a delivery vehicle for the controlled release of bioactive molecules. *Journal of controlled release : official journal of the Controlled Release Society*. 2005;109:256-74.
- [53] Payne RG, Yaszemski MJ, Yasko AW, Mikos AG. Development of an injectable, in situ crosslinkable, degradable polymeric carrier for osteogenic cell populations. Part 1. Encapsulation of marrow stromal osteoblasts in surface crosslinked gelatin microparticles. *Biomaterials*. 2002;23:4359-71.
- [54] Neidert MR, Lee ES, Oegema TR, Tranquillo RT. Enhanced fibrin remodeling in vitro with TGF-beta1, insulin and plasmin for improved tissue-equivalents. *Biomaterials*. 2002;23:3717-31.
- [55] Schmoekel H, Schense JC, Weber FE, Gratz KW, Gnani D, Muller R, et al. Bone healing in the rat and dog with nonglycosylated BMP-2 demonstrating low solubility in fibrin matrices. *Journal of orthopaedic research : official publication of the Orthopaedic Research Society*. 2004;22:376-81.
- [56] Hunter CJ, Mouw JK, Levenston ME. Dynamic compression of chondrocyte-seeded fibrin gels: effects on matrix accumulation and mechanical stiffness. *Osteoarthritis and cartilage / OARS, Osteoarthritis Research Society*. 2004;12:117-30.
- [57] Li C, Vepari C, Jin HJ, Kim HJ, Kaplan DL. Electrospun silk-BMP-2 scaffolds for bone tissue engineering. *Biomaterials*. 2006;27:3115-24.
- [58] Fini M, Motta A, Torricelli P, Giavaresi G, Nicoli Aldini N, Tschon M, et al. The healing of confined critical size cancellous defects in the presence of silk fibroin hydrogel. *Biomaterials*. 2005;26:3527-36.
- [59] Wang Y, Kim UJ, Blasioli DJ, Kim HJ, Kaplan DL. In vitro cartilage tissue engineering with 3D porous aqueous-derived silk scaffolds and mesenchymal stem cells. *Biomaterials*. 2005;26:7082-94.
- [60] Lu Q, Ganesan K, Simionescu DT, Vyavahare NR. Novel porous aortic elastin and collagen scaffolds for tissue engineering. *Biomaterials*. 2004;25:5227-37.
- [61] Chilkoti A, Christensen T, MacKay JA. Stimulus responsive elastin biopolymers: Applications in medicine and biotechnology. *Current opinion in chemical biology*. 2006;10:652-7.
- [62] Patel A, Fine B, Sandig M, Mequanint K. Elastin biosynthesis: The missing link in tissue-engineered blood vessels. *Cardiovascular research*. 2006;71:40-9.
- [63] Nishinari K, Takahashi R. Interaction in polysaccharide solutions and gels. *Current Opinion in Colloid & Interface Science*. 2003;8:396-400.
- [64] Cascone MG, Barbani N, Cristallini C, Giusti P, Ciardelli G, Lazzeri L. Bioartificial polymeric materials based on polysaccharides. *Journal of biomaterials science Polymer edition*. 2001;12:267-81.
- [65] Venugopal J, Ramakrishna S. Applications of polymer nanofibers in biomedicine and biotechnology. *Applied biochemistry and biotechnology*. 2005;125:147-58.
- [66] Khor E, Lim LY. Implantable applications of chitin and chitosan. *Biomaterials*. 2003;24:2339-49.

- [67] Ravindran S, Huang CC, George A. Extracellular matrix of dental pulp stem cells: applications in pulp tissue engineering using somatic MSCs. *Frontiers in physiology*. 2014;4:395.
- [68] George M, Abraham TE. Polyionic hydrocolloids for the intestinal delivery of protein drugs: alginate and chitosan--a review. *Journal of controlled release : official journal of the Controlled Release Society*. 2006;114:1-14.
- [69] Lee KY, Peters MC, Mooney DJ. Comparison of vascular endothelial growth factor and basic fibroblast growth factor on angiogenesis in SCID mice. *Journal of controlled release : official journal of the Controlled Release Society*. 2003;87:49-56.
- [70] Ji Y, Ghosh K, Li B, Sokolov JC, Clark RA, Rafailovich MH. Dual-syringe reactive electrospinning of cross-linked hyaluronic acid hydrogel nanofibers for tissue engineering applications. *Macromolecular bioscience*. 2006;6:811-7.
- [71] Chung C, Mesa J, Miller GJ, Randolph MA, Gill TJ, Burdick JA. Effects of auricular chondrocyte expansion on neocartilage formation in photocrosslinked hyaluronic acid networks. *Tissue engineering*. 2006;12:2665-73.
- [72] Boesel LF, Reis RL. The effect of water uptake on the behaviour of hydrophilic cements in confined environments. *Biomaterials*. 2006;27:5627-33.
- [73] Gomes ME, Ribeiro AS, Malafaya PB, Reis RL, Cunha AM. A new approach based on injection moulding to produce biodegradable starch-based polymeric scaffolds: morphology, mechanical and degradation behaviour. *Biomaterials*. 2001;22:883-9.
- [74] Lee C-T, Kung P-H, Lee Y-D. Preparation of poly(vinyl alcohol)-chondroitin sulfate hydrogel as matrices in tissue engineering. *Carbohydrate Polymers*. 2005;61:348-54.
- [75] Bassleer CT, Combal JP, Bougaret S, Malaise M. Effects of chondroitin sulfate and interleukin-1 beta on human articular chondrocytes cultivated in clusters. *Osteoarthritis and cartilage / OARS, Osteoarthritis Research Society*. 1998;6:196-204.
- [76] Naessens M, Cerdobbel A, Soetaert W, Vandamme EJ. Leuconostoc dextransucrase and dextran: production, properties and applications. *Journal of Chemical Technology and Biotechnology*. 2005;80:845-60.
- [77] Rees DA. Structure, conformation, and mechanism in the formation of polysaccharide gels and networks. *Advances in carbohydrate chemistry and biochemistry*. 1969;24:267-332.
- [78] Martson M, Viljanto J, Hurme T, Saukko P. Biocompatibility of cellulose sponge with bone. *European surgical research Europäische chirurgische Forschung Recherches chirurgicales europeennes*. 1998;30:426-32.
- [79] Grzybowski BA, Wilmer CE, Kim J, Browne KP, Bishop KJM. Self-assembly: from crystals to cells. *Soft Matter*. 2009;5.
- [80] Jayawarna V, Ali M, Jowitt TA, Miller AF, Saiani A, Gough JE, et al. Nanostructured Hydrogels for Three-Dimensional Cell Culture Through Self-Assembly of Fluorenylmethoxycarbonyl-Dipeptides. *Advanced materials*. 2006;28:611-4.
- [81] Mahler A, Reches M, Rechter M, Cohen S, Gazit E. Rigid, Self-Assembled Hydrogel Composed of a Modified Aromatic Dipeptide. *Advanced materials*. 2006;18:1365-70.

- [82] Chen L, Pont G, Morris K, Lotze G, Squires A, Serpell LC, et al. Salt-induced hydrogelation of functionalised-dipeptides at high pH. *Chemical communications*. 2011;47:12071-3.
- [83] Vegners R, Shestakova I, Kalvinsh I, Ezzell RM, Janmey PA. Use of a gel-forming dipeptide derivative as a carrier for antigen presentation. *Journal of peptide science : an official publication of the European Peptide Society*. 1995;1:371-8.
- [84] Raeburn J, Zamith Cardoso A, Adams DJ. The importance of the self-assembly process to control mechanical properties of low molecular weight hydrogels. *Chemical Society reviews*. 2013;42:5143-56.
- [85] Nguyen MK, Lee DS. Injectable biodegradable hydrogels. *Macromolecular bioscience*. 2010;10:563-79.
- [86] Guvendiren M, Lu HD, Burdick JA. Shear-thinning hydrogels for biomedical applications. *Soft Matter*. 2012;8:260-72.
- [87] Gutowska A, Bae YH, Jacobs H, Mohammad F, Mix D, Feijen J, et al. Heparin release from thermosensitive polymer coatings: in vivo studies. *Journal of biomedical materials research*. 1995;29:811-21.
- [88] Adams DJ, Holtzmann K, Schneider C, Butler MF. Self-assembly of surfactant-like peptides. *Langmuir : the ACS journal of surfaces and colloids*. 2007;23:12729-36.
- [89] Guler MO, Stupp SI. A self-assembled nanofiber catalyst for ester hydrolysis. *Journal of the American Chemical Society*. 2007;129:12082-3.
- [90] Williams BA, Lund K, Liu Y, Yan H, Chaput JC. Self-assembled peptide nanoarrays: an approach to studying protein-protein interactions. *Angewandte Chemie*. 2007;46:3051-4.
- [91] Guler MO, Soukasene S, Hulvat JF, Stupp SI. Presentation and recognition of biotin on nanofibers formed by branched peptide amphiphiles. *Nano letters*. 2005;5:249-52.
- [92] Guvendiren M, Messersmith PB, Shull KR. Self-assembly and adhesion of DOPA-modified methacrylic triblock hydrogels. *Biomacromolecules*. 2008;9:122-8.
- [93] Gunasekaran K, Ramakrishnan C, Balaram P. Beta-hairpins in proteins revisited: lessons for de novo design. *Protein engineering*. 1997;10:1131-41.
- [94] McMillan RA, Conticello VP. Synthesis and Characterization of Elastin-Mimetic Protein Gels Derived from a Well-Defined Polypeptide Precursor. *Macromolecules*. 2000;33: 4809-21.
- [95] Gulrez SKH, Al-Assaf S, Phillips GO. Hydrogels: Methods of Preparation, Characterisation and Applications. *Progress in Molecular and Environmental Bioengineering* 118 – From Analysis and Modeling to Technology Applications 2011. p. 117-50.
- [96] Zhang S. Fabrication of novel biomaterials through molecular self-assembly. *Nature biotechnology*. 2003;21:1171-8.
- [97] Davis ME, Motion JP, Narmoneva DA, Takahashi T, Hakuno D, Kamm RD, et al. Injectable self-assembling peptide nanofibers create intramyocardial microenvironments for endothelial cells. *Circulation*. 2005;111:442-50.
- [98] Hartgerink JD, Beniash E, Stupp SI. Self-assembly and mineralization of peptide-amphiphile nanofibers. *Science*. 2001;294:1684-8.

- [99] Hwang JJ, Iyer SN, Li LS, Claussen R, Harrington DA, Stupp SI. Self-assembling biomaterials: liquid crystal phases of cholesteryl oligo(L-lactic acid) and their interactions with cells. *Proceedings of the National Academy of Sciences of the United States of America*. 2002;99:9662-7.
- [100] Lee K, Silva EA, Mooney DJ. Growth factor delivery-based tissue engineering: general approaches and a review of recent developments. *J R Soc Interface*. 2011;8:153-70.
- [101] Liu W, Jawerth LM, Sparks EA, Falvo MR, Hantgan RR, Superfine R, et al. Fibrin fibers have extraordinary extensibility and elasticity. *Science*. 2006;313:634.
- [102] Dong H, Paramonov SE, Hartgerink JD. Self-assembly of alpha-helical coiled coil nanofibers. *Journal of the American Chemical Society*. 2008;130:13691-5.
- [103] Parkhe AD, Seeley SK, Gardner K, Thompson L, Lewis RV. Structural studies of spider silk proteins in the fiber. *Journal of molecular recognition : JMR*. 1997;10:1-6.
- [104] Hayashi CY, Shipley NH, Lewis RV. Hypotheses that correlate the sequence, structure, and mechanical properties of spider silk proteins. *International journal of biological macromolecules*. 1999;24:271-5.
- [105] Slotta U, Hess S, Spiess K, Stromer T, Serpell L, Scheibel T. Spider silk and amyloid fibrils: a structural comparison. *Macromolecular bioscience*. 2007;7:183-8.
- [106] Brack A, Orgel LE. Beta structures of alternating polypeptides and their possible prebiotic significance. *Nature*. 1975;256:383-7.
- [107] Aggeli A, Bell M, Boden N, Keen JN, Knowles PF, McLeish TC, et al. Responsive gels formed by the spontaneous self-assembly of peptides into polymeric beta-sheet tapes. *Nature*. 1997;386:259-62.
- [108] Zhang S, Holmes T, Lockshin C, Rich A. Spontaneous assembly of a self-complementary oligopeptide to form a stable macroscopic membrane. *Proceedings of the National Academy of Sciences of the United States of America*. 1993;90:3334-8.
- [109] Semino CE, Kasahara J, Hayashi Y, Zhang S. Entrapment of migrating hippocampal neural cells in three-dimensional peptide nanofiber scaffold. *Tissue engineering*. 2004;10:643-55.
- [110] Holmes TC, de Lacalle S, Su X, Liu G, Rich A, Zhang S. Extensive neurite outgrowth and active synapse formation on self-assembling peptide scaffolds. *Proceedings of the National Academy of Sciences of the United States of America*. 2000;97:6728-33.
- [111] Collier JH, Hu BH, Ruberti JW, Zhang J, Shum P, Thompson DH, et al. Thermally and photochemically triggered self-assembly of peptide hydrogels. *Journal of the American Chemical Society*. 2001;123:9463-4.
- [112] Jung JP, Nagaraj AK, Fox EK, Rudra JS, Devgun JM, Collier JH. Co-assembling peptides as defined matrices for endothelial cells. *Biomaterials*. 2009;30:2400-10.
- [113] Rudra JS, Tian YF, Jung JP, Collier JH. A self-assembling peptide acting as an immune adjuvant. *Proceedings of the National Academy of Sciences of the United States of America*. 2010;107:622-7.
- [114] Ozbas B, Kretsinger J, Rajagopal K, Schneider JP, Pochan DJ. Salt-Triggered Peptide Folding and Consequent Self-Assembly into Hydrogels with Tunable Modulus. *Macromolecules*. 2004;37:7331-7.

- [115] Rajagopal K, Lamm MS, Haines-Butterick LA, Pochan DJ, Schneider JP. Tuning the pH responsiveness of beta-hairpin peptide folding, self-assembly, and hydrogel material formation. *Biomacromolecules*. 2009;10:2619-25.
- [116] Yang Z, Liang G, Ma M, Gao Y, Xu B. Conjugates of naphthalene and dipeptides produce molecular hydrogelators with high efficiency of hydrogelation and superhelical nanofibers. *J Mater Chem*. 2007;17:850-4.
- [117] Yu YC, Pakalns T, Dori Y, McCarthy JB, Tirrell M, Fields GB. Construction of biologically active protein molecular architecture using self-assembling peptide-amphiphiles. *Methods in enzymology*. 1997;289:571-87.
- [118] Anderson JM, Andukuri A, Lim DJ, Jun HW. Modulating the gelation properties of self-assembling peptide amphiphiles. *ACS nano*. 2009;3:3447-54.
- [119] Löwik DWPM, Shklyarevskiy IO, Ruizendaal L, Christianen PCM, Maan JC, Hest JCMv. A Highly Ordered Material from Magnetically Aligned Peptide Amphiphile Nanofiber Assemblies. *Advanced materials*. 2007;19:1191-5.
- [120] Stendahl JC, Rao MS, Guler MO, Stupp SI. Intermolecular Forces in the Self-Assembly of Peptide Amphiphile Nanofibers. *Advanced functional materials*. 2006;16:499-508.
- [121] Niece KL, Czeisler C, Sahni V, Tysseling-Mattiace V, Pashuck ET, Kessler JA, et al. Modification of gelation kinetics in bioactive peptide amphiphiles. *Biomaterials*. 2008;29:4501-9.
- [122] Silva GA, Czeisler C, Niece KL, Beniash E, Harrington DA, Kessler JA, et al. Selective differentiation of neural progenitor cells by high-epitope density nanofibers. *Science*. 2004;303:1352-5.
- [123] Beniash E, Hartgerink JD, Storrie H, Stendahl JC, Stupp SI. Self-assembling peptide amphiphile nanofiber matrices for cell entrapment. *Acta biomaterialia*. 2005;1:387-97.
- [124] Rajangam K, Behanna HA, Hui MJ, Han X, Hulvat JF, Lomasney JW, et al. Heparin binding nanostructures to promote growth of blood vessels. *Nano letters*. 2006;6:2086-90.
- [125] Keeley FW, Bellingham CM, Woodhouse KA. Elastin as a self-organizing biomaterial: use of recombinantly expressed human elastin polypeptides as a model for investigations of structure and self-assembly of elastin. *Philosophical transactions of the Royal Society of London Series B, Biological sciences*. 2002;357:185-9.
- [126] Mecham RP, Broekelmann T, Davis EC, Gibson MA, Brown-Augsburger P. Elastic fibre assembly: macromolecular interactions. *Ciba Foundation symposium*. 1995;192:172-81; discussion 81-4.
- [127] Betre H, Ong SR, Guilak F, Chilkoti A, Fermor B, Setton LA. Chondrocytic differentiation of human adipose-derived adult stem cells in elastin-like polypeptide. *Biomaterials*. 2006;27:91-9.
- [128] Cirulis JT, Keeley FW. Kinetics and morphology of self-assembly of an elastin-like polypeptide based on the alternating domain arrangement of human tropoelastin. *Biochemistry*. 2010;49:5726-33.
- [129] Reiersen H, Clarke AR, Rees AR. Short elastin-like peptides exhibit the same temperature-induced structural transitions as elastin polymers: implications for protein engineering. *Journal of molecular biology*. 1998;283:255-64.

- [130] Yamaoka T, Tamura T, Seto Y, Tada T, Kunugi S, Tirrell DA. Mechanism for the phase transition of a genetically engineered elastin model peptide (VPGIG)₄₀ in aqueous solution. *Biomacromolecules*. 2003;4:1680-5.
- [131] Ayres L, Vos MRJ, Adams PJHM, Shklyarevskiy IO, Hest JCMv. Elastin-Based Side-Chain Polymers Synthesized by ATRP. *Macromolecules*. 2003;36:5967-73.
- [132] Wright ER, Conticello VP. Self-assembly of block copolymers derived from elastin-mimetic polypeptide sequences. *Advanced drug delivery reviews*. 2002;54:1057-73.
- [133] Nagapudi K, Brinkman WT, Thomas BS, Park JO, Srinivasarao M, Wright E, et al. Viscoelastic and mechanical behavior of recombinant protein elastomers. *Biomaterials*. 2005;26:4695-706.
- [134] Adams DJ, Topham PD. Peptide conjugate hydrogelators. *Soft Matter*. 2010;6:3707-21.
- [135] Kim W, Thevenot J, Ibarboure E, Lecommandoux S, Chaikof EL. Self-assembly of thermally responsive amphiphilic diblock copolypeptides into spherical micellar nanoparticles. *Angewandte Chemie*. 2010;49:4257-60.
- [136] Nettles DL, Haider MA, Chilkoti A, Setton LA. Neural network analysis identifies scaffold properties necessary for in vitro chondrogenesis in elastin-like polypeptide biopolymer scaffolds. *Tissue engineering Part A*. 2010;16:11-20.
- [137] Betre H, Setton LA, Meyer DE, Chilkoti A. Characterization of a genetically engineered elastin-like polypeptide for cartilaginous tissue repair. *Biomacromolecules*. 2002;3:910-6.
- [138] Banta S, Wheeldon IR, Blenner M. Protein engineering in the development of functional hydrogels. *Annual review of biomedical engineering*. 2010;12:167-86.
- [139] Alber T. Structure of the leucine zipper. *Current opinion in genetics & development*. 1992;2:205-10.
- [140] Landschulz WH, Johnson PF, McKnight SL. The leucine zipper: a hypothetical structure common to a new class of DNA binding proteins. *Science*. 1988;240:1759-64.
- [141] Petka WA, Harden JL, McGrath KP, Wirtz D, Tirrell DA. Reversible hydrogels from self-assembling artificial proteins. *Science*. 1998;281:389-92.
- [142] Wang C, Stewart RJ, Kopecek J. Hybrid hydrogels assembled from synthetic polymers and coiled-coil protein domains. *Nature*. 1999;397:417-20.
- [143] Shen W, Lammertink RGH, Sakata JK, Kornfield JA, Tirrell DA. Assembly of an Artificial Protein Hydrogel through Leucine Zipper Aggregation and Disulfide Bond Formation. *Macromolecules*. 2005;38:3909-16.
- [144] Shen W, Zhang K, Kornfield JA, Tirrell DA. Tuning the erosion rate of artificial protein hydrogels through control of network topology. *Nat Mater*. 2006;5:153-8.
- [145] Ryan SJ, Kennan AJ. Variable stability heterodimeric coiled-coils from manipulation of electrostatic interface residue chain length. *Journal of the American Chemical Society*. 2007;129:10255-60.
- [146] Boyan BD, Hummert TW, Dean DD, Schwartz Z. Role of material surfaces in regulating bone and cartilage cell response. *Biomaterials*. 1996;17:137-46.
- [147] Elbert DL, Hubbell JA. Surface Treatments of Polymers for Biocompatibility. *Annual Review of Materials Science*. 1996;26:365-94.

- [148] Hern DL, Hubbell JA. Incorporation of adhesion peptides into nonadhesive hydrogels useful for tissue resurfacing. *Journal of biomedical materials research*. 1998;39:266-76.
- [149] Benoit DS, Anseth KS. The effect on osteoblast function of colocalized RGD and PHSRN epitopes on PEG surfaces. *Biomaterials*. 2005;26:5209-20.
- [150] Dai W, Belt J, Saltzman WM. Cell-binding peptides conjugated to poly(ethylene glycol) promote neural cell aggregation. *Bio/technology*. 1994;12:797-801.
- [151] Hosseinkhani H, Hiraoka Y, Li CH, Chen YR, Yu DS, Hong PD, et al. Engineering three-dimensional collagen-IKVAV matrix to mimic neural microenvironment. *ACS chemical neuroscience*. 2013;4:1229-35.
- [152] Bellamkonda R, Ranieri JP, Aebischer P. Laminin oligopeptide derivatized agarose gels allow three-dimensional neurite extension in vitro. *Journal of neuroscience research*. 1995;41:501-9.
- [153] Derda R, Li L, Orner BP, Lewis RL, Thomson JA, Kiessling LL. Defined substrates for human embryonic stem cell growth identified from surface arrays. *ACS chemical biology*. 2007;2:347-55.
- [154] Stauffer WR, Cui XT. Polypyrrole doped with 2 peptide sequences from laminin. *Biomaterials*. 2006;27:2405-13.
- [155] Kisiel M, Martino MM, Ventura M, Hubbell JA, Hilborn J, Ossipov DA. Improving the osteogenic potential of BMP-2 with hyaluronic acid hydrogel modified with integrin-specific fibronectin fragment. *Biomaterials*. 2013;34:704-12.
- [156] Hubbell JA, Massia SP, Drumheller PD. Surface-grafted cell-binding peptides in tissue engineering of the vascular graft. *Annals of the New York Academy of Sciences*. 1992;665:253-8.
- [157] Elbert DL, Hubbell JA. Surface Treatments of Polymers for Biocompatibility. *Annual Review of Materials Science*. 1996;26:365-94.
- [158] Shin H, Jo S, Mikos AG. Biomimetic materials for tissue engineering. *Biomaterials*. 2003;24:4353-64.
- [159] Hersel U, Dahmen C, Kessler H. RGD modified polymers: biomaterials for stimulated cell adhesion and beyond. *Biomaterials*. 2003;24:4385-415.
- [160] Mi L, Fischer S, Chung B, Sundelacruz S, Harden JL. Self-assembling protein hydrogels with modular integrin binding domains. *Biomacromolecules*. 2006;7:38-47.
- [161] Fischer SE, Mi L, Mao HQ, Harden JL. Biofunctional coatings via targeted covalent cross-linking of associating triblock proteins. *Biomacromolecules*. 2009;10:2408-17.
- [162] Fischer SE, Liu X, Mao HQ, Harden JL. Controlling cell adhesion to surfaces via associating bioactive triblock proteins. *Biomaterials*. 2007;28:3325-37.
- [163] Ghosh K, Ingber DE. Micromechanical control of cell and tissue development: implications for tissue engineering. *Advanced drug delivery reviews*. 2007;59:1306-18.
- [164] Wang N, Tytell JD, Ingber DE. Mechanotransduction at a distance: mechanically coupling the extracellular matrix with the nucleus. *Nature reviews Molecular cell biology*. 2009;10:75-82.

- [165] Ingber DE. Cellular mechanotransduction: putting all the pieces together again. *FASEB journal : official publication of the Federation of American Societies for Experimental Biology*. 2006;20:811-27.
- [166] Guvendiren M, Burdick JA. Stem cell response to spatially and temporally displayed and reversible surface topography. *Advanced healthcare materials*. 2013;2:155-64.
- [167] Discher DE, Mooney DJ, Zandstra PW. Growth factors, matrices, and forces combine and control stem cells. *Science*. 2009;324:1673-7.
- [168] Engler AJ, Sen S, Sweeney HL, Discher DE. Matrix elasticity directs stem cell lineage specification. *Cell*. 2006;126:677-89.
- [169] DeKosky BJ, Dormer NH, Ingavle GC, Roatch CH, Lomakin J, Detamore MS, et al. Hierarchically designed agarose and poly(ethylene glycol) interpenetrating network hydrogels for cartilage tissue engineering. *Tissue engineering Part C, Methods*. 2010;16:1533-42.
- [170] Haque MA, Kurokawa T, Gong JP. Super tough double network hydrogels and their application as biomaterials. *Polymer*. 2012;53:1805-22.
- [171] Huang G, Zhang X, Xiao Z, Zhang Q, Zhou J, Xu F, et al. Cell-encapsulating microfluidic hydrogels with enhanced mechanical stability. *Soft Matter*. 2012;14:10687-94.
- [172] Bryant SJ, Anseth KS, Lee DA, Bader DL. Crosslinking density influences the morphology of chondrocytes photoencapsulated in PEG hydrogels during the application of compressive strain. *Journal of orthopaedic research : official publication of the Orthopaedic Research Society*. 2004;22:1143-9.
- [173] Bryant SJ, Chowdhury TT, Lee DA, Bader DL, Anseth KS. Crosslinking density influences chondrocyte metabolism in dynamically loaded photocrosslinked poly(ethylene glycol) hydrogels. *Annals of biomedical engineering*. 2004;32:407-17.
- [174] Shin SR, Bae H, Cha JM, Mun JY, Chen YC, Tekin H, et al. Carbon nanotube reinforced hybrid microgels as scaffold materials for cell encapsulation. *ACS nano*. 2012;6:362-72.
- [175] Schnepf ZAC, Gonzalez-McQuire R, Mann S. Hybrid Biocomposites Based on Calcium Phosphate Mineralization of Self-Assembled Supramolecular Hydrogels. *Advanced materials*. 2006;18:1869-72.
- [176] Burnham NA, Colton RJ. Measuring the nanomechanical properties and surface forces of materials using an atomic force microscope. *Journal of Vacuum Science & Technology A* 1989;7:2906e13.
- [177] Tripathy S, Berger EJ. Measuring viscoelasticity of soft samples using atomic force microscopy. *Journal of biomechanical engineering*. 2009;131:094507.
- [178] Cohen SR, Kalfon-Cohen E. Dynamic nanoindentation by instrumented nanoindentation and force microscopy: a comparative review. *Beilstein journal of nanotechnology*. 2013;4:815-33.
- [179] Cha C, Jeong JH, Shim J, Kong H. Tuning the dependency between stiffness and permeability of a cell encapsulating hydrogel with hydrophilic pendant chains. *Acta biomaterialia*. 2011;7:3719-28.
- [180] Cha C, Kim SY, Cao L, Kong H. Decoupled control of stiffness and permeability with a cell-encapsulating poly(ethylene glycol) dimethacrylate hydrogel. *Biomaterials*. 2010;31:4864-71.

- [181] Vo TN, Kasper FK, Mikos AG. Strategies for controlled delivery of growth factors and cells for bone regeneration. *Advanced drug delivery reviews*. 2012;64:1292-309.
- [182] DeLong SA, Moon JJ, West JL. Covalently immobilized gradients of bFGF on hydrogel scaffolds for directed cell migration. *Biomaterials*. 2005;26:3227-34.
- [183] Saik JE, Gould DJ, Watkins EM, Dickinson ME, West JL. Covalently immobilized platelet-derived growth factor-BB promotes angiogenesis in biomimetic poly(ethylene glycol) hydrogels. *Acta biomaterialia*. 2011;7:133-43.
- [184] Dvir T, Timko BP, Kohane DS, Langer R. Nanotechnological strategies for engineering complex tissues. *Nature nanotechnology*. 2011;6:13-22.
- [185] Freeman I, Kedem A, Cohen S. The effect of sulfation of alginate hydrogels on the specific binding and controlled release of heparin-binding proteins. *Biomaterials*. 2008;29:3260-8.
- [186] Martino MM, Hubbell JA. The 12th-14th type III repeats of fibronectin function as a highly promiscuous growth factor-binding domain. *FASEB journal : official publication of the Federation of American Societies for Experimental Biology*. 2010;24:4711-21.
- [187] Burgess WH, Maciag T. The heparin-binding (fibroblast) growth factor family of proteins. *Annual review of biochemistry*. 1989;58:575-606.
- [188] Seif-Naraghi SB, Horn D, Schup-Magoffin PJ, Christman KL. Injectable extracellular matrix derived hydrogel provides a platform for enhanced retention and delivery of a heparin-binding growth factor. *Acta biomaterialia*. 2012;8:3695-703.
- [189] Sakiyama-Elbert SE, Hubbell JA. Controlled release of nerve growth factor from a heparin-containing fibrin-based cell ingrowth matrix. *Journal of controlled release : official journal of the Controlled Release Society*. 2000;69:149-58.
- [190] Sakiyama-Elbert SE, Hubbell JA. Development of fibrin derivatives for controlled release of heparin-binding growth factors. *Journal of controlled release : official journal of the Controlled Release Society*. 2000;65:389-402.
- [191] Sakiyama SE, Schense JC, Hubbell JA. Incorporation of heparin-binding peptides into fibrin gels enhances neurite extension: an example of designer matrices in tissue engineering. *FASEB journal : official publication of the Federation of American Societies for Experimental Biology*. 1999;13:2214-24.
- [192] Lee KY, Mooney DJ. Alginate: properties and biomedical applications. *Progress in polymer science*. 2012;37:106-26.
- [193] Kolambkar YM, Dupont KM, Boerckel JD, Huebsch N, Mooney DJ, Hutmacher DW, et al. An alginate-based hybrid system for growth factor delivery in the functional repair of large bone defects. *Biomaterials*. 2011;32:65-74.
- [194] Gajjaraman S, He G, Narayanan K, George A. Biological assemblies provide novel templates for the synthesis of hierarchical structures and facilitate cell adhesion. *Advanced functional materials*. 2008;18:3972-80.
- [195] He G, Dahl T, Veis A, George A. Nucleation of apatite crystals in vitro by self-assembled dentin matrix protein 1. *Nat Mater*. 2003;2:552-8.
- [196] Ravindran S, Gao Q, Kotecha M, Magin RL, Karol S, Bedran-Russo A, et al. Biomimetic extracellular matrix-incorporated scaffold induces osteogenic gene

expression in human marrow stromal cells. *Tissue engineering Part A*. 2012;18:295-309.

[197] Yin Z, Schmid TM, Yasar TK, Liu Y, Royston TJ, Magin RL. Mechanical Characterization of Tissue-Engineered Cartilage Using Microscopic Magnetic Resonance Elastography. *Tissue engineering Part C, Methods*. 2014.

[198] Granlund HKaC-fWaG. Local multiscale frequency and bandwidth estimation. In *Proceedings of IEEE International Conference on Image Processing* 1994. p. 36-40.

[199] Ravindran S, Song Y, George A. Development of three-dimensional biomimetic scaffold to study epithelial-mesenchymal interactions. *Tissue engineering Part A*. 2010;16:327-42.

[200] Weadock KS, Miller EJ, Bellincampi LD, Zawadsky JP, Dunn MG. Physical crosslinking of collagen fibers: comparison of ultraviolet irradiation and dehydrothermal treatment. *Journal of biomedical materials research*. 1995;29:1373-9.

[201] Haugh MG, Murphy CM, McKiernan RC, Altenbuchner C, O'Brien FJ. Crosslinking and mechanical properties significantly influence cell attachment, proliferation, and migration within collagen glycosaminoglycan scaffolds. *Tissue engineering Part A*. 2011;17:1201-8.

[202] Yodkhum K, Phaechamud T. Hydrophobic chitosan sponges modified by aluminum monostearate and dehydrothermal treatment as sustained drug delivery system. *Materials science & engineering C, Materials for biological applications*. 2014;42:715-25.

[203] Murakami M, Saito T, Tabata Y. Controlled release of sphingosine-1-phosphate agonist with gelatin hydrogels for macrophage recruitment. *Acta biomaterialia*. 2014;10:4723-9.

[204] Billiet T, Vandenhaute M, Schelfhout J, Van Vlierberghe S, Dubruel P. A review of trends and limitations in hydrogel-rapid prototyping for tissue engineering. *Biomaterials*. 2012;33:6020-41.

[205] Baker BM, Chen CS. Deconstructing the third dimension: how 3D culture microenvironments alter cellular cues. *Journal of cell science*. 2012;125:3015-24.

[206] Mohsin MA, Berry JP, Treloar LRG. Dynamic Mechanical-Properties of Polybutadiene Rubbers. *Polymer*. 1985;26:1463-8.

[207] Chirila TV, Hong Y. Poly(1-vinyl-2-pyrrolidinone) hydrogels as vitreous substitutes: a rheological study. *Polym Int*. 1998;46:183-95.

[208] Sieminski AL, Was AS, Kim G, Gong H, Kamm RD. The stiffness of three-dimensional ionic self-assembling peptide gels affects the extent of capillary-like network formation. *Cell biochemistry and biophysics*. 2007;49:73-83.

[209] Zhu W, Mow VC, Koob TJ, Eyre DR. Viscoelastic shear properties of articular cartilage and the effects of glycosidase treatments. *Journal of orthopaedic research : official publication of the Orthopaedic Research Society*. 1993;11:771-81.

[210] Lopez O, Amrami KK, Manduca A, Ehman RL. Characterization of the dynamic shear properties of hyaline cartilage using high-frequency dynamic MR elastography. *Magnetic resonance in medicine : official journal of the Society of Magnetic Resonance in Medicine / Society of Magnetic Resonance in Medicine*. 2008;59:356-64.

- [211] Berglund JD, Mohseni MM, Nerem RM, Sambanis A. A biological hybrid model for collagen-based tissue engineered vascular constructs. *Biomaterials*. 2003;24:1241-54.
- [212] Rowland CR, Lennon DP, Caplan AI, Guilak F. The effects of crosslinking of scaffolds engineered from cartilage ECM on the chondrogenic differentiation of MSCs. *Biomaterials*. 2013;34:5802-12.
- [213] Hershko A, Ciechanover A. Mechanisms of intracellular protein breakdown. *Annual review of biochemistry*. 1982;51:335-64.
- [214] DeForest CA, Anseth KS. Advances in bioactive hydrogels to probe and direct cell fate. *Annual review of chemical and biomolecular engineering*. 2012;3:421-44.
- [215] Ivannikov MV, Macleod GT. Mitochondrial free Ca^{2+} levels and their effects on energy metabolism in *Drosophila* motor nerve terminals. *Biophys J*. 2013;104:2353-61.
- [216] Warren SM, Nacamuli RK, Song HM, Longaker MT. Tissue-engineered bone using mesenchymal stem cells and a biodegradable scaffold. *The Journal of craniofacial surgery*. 2004;15:34-7.
- [217] Raynaud S, Champion E, Bernache-Assollant D, Thomas P. Calcium phosphate apatites with variable Ca/P atomic ratio I. Synthesis, characterisation and thermal stability of powders. *Biomaterials*. 2002;23:1065-72.
- [218] Song J, Saiz E, Bertozzi CR. A new approach to mineralization of biocompatible hydrogel scaffolds: an efficient process toward 3-dimensional bonelike composites. *Journal of the American Chemical Society*. 2003;125:1236-43.
- [219] Song J, Malathong V, Bertozzi CR. Mineralization of synthetic polymer scaffolds: a bottom-up approach for the development of artificial bone. *Journal of the American Chemical Society*. 2005;127:3366-72.
- [220] Azami M, Moosavifar MJ, Baheiraei N, Moztarzadeh F, Ai J. Preparation of a biomimetic nanocomposite scaffold for bone tissue engineering via mineralization of gelatin hydrogel and study of mineral transformation in simulated body fluid. *Journal of biomedical materials research Part A*. 2012;100:1347-55.
- [221] Jiang H, Su W, Mather PT, Bunning TJ. Rheology of highly swollen chitosan/polyacrylate hydrogels. *Polymer*. 1999;40:4593-602.
- [222] Arinzech TL, Tran T, McAlary J, Daculsi G. A comparative study of biphasic calcium phosphate ceramics for human mesenchymal stem-cell-induced bone formation. *Biomaterials*. 2005;26:3631-8.
- [223] Muller P, Bulnheim U, Diener A, Luthen F, Teller M, Klinkenberg ED, et al. Calcium phosphate surfaces promote osteogenic differentiation of mesenchymal stem cells. *Journal of cellular and molecular medicine*. 2008;12:281-91.
- [224] Shui C, Spelsberg TC, Riggs BL, Khosla S. Changes in Runx2/Cbfa1 expression and activity during osteoblastic differentiation of human bone marrow stromal cells. *Journal of bone and mineral research : the official journal of the American Society for Bone and Mineral Research*. 2003;18:213-21.
- [225] Zhao Z, Zhao M, Xiao G, Franceschi RT. Gene transfer of the Runx2 transcription factor enhances osteogenic activity of bone marrow stromal cells in vitro and in vivo. *Molecular therapy : the journal of the American Society of Gene Therapy*. 2005;12:247-53.

- [226] George A, Sabsay B, Simonian PA, Veis A. Characterization of a novel dentin matrix acidic phosphoprotein. Implications for induction of biomineralization. *The Journal of biological chemistry*. 1993;268:12624-30.
- [227] MacDougall M, Gu TT, Simmons D. Dentin matrix protein-1, a candidate gene for dentinogenesis imperfecta. *Connective tissue research*. 1996;35:267-72.
- [228] Thotakura SR, Karthikeyan N, Smith T, Liu K, George A. Cloning and characterization of rat dentin matrix protein 1 (DMP1) gene and its 5'-upstream region. *The Journal of biological chemistry*. 2000;275:10272-7.
- [229] Kulkarni GV, Chen B, Malone JP, Narayanan AS, George A. Promotion of selective cell attachment by the RGD sequence in dentine matrix protein 1. *Archives of oral biology*. 2000;45:475-84.
- [230] Luo S, Mao C, Lee B, Lee AS. GRP78/BiP is required for cell proliferation and protecting the inner cell mass from apoptosis during early mouse embryonic development. *Molecular and cellular biology*. 2006;26:5688-97.
- [231] Ravindran S, Gao Q, Ramachandran A, Sundivakkam P, Tiruppathi C, George A. Expression and distribution of grp-78/bip in mineralizing tissues and mesenchymal cells. *Histochemistry and cell biology*. 2012;138:113-25.
- [232] Murakami T, Saito A, Hino S, Kondo S, Kanemoto S, Chihara K, et al. Signalling mediated by the endoplasmic reticulum stress transducer OASIS is involved in bone formation. *Nature cell biology*. 2009;11:1205-11.
- [233] Deshpande AS, Fang PA, Zhang X, Jayaraman T, Sfeir C, Beniash E. Primary structure and phosphorylation of dentin matrix protein 1 (DMP1) and dentin phosphophoryn (DPP) uniquely determine their role in biomineralization. *Biomacromolecules*. 2011;12:2933-45.
- [234] George A, Srinivasan R, Thotakura S, Veis A. The phosphophoryn gene family: identical domain structures at the carboxyl end. *European journal of oral sciences*. 1998;106 Suppl 1:221-6.
- [235] Park JS, Chu JS, Tsou AD, Diop R, Tang Z, Wang A, et al. The effect of matrix stiffness on the differentiation of mesenchymal stem cells in response to TGF-beta. *Biomaterials*. 2011;32:3921-30.
- [236] Li Z, Gong Y, Sun S, Du Y, Lu D, Liu X, et al. Differential regulation of stiffness, topography, and dimension of substrates in rat mesenchymal stem cells. *Biomaterials*. 2013;34:7616-25.
- [237] Lu D, Luo C, Zhang C, Li Z, Long M. Differential regulation of morphology and stemness of mouse embryonic stem cells by substrate stiffness and topography. *Biomaterials*. 2014;35:3945-55.
- [238] Nava MM, Raimondi MT, Pietrabissa R. Controlling self-renewal and differentiation of stem cells via mechanical cues. *Journal of biomedicine & biotechnology*. 2012;2012:797410.
- [239] Eapen A, Sundivakkam P, Song Y, Ravindran S, Ramachandran A, Tiruppathi C, et al. Calcium-mediated stress kinase activation by DMP1 promotes osteoblast differentiation. *The Journal of biological chemistry*. 2010;285:36339-51.
- [240] Ye L, Mishina Y, Chen D, Huang H, Dallas SL, Dallas MR, et al. Dmp1-deficient mice display severe defects in cartilage formation responsible for a chondrodysplasia-like phenotype. *The Journal of biological chemistry*. 2005;280:6197-203.

- [241] Nie X, Luukko K, Kettunen P. BMP signalling in craniofacial development. *The International journal of developmental biology*. 2006;50:511-21.
- [242] Ducy P, Karsenty G. The family of bone morphogenetic proteins. *Kidney international*. 2000;57:2207-14.
- [243] Cho TJ, Gerstenfeld LC, Einhorn TA. Differential temporal expression of members of the transforming growth factor beta superfamily during murine fracture healing. *Journal of bone and mineral research : the official journal of the American Society for Bone and Mineral Research*. 2002;17:513-20.
- [244] Nakamura S, Matsumoto T, Sasaki J, Egusa H, Lee KY, Nakano T, et al. Effect of calcium ion concentrations on osteogenic differentiation and hematopoietic stem cell niche-related protein expression in osteoblasts. *Tissue engineering Part A*. 2010;16:2467-73.
- [245] Sasano Y, Zhu JX, Kamakura S, Kusunoki S, Mizoguchi I, Kagayama M. Expression of major bone extracellular matrix proteins during embryonic osteogenesis in rat mandibles. *Anatomy and embryology*. 2000;202:31-7.
- [246] Lee JL, Wang MJ, Sudhir PR, Chen GD, Chi CW, Chen JY. Osteopontin promotes integrin activation through outside-in and inside-out mechanisms: OPN-CD44V interaction enhances survival in gastrointestinal cancer cells. *Cancer research*. 2007;67:2089-97.
- [247] Turk BE, Huang LL, Piro ET, Cantley LC. Determination of protease cleavage site motifs using mixture-based oriented peptide libraries. *Nature biotechnology*. 2001;19:661-7.
- [248] Chen G, Deng C, Li YP. TGF-beta and BMP signaling in osteoblast differentiation and bone formation. *International journal of biological sciences*. 2012;8:272-88.

VITA

Name: Chun-Chieh Huang

Education: Ph.D., Bioengineering, University of Illinois at Chicago, Chicago, USA, 2014
M.S., Biomedical Engineering, National Taiwan University, Taipei, Taiwan, 2005
B.S., Material Science and Engineering, National Chiao Tung University, Hsinchu, Taiwan, 2003

Awards: The Second Place Pre-Doctoral Basic Science Young Investigators Awards, American Association for Dental Research Chicago Section, Chicago, USA, 2010

Publications: CC Huang, S Ravindran, Z Yin, A George. 3-D self-assembling leucine zipper hydrogel with tunable properties for tissue engineering. *Biomaterials*. 2014; 35: 5316-5326.

S Ravindran, Y Zhang, CC Huang, A George. Odontogenic induction of dental stem cells by extracellular matrix-inspired three-dimensional scaffold. *Tissue Eng Part A*. 2014; 20: 92-102.

Y Zhang, Y Song, S Ravindran, Q Gao, CC Huang, A Ramachandran, A Kulkarni, A George. *J Dent Res*. 2014; 93: 155-161.

S Ravindran, CC Huang, A George. Extracellular matrix of dental pulp stem cells: applications in pulp tissue engineering using somatic MSCs. *Front Physiol*. 2013; 4: 395.

A George, CC Huang. Bioinspired Strategies for Hard Tissue Regeneration. *Advances in Biomimetics*. InTech; 2011.

YC Huang, CC Huang, YY Huang, KS Chen. Surface modification and characterization of chitosan or PLGA membrane with laminin by chemical and oxygen plasma treatment for neural regeneration. *J Biomed Mater Res A*. 2007; 82: 842-51.

YC Huang, YY Huang, CC Huang, HC Liu. Manufacture of porous polymer nerve conduits through a lyophilizing and wire-heating process. *J Biomed Mater Res B Appl Biomater*. 2005; 74: 659-664.